Aalborg Universitet

Characterisation and Modelling of Measured Massive MIMO Channels

Martinez, Alex Oliveras

CORRECTION NOTE CONCERNING

TITLE: Characterisation and Modelling of Measured Massive MIMO Channels

AUTHOR: Àlex Oliveras Martínez

DESCRIPTION:
There are corrections to the following pages:

Introduction:
       Summary of Papers
              Paper C (Pg. 18)
              Paper E (Pg. 20)

Papers:
       Paper C
              Copyright (Pg. 66)
              3 Channel hardening (Pg. 70-73)
              Conclusions (Pg. 77)
       Paper E
              4 Channel hardening (Pg. 110-116)
              Conclusions (Pg.121-123)

The corrections are located at the beginning of this file.

SUMMARY OF PAPERS: PAPER C (PG. 18)

4.3 Paper C

Massive MIMO Properties based on Measured Channels: Channel Hardening, User Decorrelation and Channel Sparcity
50th Asilomar Conference on Signals, Systems, and Computers, IEEE pp. 1804-1808, 2016

Motivation

Some signal processing methods for massive MIMO extensively exploit some properties of the channel that has not been deeply studied in measured channels. These properties are: Channel hardening, orthogonality of the channel vectors of users at specific distances between them, and dimension of the signal subspace. This work is motivated by the lack of study of the mentioned properties.

Paper content

This study is based on two massive MIMO measurement campaigns. The first one has 64 base station antennas and 8 dual-antenna users in an indoor scenario similar to a shopping mall. The second measurement campaign has 128 antennas at the base station and 2 dual-antenna users in an outdoor scenario that could be used as a concert venue. To study the channel hardening we look at the standard deviation over channel realizations of the average power across the array. The orthogonality of the channel vector of the users is computed for specific positions of the users. Finally we observe the eigenvalue profile for the channel of a single user, and the angle of arrival using a steering vector beam-sweeping.

Main results

First we observe that the average power of the channel across the array becomes more stable when the number of base station antennas increases. However the hardening is not as strong as in Gaussian channels due to the correlation between links. In addition, adding more antennas with high power does not improve the channel hardening. Increasing the aperture of the base station array increases the hardening effect. We also observe a clear relationship between the orthogonality of the channel vector of the users with the distance between these users in NLoS. The analysis of the eigenvalue profile shows a larger dimension of the signal subspace for NLoS channels compared to LoS. However, the smoothness in the profile does not reveal a clear number for the dimension of the subspace. The angle of arrival shows a rich scattering environment.

SUMMARY OF PAPERS: PAPER E (PG. 20)

4.5 Paper E

An Experimental Study of Massive MIMO Properties in 5G Scenarios
Under major revision by IEEE Transactions on Antennas and Propagation

Motivation

The motivation for this publication is to study three main characteristics of massive MIMO that are used in some signal processing techniques, but they have never been deeply studied in measured channels. These characteristics are: channel hardening, multi-user consistency and dimension of the signal subspace. Two massive MIMO measurement campaigns are used to study these topics.

Paper content

This publication analyses two massive MIMO measurement campaigns. The first one uses 64 BS antennas and it serves 8 dual-antenna users. The scenario is a large indoor venue. The second measurement campaign uses 128 BS antennas serving 2 dual-antenna users. The measurements are recorded in an outdoor venue. The standard deviation of the average power across the arrays is used as a measure of the hardening of the channel. The results are presented for an increasing number of BS antennas (i.e. increasing the aperture of the array) and the different arrays and scenarios are also compared. The channel vector orthogonality is presented for specific distances between the users together with its impact to the matched filter capacity. Finally, to study the dimension of the subspace of the signal, we present the power profile of the eigenvalues for several measured scenarios, and the beamforming angle-of-arrival.

Main results

The results presented in this publication show the increase of the channel hardening effect when increasing the number of BS antennas with similar power. However, increasing the number of antennas with high power is detrimental for the channel hardening. They also show that larger aperture arrays achieve larger hardening due to better separated antennas and gathering more diversity. The results also show that in NLoS scenarios the distance between the users is determinant for the channel vector orthogonality. In LoS scenarios it is the beampattern of the array which influences the channel vector orthogonality. Finally, the profile of eigenvalues does not show a clear subspace occupied by the signal, but the angle-of-arrival shows energy scattered in all directions.

PAPER C: COPYRIGHT (PG. 66)

PAPER C: 3 CHANNEL HARDENING (PG. 70-73)

Fig. C.1: Base station array formed by 8 sets (sub-arrays) with 16 elements.

2.3 Channel sounder and normalization

The measurements were made with a correlation based channel sounder operating at 5.8 GHz and with a bandwidth of 100 MHz. The sounder measures a 8x16 MIMO channel fully in parallel in indoor-64 and 8x4 in outdoor-128, which is further extended by connecting the elements of each antenna set via a fast switch. During the measurements the 64x16 and 128x4 massive MIMO channels are sampled at a rate of 60 Hz during 20 s, for a total of 1200 channel realizations.

We use the Fourier Transform of the channel impulse responses obtained from the sounder and use the narrow band channel at the central frequency for analysis. We denote $\mathbf{h}_k(r) \in \mathbb{C}^{M \times 1}$ as the channel vector from user $k \in \{1, ..., 8\}$ in indoor-64 and $k \in \{1, 2\}$ in outdoor-128 to the BS array for channel realization $r \in \{1, ..., R\}$, where $R = 1200$ is the total number of channel realizations. $M = 64$ in indoor-64 and $M = 128$ in outdoor-128, is the number of BS elements. $h_{mk}(r)$ is the mth entry of the vector, corresponding to the mth element of the BS array.

The channel vectors are normalized as follows:

$$\overline{\mathbf{h}}_k(r) = \frac{\mathbf{h}_k(r)}{\sqrt{\sum_{r=1}^{R} \|\mathbf{h}_k(r)\|^2}} \sqrt{MR} \tag{C.1}$$

where $\|\cdot\|$ is the euclidean norm. This normalization creates a virtual power gain control that removes the user power imbalance but we keeps the differences among BS elements. We note that the average value of each channel coefficient is equal to 1.

3 Channel hardening

Firstly we analyze the channel hardening property of the massive MIMO system in our measurements as a function of the number of antennas at the BS. The metric of interest is the sum of the channel power over the antennas for one given snapshot. This corresponds to a post-processing by matched filtering. We show the standard deviation over realizations of the average power per antenna.

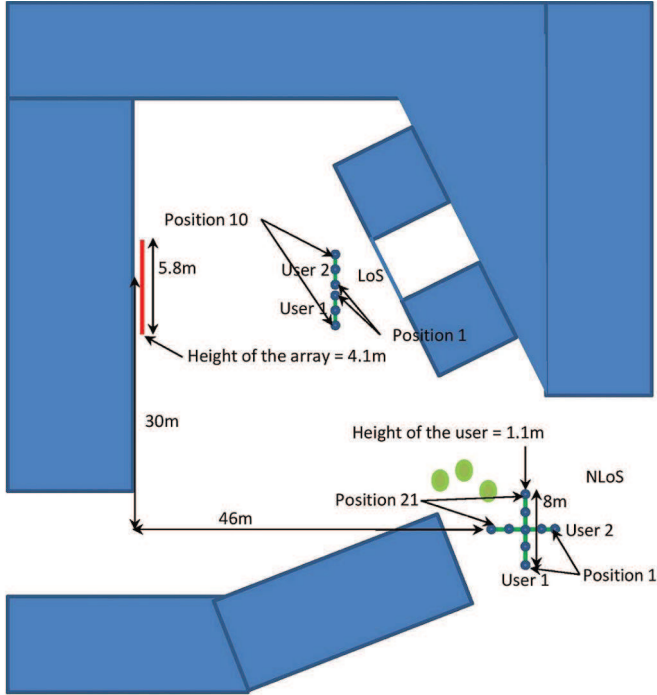**Fig. C.2:** 2 users in a NLOS scenario holding a 2 antennas mockup.

Fig. C.3: Floor map of the courtyard. Showing the positions of the users in orthogonal lines. Each lines has 21 positions.

For a selected subset of M' antennas, we compute the average power per

antenna for user k and snapshot r as:

$$\overline{P}_k(r) = \frac{1}{M'} \sum_{m=1}^{M'} |h_{mk}(r)|^2 \qquad (C.2)$$

The standard deviation is computed over the R realizations of the channel as

$$Std_k = \sqrt{\frac{1}{R}\sum_{r=1}^{R}(\overline{P}_k(r) - \mu)^2} \qquad (C.3)$$

where $\mu = \frac{1}{R}\sum_{r=1}^{R}\overline{P}_k(r)$ is the mean power over the snapshots.

We distinguish two situations. First, the power variations across the array are removed using C.4. Second, the power variations across the array are maintained using the normalization described in C.1.

In order to remove the power variations across the array the channel coefficient is normalized as follows:

$$\overline{h}_{mk}(r) = \frac{h_{mk}(r)}{\sqrt{\sum_{r=1}^{R}|h_{mk}(r)|^2}}\sqrt{R} \qquad (C.4)$$

where $|\cdot|$ is the absolute value. This normalization creates a virtual power gain control that removes the user power imbalance and the differences among BS elements.

Fig. C.4 shows the results of the std for both normalizations in the NLoS scenario and user 1 antenna b in the first position. The antennas are selected in a consecutive order starting from the right side of the array in Fig. C.1. In addition the power of each antenna averaged over the channel realizations is presented. We observe that the channel hardening is affected by two factors. Adding more antennas with similar power reduces the std and adding more antennas with higher power increases the std. The first is a consequence of the law of large numbers and it contributes to the channel hardening of the massive MIMO channel. However, due to the large aperture of the massive MIMO arrays large power variations are observed across the array. These power variations can be detrimental for the channel hardening.

In Fig. C.4 we see a decrease of the std for the first 16 antennas because their power is similar. The large power of the antennas 16 to 40 increases the std, which decreases after antenna 60 because the power of the antennas is reduced again. These effects are reduced in the std after removing the power variations across the array using the normalization presented in C.4.

In the following we keep the power variations across the array using equation E.1. In order to have more representative results, the std is averaged over all the positions of the subset of M' consecutive antennas over the array, and all the user elements.

Fig. C.5 shows the results in the LOS and NLOS scenario of outdoor-128. We compare the results with an independent identically distributed Gaussian

random channel with same average power (named Gaussian in the figure). We observe that the variation of the average channel energy decreases when increasing the number of base station antennas. Those measurements show a channel hardening in measured massive MIMO channels, but the measured hardening is not as strong as in the Gaussian channel.

We observe similar results in the slopes LOS and NLOS scenarios. These results are similar for other positions of the users.

In NLOS the standard deviation is consistently larger than the LOS case, i.e., the hardening is less than in the LOS environment. This is possible since not only the LOS component is reduced but also the distribution of the other components arriving via scattering is changed. Although the LOS component is blocked in the measured NLOS scenario, the main part of the energy is still expected from a few directions with relatively strong components, and thus not like the ideal Gaussian channel.

One way to define the hardening is as the ratio of the standard deviation obtained with a single antenna to the standard deviation obtained with 128 elements. With this definition the hardening for the simulated Gaussian case is about 21 dB while it is about 6 dB for the measured LOS and NLOS channels. While the difference between the simulated and measured channels is more than 10 dB, the observed hardening is still significant.

As a conclusion, from our measurements, we have observed a channel hardening as the number of antennas increases. The hardening slope is weaker than in the Gaussian channel case and can result in a significant gap in the standard deviation of the average power per antenna. We also observed the two factors influencing the hardening: Adding more antennas with the same power reduces the std, and adding more antennas with higher power increases the std.

4 User decorrelation

We focus on the scalar product of the channel vectors of 2 users with specific separation, defined for snapshot r as

$$SP(r) = \frac{\left| \overline{\mathbf{h}}_1(r)^H \overline{\mathbf{h}}_2(r) \right|}{\left\| \overline{\mathbf{h}}_1(r) \right\| \left\| \overline{\mathbf{h}}_2(r) \right\|} \tag{C.5}$$

where $|\cdot|$ is the absolute value, and the superscript H denotes the conjugate transpose. We show the average value of $SP(r)$ over the different snapshots of a same measurement.

Fig. C.6 shows the result in the NLOS scenario for different numbers of antennas. The antennas are chosen in a consecutive order from the first antenna in the left side of the array. Looking at the maximum number of base
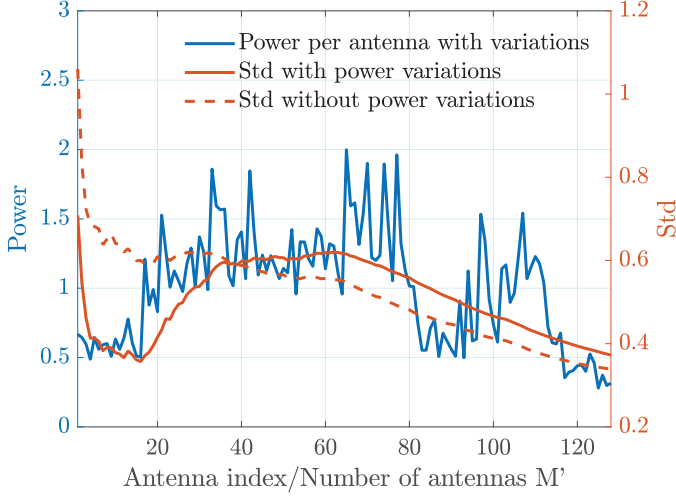
Fig. C.4: Power of each antenna averaged over realizations. Std over realization of the average power in the subset of antennas, with and without removing the power variations across the array. NLoS Scenario, with User 1 antenna b in the first position.
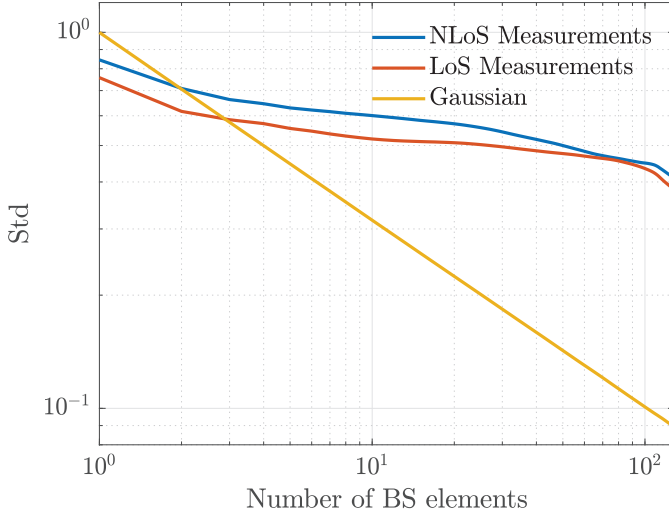
Fig. C.5: Std over realization of the average power in the subset of antennas, without removing the power variations across the array. NLoS and LoS scenarios.

station antennas (i.e. 128 antennas) we observe that the closer the users are, the larger the scalar product is. The decorrelation distance can be obtained for a target correlation. For a correlation of 0.25, the decorrelation distance is approximately 65 cm (12 times the wavelength). For a smaller number of

PAPER C: CONCLUSIONS (PG. 77)

6   Conclusion

Two measurement campaigns are used to investigate three prominent properties of massive MIMO channels: channel hardening, user decorrelation and channel angular spread. The first measurement campaign involves a 64-antenna base station and the second ones involves a 128-antenna base station. The measurements show a channel hardening for both LOS and NLOS scenario brought by massive MIMO, but that can be significantly weaker than in the Gaussian channel case. We observed the benefits of having more antennas with similar power, and the drawback of adding high power antennas. Correlation properties are different in both LOS and NLOS. In LOS, correlation is determined by the angular resolution of the array and its ability to separate the users spatially. In NLOS, the measurements suggest common paths or clusters that cannot be resolved by the array, when the users are in close proximity. Finally, in a rich indoor scattering environment, the channel appears to occupy a large part of the angular space defined by the massive array.

References

[1] A. Osseiran, J. F. Monserrat, and P. Marsch, *5G Mobile and Wireless Communications Technology*, 1st ed.   Cambridge University Press, 2016.

[2] T. L. Marzetta, "Noncooperative cellular wireless with unlimited numbers of base station antennas," *IEEE Transactions on Wireless Communications*, vol. 9, no. 11, pp. 3590–3600, 2010.

[3] F. Rusek, D. Persson, B. K. Lau, E. G. Larsson, T. L. Marzetta, O. Edfors, and F. Tufvesson, "Scaling Up MIMO: Opportunities and Challenges with Very Large Arrays," *IEEE Signal Processing Magazine*, vol. 13, no. 1, pp. 40–60, 2013.

[4] E. G. Larsson, O. Edfors, F. Tufvesson, and T. L. Marzetta, "Massive MIMO for Next Generation Wireless Systems," *IEEE Communications Magazine*, vol. 52, no. 2, pp. 186–195, 2014.

[5] A. Adhikary, J. Nam, J.-Y. Ahn, and G. Caire, "Joint Spatial Division and Multiplexing," *IEEE Transactions on information theory*, vol. 59, no. 10, pp. 6441–6463, 2013.

[6] H. Yin, L. Cottatellucci, D. Gesbert, R. R. Muller, and G. He, "Pilot decontamination using combined angular and amplitude based projections in massive MIMO systems," in *2015 IEEE 16th International Workshop on*

PAPER E: 4 CHANNEL HARDENING (PG. 110-116)

Fig. E.5: BS array with 8 sets of 16 elements

estimated to be 27 dB and 20 dB for the 64-mMIMO and 128-mMIMO respectively with a 5 percentile of 13 dB and 6 dB respectively.

3.2 Narrowband channel and Normalization

We focus on the analysis of a narrow band channel obtained via Fourier transform of the measured impulse responses. We disregard all the frequencies except the central one with a bandwidth of 2 MHz. We denote $\mathbf{h}_k^{(n)}(r) \in \mathbb{C}^{M \times 1}$ as the channel vector from antenna $n \in \{a, b\}$ in the handset of user $k \in \{1, ..., 8\}$ in 64-mMIMO and $k \in \{1, 2\}$ in 128-mMIMO to the BS array at channel realization $r \in \{1, ..., R\}$, where $R = 1200$. $M = 64$ in 64-mMIMO and $M = 128$ in 128-mMIMO is the number of BS elements. $h_{mk}^{(n)}(r)$ is the mth entry of the vector, corresponding to the mth element of the BS array. We call $\mathbf{H}(r) \in \mathbb{C}^{M \times KN}$ the full 64×16 channel matrix in 64-mMIMO and 128×4 in 128-mMIMO. $K = 8$ is the number of users in 64-mMIMO and $K = 2$ in 128-mMIMO, $N = 2$ is the number of antennas per user. The two channel vectors of user k at realization r are placed in two consecutive columns of $\mathbf{H}(r)$.

Normalizing the channel we create a virtual power gain control, where the received energy from each user antenna is normalized as:

$$\overline{\mathbf{h}}_k^{(n)}(r) = \frac{\mathbf{h}_k^{(n)}(r)}{\sqrt{\sum_{r=1}^{R} \left\| \mathbf{h}_k^{(n)}(r) \right\|^2}} \sqrt{MR} \tag{E.1}$$

where $\|\cdot\|$ is the Euclidean norm.

With this normalization, we remove the user impact and handset antenna power imbalance but we keep the differences among BS elements. We denote $\overline{\mathbf{H}}(r) \in \mathbb{C}^{M \times KN}$ as the channel matrix made out of the normalized vectors in (E.1).

4 Channel hardening

One of the most promising features of massive MIMO is its capability to harden the channel. In other words, the fast fading is reduced and the noise is

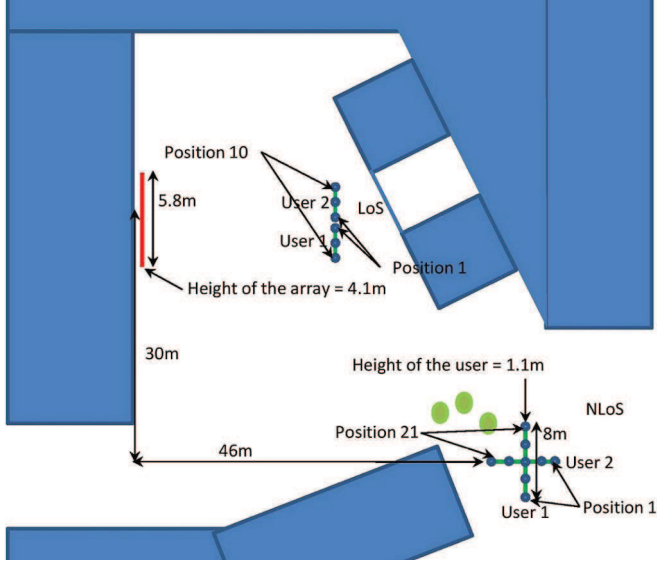**Fig. E.6:** Scenario in LoS and scenario in NLoS

Fig. E.7: 2 users holding the sticks to keep the separation constant

averaged out as a result of the law of large numbers [20]. Channel hardening allows to allocate resources in a longer time period, since the fast variations of the channel vanishes. In addition, the signal power of each user is more stable, so the outage probability is reduced.

4.1 Standard deviation of the mean power

To study the channel hardening effect, we compute the standard deviation of the mean power across the antennas of the BS array. The mean power is

$$\overline{P}_k^{(n)}(r) = \frac{1}{M'} \sum_{m=1}^{M'} \left| \overline{h}_{mk}^{(n)}(r) \right|^2 \tag{E.2}$$

where M' is the selected number of BS elements. The standard deviation is computed over the R realizations of the channel as

$$Std_k^{(n)} = \sqrt{ \frac{\sum_{r=1}^{R} \left(\overline{P}_k^{(n)}(r) - \mu \right)^2}{R-1} } \tag{E.3}$$

where $\mu = \frac{1}{R} \sum_{r=1}^{R} \overline{P}_k^{(n)}(r)$ is the mean power over the realizations.

We distinguish two situations. First, the power variations across the array are removed using E.4. Second, the power variations across the array are maintained using the normalization described in E.1.

In order to remove the power variations across the array the channel coefficient is normalized as follows:

$$\overline{h}_{mk}(r) = \frac{h_{mk}(r)}{\sqrt{\sum_{r=1}^{R} |h_{mk}(r)|^2}} \sqrt{R} \tag{E.4}$$

where $|\cdot|$ is the absolute value. This normalization creates a virtual power gain control that removes the user power imbalance and the differences among BS elements.

Fig. E.8 shows the results of the standard deviation for both normalizations in the NLoS scenario and user 1 antenna b in the first position. The antennas are selected in a consecutive order starting from the right side of the array in Fig. E.5. In addition the power of each antenna averaged over the channel realizations is presented. We observe that the channel hardening is affected by two factors. Adding more antennas with similar power reduces the standard deviation and adding more antennas with higher power increases the standard deviation. The first is a consequence of the law of large numbers and it contributes to the channel hardening of the massive MIMO channel. However, due to the large aperture of the massive MIMO arrays large power variations are observed across the array. These power variations can be detrimental for the channel hardening.

In Fig. E.8 we see a decrease of the standard deviation for the first 16 antennas because their power is similar. The large power of the antennas 16 to 40 increases the standard deviation, which decreases after antenna 60 because the power of the antennas is reduced again. These effects are reduced
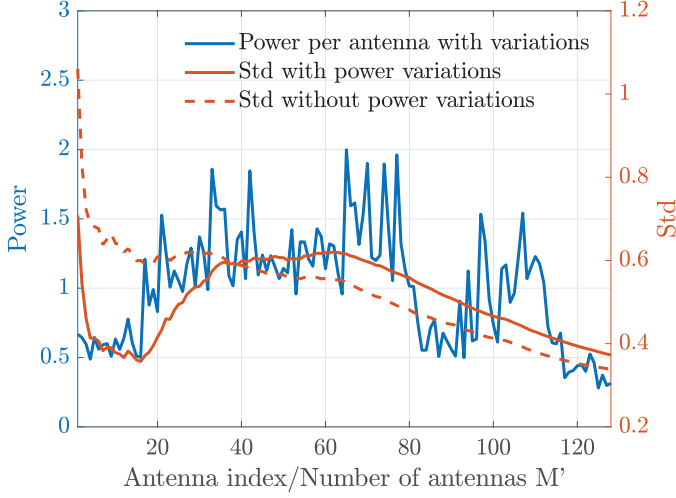
Fig. E.8: Power of each antenna averaged over realizations. Standard deviation over realization of the average power in the subset of antennas, with and without removing the power variations across the array. NLoS Scenario, with User 1 antenna b in the first position.

in the standard deviation after removing the power variations across the array using the normalization presented in E.4.

In the following we keep the power variations across the array using equation E.1. In order to have more representative results, the standard deviation is averaged over all the positions of the subset of M' consecutive antennas over the array, and all the user elements.

First we focus on 64-mMIMO. Fig. E.9 shows the standard deviation of the mean power in the S-LoS $\perp$ scenario. The results for a theoretical Gaussian channel are used as a reference model.

The results show a decrease of channel variations when increasing the number of BS antennas. The VLA has the most hardening effect, followed by the LA which in turn is better than the C2D array. When the aperture of the array increases some of the antennas become more separated, likely creating less correlated channels and more hardening. We observe a rising of the standard deviation when the number of BS antennas is very high. The reason is the effect of power variations across the array. Even if we averaged for different positions of the subset of antennas, for certain number of antennas M', the antennas in the middle of the array might be included more times in the subset than the antennas at the edges. However, when the number of antennas in the subset is small or large, all the antennas are included approximately the same number of times in the subset.

In order to have a broader view of the result, in Fig. E.10 we plot the same metric for the maximum number of elements in the BS array (i.e. 64
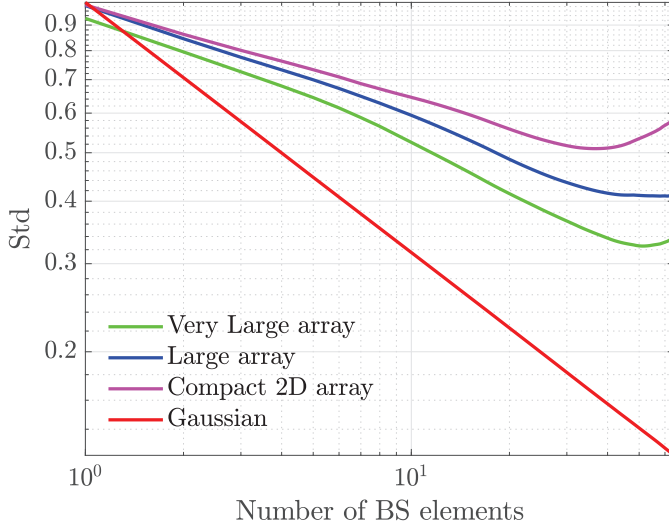
Fig. E.9: Standard deviation of the mean power, average over subarray position and users, S-LoS ⊥

antennas), taking the statistics across the 16 user antennas, for each array and scenario measured, which gives 16 samples per box. The boxplot shows the first and third quartiles as the bottom and top of the box, and the line inside the box is the second quartile (i.e. the median). The median of the 16 user antennas shows that for all the scenarios, except the S-NLoS, the VLA has the strongest channel hardening, followed by the LA which in turn is better than the C2D. Thus, the conclusions obtained in Fig. E.9 can be generalized in a statistical sense for most of the scenarios.

Second we focus on 128-mMIMO. We also keep the power variations across the array, and we average over all possible subsets of antennas and the different user antennas. Fig. E.11 shows the standard deviation of the mean power in both LoS and NLoS scenarios. The Gaussian channel is also plotted as a reference. The results show a hardening effect in the channel. The standard deviation is larger for the NLoS scenario than for the LoS one.

In order to quantify the hardening we look at the ratio of the mean standard deviation obtained with 1 antenna to the mean standard deviation obtained with 128 antennas. In the Gaussian channel the ratio is 21 dB, while in the LoS it is 6 dB and in the NLoS it is 10 dB. Even if there is certain difference between the Gaussian channel and the measured channels, the measured hardening is still significant.

In order to generalize the results, we look at the statistics over users and their positions. In Fig. E.12 we show the same metric for 128 BS antennas taking the statistics over the 4 user antennas and all the measured positions
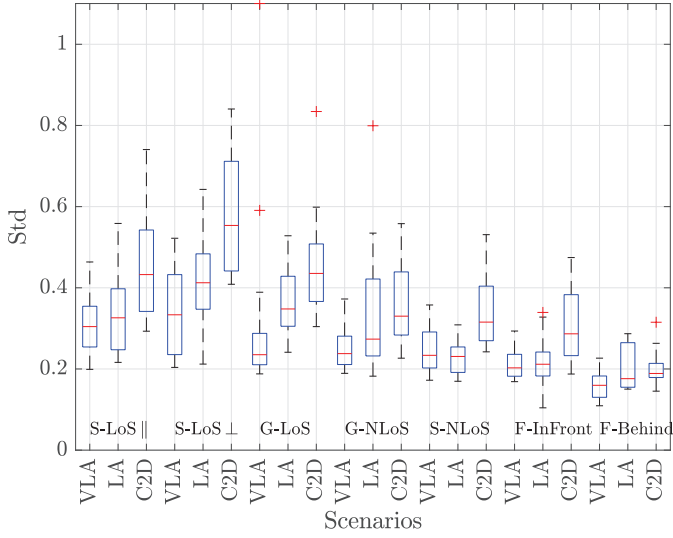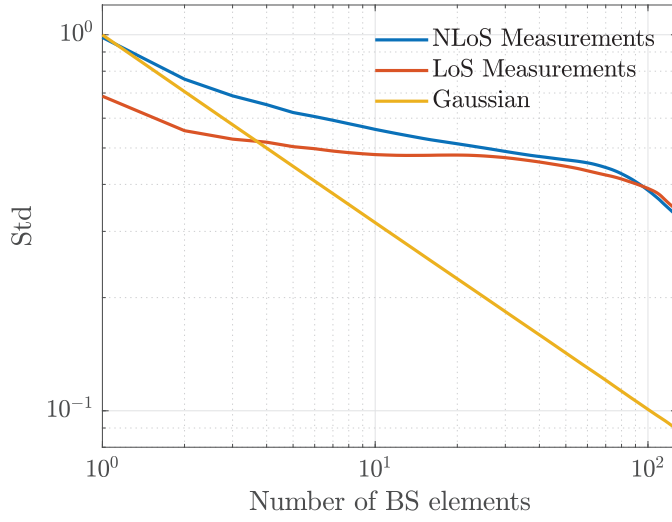
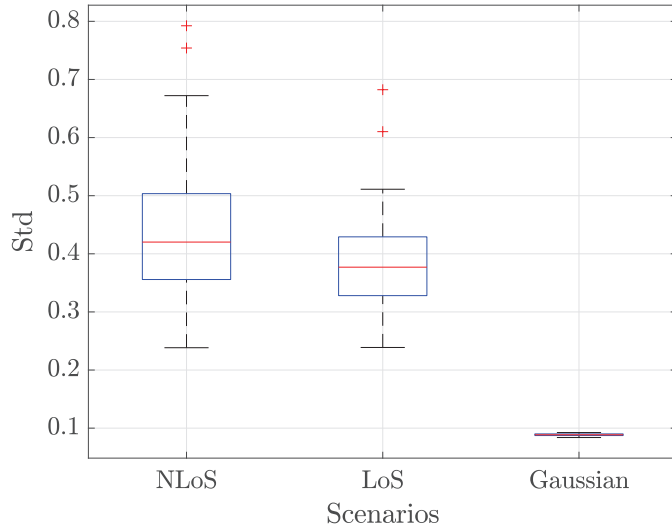**Fig. E.10:** Boxplot of the standard deviation of the mean power with 64 BS antennas, all the scenarios

of the users, which gives 84 samples for the NLoS scenario and the Gaussian channel boxes, and 40 samples for the LoS scenario box. We observe that the measured channels show a larger dispersion compared with the Gaussian channel as it is expected due to variation in the surroundings, hand grip, etc. We also observe the stronger hardening in the LoS scenario compared with the NLoS scenario. The NLoS scenario in some cases achieve as much hardening as the LoS but the median and the inter-quartile range is smaller for the LoS scenario.

In order to understand the degree of scattering in the measurements we use the method of moments to calculate the Rician K factor [21]. Computing the statistics for all the antenna links, and distances between users, the 10 and 90 percentiles and the mean are: $-0.8\,$dB, $8.2\,$dB, $4.1\,$dB, respectively for the LoS Parallel scenario and $-3.1\,$dB, $7.1\,$dB, $2\,$dB for the NLoS scenario. Note the method of moments K factor estimation is known to be poor for low SNR [22]. Hence, a small fraction of clearly erroneous results were omitted from the statistics.

As a conclusion, we observe the channel hardening effect when the number of BS antennas increases, but not as strong as the Gaussian channel. We distinguish two effects that impact the channel hardening. To increase the number of antennas in the array with similar power, increases the hardening. However, increasing the number of antennas with high power reduces the hardening. We also showed the improvement brought by increasing the aperture of the array, and the impact of the LoS or NLoS scenarios.
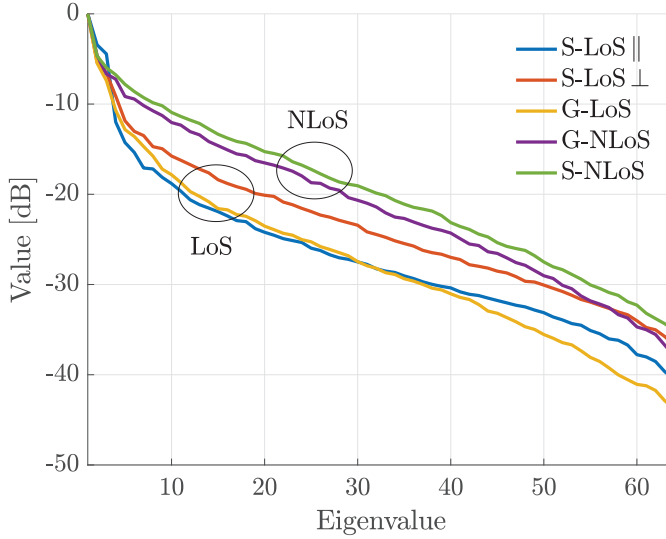
Fig. E.11: Standard deviation of the mean power, average over subarray position and users, NLoS 0.57m and LoS 0.6m between users

Fig. E.12: Boxplot of the standard deviation of the mean power with 128 BS antennas

5 Multi-user orthogonality and Sum-Rate

PAPER E: CONCLUSIONS (PG.121-123)

Fig. E.18: Normalized eigenvalues profile, User 1 antenna a, C2D, all scenarios with user

For the LoS scenarios the total energy is generally concentrated on fewer eigenvalues, compared to the NLOS scenarios. For example a level of $-15\,\mathrm{dB}$ is reached at about 10 eigenvalues or less for the LoS scenarios, whereas about 20 eigenvalues are needed to reach that level in the NLoS scenarios. However, all the profiles are decaying smoothly, so that determining the rank of the spatial covariance matrix effectively depends on the choice of threshold.

The smoothness of the curves can be attributed to limitations of practical measurements such as the limited number of measurements, a degree of non-stationarity of the channel, and inevitable imperfections like noise and spurious signals.

Insight into the channel rank properties can also be gained by analysing angle of arraivals. Fig. E.19 shows average beamforming spectra (Hamming weighted) obtained with the LA, Set 3 in both LoS and NLoS with different users. While it is possible to identify a main angle of arrival for the case of a nearby LOS user, it is also clear that the distribution over angle is much more even in the NLOS scenarios, as expected from the eigenvalue distributions in Fig. E.18. Even if the users have a dominant path, we observe energy scattered in other angles, as also reported in [3, 5].

7   Conclusion

This paper investigates three major characteristics of massive MIMO channels that are widely accepted and used in most of the theoretical studies, but they
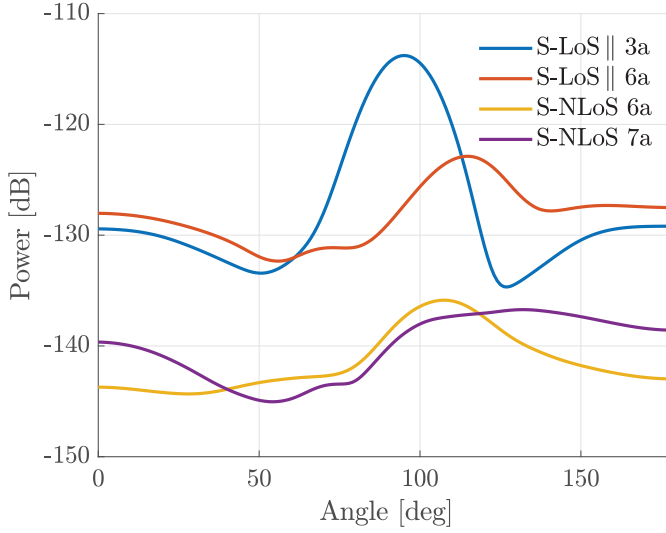
Fig. E.19: Beamforming angle of arrival averaged over channel realizations, Large Array, set 3

have, to the best of our knowledge, never been verified in measured propagation channels. These characteristics are the channel hardening in terms of mean power across the array, user orthogonality for specific distances between users and the rank of the spatial covariance matrix.

The presented results show the channel hardening effect of the massive MIMO channels. The study shows how the standard deviation of the mean power across the BS array decreases when the number of elements of similar power in the array increases, but not when the new antennas have high power. We also show the stronger hardening brought by increasing the aperture of the array.

This study also shows the sum-rate of the matched filter precoder of two users separated certain distances. The results show that in NLoS scenarios, the sum-rate decreases when the users are close to each other. In LoS scenarios the sum-rate depends on the exact position of the users respect to the beam created by the array. It makes clear the importance of taking into account the distance between users to model the system.

Finally in the study on the rank of the spatial covariance matrix, the profile of eigenvalues of the covariance matrix does not show a clear group of effective eigenvalues. Looking at the angle-of-arrival of the signal it is clear the energy is scattered in multiple directions, except in LoS with users very close to the BS array.

CHARACTERISATION AND MODELLING OF MEASURED MASSIVE MIMO CHANNELS

BY
ÀLEX OLIVERAS MARTÍNEZ

DISSERTATION SUBMITTED 2017

Characterisation and Modelling of Measured Massive MIMO Channels

Ph.D. Dissertation

Àlex Oliveras Martínez

Dissertation submitted December 18, 2017

Abstract

Massive MIMO is defined as a cellular system comprising a very large number of antennas at the base station serving multiple users in the same time-frequency resource. Theoretical studies attribute great benefits to this technology, for example high spectral efficiency, low probability of error and energy efficiency. However, the channel models used to study the performance of massive MIMO are over simplified and might not represent the reality.

This thesis presents the analysis of measured massive MIMO channels in order to better understand its characteristics and their impact into real implementations. The measurements used in this thesis are highly realistic. New deployment scenarios for the 5G are studied, similar to shopping malls and outdoor concert venues, both in LoS and NLoS. The measurements involve multiple dynamic users holding a two-antennas mockup handset and they are allowed to have their own handgrip.

The study of this measured channels brings insight on characteristics that can be exploited by signal processing techniques or they can be use to create better channel models. For example the degree of multi-user multiplexing that the channel offers, the orthogonality of the channel vectors of different users, the conditioning of the channel for two antennas in the same handset, etc. The thesis has a strong focus on the impact of the aperture of the array. Finally this thesis proposes some topics to modify in WINNER-type channel models to adapt them to massive MIMO channels.

Resumé

Massive MIMO defineres som et cellulært system med et meget stort antal antenner på basisstationen og som på samme tid servicerer flere brugere på samme tid og på samme frekvens. Teoretiske studier tillægger denne teknologi mange gode egenskaber, såsom stor spektral effektivitet, lav fejlsandsynlighed og stor energieffektivitet. Kanalmodellerne som er blevet brugt til disse studier er dog oversimplificerede og repræsenterer måske ikke virkeligheden tilstrækkeligt godt.

Denne afhandling præsenterer en analyse af målte massive MIMO kanaler med henblik på en bedre forståelse af kanalens karakteristika og påvirkning af faktiske implementeringer. Målingerne som bruges i denne afhandling er opnået under meget realistiske forhold. De nye udrulningsscenarier for 5G studeres, som ligner indkøbscentre og udendørs koncertspillesteder, i line of sight (LOS) såvel som non line of sight (NLOS) betingelser. Målingerne involverer flere brugere i bevægelse, hver med en håndset model med to antenner, som holdes i hånden på en måde valgt af den enkelte bruger.

Studiet af de målte kanaler giver indsigt i karakteristika som kan udnyttes med signalprocesseringsteknikker eller kan bruges til at skabe bedre kanalmodeller. Eksempelvis graden af multi-bruger multipleksing som kanalen muliggør, orthogonaliteten af kanalvektorerne svarende til de forskellige brugere, kanalbetingelserne for to antenner i samme håndset, etc. Afhandlingen har kraftigt fokus på indvirkningen af arrayets apertur. Afslutningsvis gives ændringsforslag til kanalmodeller af WINNER-typen med henblik på tilpasning til massive MIMO kanaler.

Contents

Contents

Contents

Contents

Thesis Details

Thesis title:	Characterisation and Modelling of Measured Massive MIMO Channels
PhD Student:	Àlex Oliveras Martínez
PhD Supervisor:	Assoc. Prof. Elisabeth De Carvalho, Aalborg University
PhD Co-supervisor:	Prof. Petar Popovski, Aalborg University

The main body of this thesis consists of the following papers.

[F] *Accepted:* À. O. Martínez, P. Popovski, J. Ø. Nielsen, E. De Carvalho, "Experimental Study of the Benefits of a Second Antenna at the User Side in a Massive MIMO System," Accepted by IEEE Access.

[D] *Submitted:* À. O. Martínez, E. De Carvalho, J. Ø. Nielsen, "Impact of Array Aperture in Massive MIMO: a Measurement based Study," Submitted to IEEE Transactions on Antennas and Propagation.

[E] *Under major revision:* À. O. Martínez, J. Ø. Nielsen, E. De Carvalho, P. Popovski, "An Experimental Study of Massive MIMO Properties in 5G Scenarios," Submitted to IEEE Transactions on Antennas and Propagation.

[C] *Published:* À. O. Martínez, E. De Carvalho, J. Ø. Nielsen, "Massive MIMO Properties based on Measured Channels: Channel Hardening, User Decorrelation and Channel Sparsity," Asilomar, November 2016.

[G] *Published:* À. O. Martínez, P. Eggers, E. De Carvalho, "Geometry-Based Stochastic Channel Models for 5G: Extending Key Features for Massive MIMO," PIMRC, September 2016.

[B] *Published:* À. O. Martínez, E. De Carvalho, J. Ø. Nielsen, J. Lishuai, "Frequency Dependence of Measured Massive MIMO Channel Properties," VTC, May 2016.

[A] *Published:* À. O. Martínez, E. De Carvalho, J. Ø. Nielsen, "Towards Very Large Aperture Massive MIMO: a measurement based study," Globecom Workshop, December 2014.

In addition to the main papers, the following publications have also been made.

[6] *Published:* L. Jing, E. De Carvalho, P. Popovski, À. O. Martínez, "Design and Performance Analysis of Non-Coherent Detection Systems with Massive Receiver Arrays," Transactions on Signal Processing, IEEE, 2016.

[5] *Published:* W. Fan, P. Kyösti, J. Nuutinen, À. O. Martínez, J.Ø. Nielsen, G. F. Pedersen, "Generating Spatial Channel Models in Multi-probe Anechoic Chamber Setups," VTC, May 2016.

[4] *Technical report:* À. O. Martínez, E. De Carvalho, P. Eggers, "Modeling and Characterization of the Massive MIMO Channel," Cooperation project Huawei - AAU, Technical Report M9-M12, October 2015.

[3] *Technical report:* À. O. Martínez, E. De Carvalho, P. Eggers, "Modeling of the Massive MIMO Wireless Backhaul Channel," Cooperation project Huawei - AAU, Technical Report M7-M8, June 2015.

[2] *Technical report:* À. O. Martínez, L. Jing, E. De Carvalho, P. Eggers, "Modeling and Characterization of the Massive MIMO Channel," Cooperation project Huawei - AAU, Technical Report M1-M6, April 2015.

[1] *Published:* À. O. Martínez, E. De Carvalho, P. Popovski, G. F. Pedersen, "Energy detection using very large antenna array receivers," Asilomar, November 2014.

Preface

During the course of this Ph.D. I realized that research is an endless process. Like the Darwinian theory of biological evolution each step is build on a chain of previous achievements. As it happens with species, the branches of knowledge evolve. Sometimes a branch in the tree of knowledge extinguishes because it is not relevant for the current state of society and sometimes an innovative idea starts a new branch like it happened with massive MIMO. Different topics might merge together, or results obtained in one field can be used in another one. Altogether, is our duty as researchers to keep the constant evolution of knowledge.

I also realized that constant learning and effort is necessary to keep improving the tree of knowledge. And it is this effort that also evolves the researcher, and makes him a better person. During the Ph.D. several qualities of the researcher are developed, for example: perseverance, determination, patience, efficiency. Researcher and knowledge evolve together fuelled by the same effort.

However, now a days, research is not done alone as in Darwin's time. During the three years of my Ph.D. I had the support of numerous people, and here I would like to mention them. The research in this thesis was supervised by Elisabeth de Carvalho and co-supervised by Petar Popovski. I highly appreciate the contribution of Jesper Ødum Nielsen with his expertise and good advise. Finally, I would like to express my gratitude to my family and friends for their support.

Àlex Oliveras Martínez
Aalborg University, December 18, 2017

Preface

Part I

Introduction

Introduction

1 Background

1.1 From MIMO to massive MIMO

Massive Multiple-Input Multiple-Output (MIMO) was concived as a cellular communications system with base stations (BS) comprising a large number of antennas serving a smaller number of single-antenna users in the same time-frequency resource [48]. Such amount of antennas renders an excess of degrees of freedom (DoF) in the channel that can be exploited to increase the throughput, reliability and energy efficiency of the communications channel [56]. In this system, simple linear precoding techniques achieve close to optimal performances [51]. In addition, the extra DoF can be utilized to mitigate the hardware impairments, so low-cost low-precision components can be used in massive MIMO systems [6]. Massive MIMO is an evolution of MIMO techniques and it establishes a new course for wireless communications. The benefits of massive MIMO makes it a promising technology for the fifth generation (5G) of cellular networks [9].

The physical world offers several resources that can be exploited by wireless communications systems to transmit information from one point to another. Traditionally only time and frequency were used as a medium to transmit independent streams of information. With antenna arrays a new dimension could be used: space. Using MIMO techniques, multiple antennas can be used to transmit multiple data streams in the same time-frequency resource using the spatial dimension of the channel [16]. Signal processing combines the signals of each antenna in the proper way to increase the amount of transmitted information or reduce the probability of error. The large number of BS antennas in massive MIMO offers a new set of advantages. Increasing the number of BS antennas permits to better exploit the characteristics of the space dimension of the channel. However, the throughput of the system not only depends on the number of antennas, but also on the DoF offered by the physical environment. The angular spread of the signal and the aperture of the BS array are fundamental factors that influence the DoF. In order to have

3

a better insight on the implications of the environment in the performance of the communications systems it is necessary to study the properties of the channel matrix.

1.2   Favorable propagation

Traditional MIMO has a small number of BS antennas that, even if it is an improvement from single-input single-output (SISO) systems, has some drawbacks.

One of the most remarkable drawbacks of MIMO systems is the inter-user interference. If the channel vector of two users is similar to each other some of the information transmitted to one user is received by the other user, which causes interference and harms the communication. Here, channel vector refers to the set of phasors describing the propagation (attenuation and phase shift) from the BS antennas to each user. It is also called spatial signature since it is strictly related to the position of the user in relation to the BS and the physical environment.

Evolving from MIMO to massive MIMO permits to reduce the inter-user interference. The reason is that the large number of BS antennas makes the channel vectors longer. In random matrix theory, using models with independent identically distributed (i.i.d.) complex Gaussian entries, when increasing the length of the vectors the scalar product between different vectors grows at lesser rate than the scalar product of a vector with itself, therefore the correlation between channel vectors asymptotically vanishes [48]. In other words, the diagonal elements of the Gramian of the channel matrix grow faster than the off-diagonal elements when the number of BS antennas grows.

The propagation channels can be very different from the simplified models and not always massive MIMO channels will have i.i.d. complex Gaussian entries. The channel condition to achieve mutual orthogonality between channel vectors is called favorable propagation [50] and it highly depends on the BS array and the physical environment.

Increasing the aperture of the array is a key factor to achieve favorable propagation. When increasing the number of antennas with a fixed aperture of the array the asymptotic orthogonality of the channel vectors of the user saturates [49]. In this fixed aperture scenarios the energy efficiency also saturates and it can not be improved by increasing the number of antennas [4, 5].

Channel measurements are necessary to better understand the conditions that make favorable propagation possible. The Gramian matrix in indoor scenarios and with different array shapes is studied in Paper A, Paper B, and Paper D. The study of the Gramian of measured channels also helps to assess the accuracy of simplified i.i.d. Gaussian models.

1.3 User Multiplexing

Massive MIMO is conceived as a multi-user MIMO system. The main difference with a single-user MIMO system is that the users are physically separated and they can not code or decode the information jointly [52]. This means that the processing has to be done at the BS. However, most of the benefits of single-user MIMO can be obtained in multi-user scenarios. Multi-user MIMO allows to transmit independent data streams to the different users, and increase the sum-rate of the system. In single-user systems, the DoF achieved by having multiple antennas at the BS are used to increase the user rates or the reliability. Instead, in multi-user systems, the DoF are used for the spatial separation of the users, so they can be served in the same time frequency rescourse [27]. Massive MIMO enhances the benefits of MIMO technologies to transmit multiple data streams simultaneously in the same time-frequency resource. The use of multiple antennas at the BS allows to focus the signal into specific regions of the space, where the intended user is located, and reduce the signal energy in other regions, to avoid interfering with other users. With massive MIMO, the signal can be focused in smaller portions of space, which brings larger gains in the throughput of the system.

To control the direction of the transmitted signal, MIMO takes advantage of the constructive and destructive patterns when adding the multiple waves from different antennas. Setting the proper weight and phase in each transmit antenna allows to control where the signals add up constructively and where destructively. Precoders are designed to fulfil this function, and they rely on proper estimation of the channel to succeed in their task.

Channel estimation in MIMO systems is achieved by transmitting pilot signals during a training period. A feedback of the estimated channel is sent to the transmitter. If the channel is reciprocal in the uplink and downlink, the estimated channel can be used in both directions, which avoids to estimate the channels twice. This is what happens in time division duplexing (TDD), where the uplink and downlink are allocated in the same frequency. This is particularly interesting in massive MIMO since the large number of BS antennas makes it infeasible to transmit orthogonal pilot signals in the downlink. Nevertheless, most of the existing communications systems work in frequency division duplexing (FDD), so the adoption of massive MIMO would be easier if it could be used in FDD [8]. Even if some advances have been made towards FDD massive MIMO, this is still an open research topic.

Precoders modify the transmitted signal in order to produce the desired constructive/destructive addition of the waves. Each precoder is designed to achieve a different goal. Linear precoders are recognized by their simplicity, however they suffer from inter-user interference. With the channel orthogonality brought by massive MIMO, these precoders become nearly optimal [38].

The user multiplexing not only depends on the precoders and the number of antennas. The physical environment has a big impact on allowing the antennas to separate the different data streams. We talk about the conditioning of the channel matrix. The rank of the channel matrix represent the number of independent data streams that can be transmitted through the channel [59]. However, not all data streams can support the same amount of data. A singular value decomposition of the channel permits to to represent it as multiple independent sub-channels and the squared of the singular value describes the received power in that sub-channel [1]. Therefore, the rank of the channel, as the number of independent data streams is not representative of the quality of the channel. Another metric like the normalized parallel channel gain (NPCG), which is a normalized sum of eigenvalues, can be more representative of the multiplexing potencial of the channel [12]. This metric is used in Paper A, Paper B, and Paper D and it is a better representation of the multi-user multiplexing gain of the channel, compared to the rank, because each sub-channel is weighted by its corresponding eigenvalue.

1.4   Users with multiple antennas

In single-antenna users scenarios massive MIMO rely on having multiple users to transmit them independent data streams and increase the sum-rate of the system. However, multiple antennas in the same user handset can be exploited to achieve higher data rates to each individual user. In 1.3 we explained how independent data streams can be transmitted to different users. The same principle can be applied in order to transmit multiple data streams to a single user. Nevertheless, the situation is more challenging because the antennas belonging to the same user are confined in a very small space yielding to high correlation. Therefore, in traditional MIMO, if there are enough users in the system it is better to allocate a single data stream per user, since they are less correlated than multiple antennas in the same user [7]. The properties of massive MIMO decorrelating the channel vectors can have a big impact in this situation, and the channels of antennas in the same user's handset could become orthogonal.

The singular values of the channel matrix are affected by the orthogonality between the channel vectors. Completely orthogonal channels have equal singular values. Completely correlated channels have one singular value equal to zero. The condition number is the ratio between the largest eigenvalue and the smallest one. Studying the condition number, like in papers A, B, and D we observe the orthogonality between the channels.

The use of multiple antennas at the user side is of capital importance in near field scenarios. These scenarios are among the ones defined by METIS for the new 5G systems [36] and they are going to be common in massive MIMO deployments. In near field scenarios the plane wave assumption is

not valid any more and the channel has to be described by spherical waves. Studies using spherical waves show that even in LoS scenarios the spherical waves help to decorrelate the antennas of the user and boost the throughput [35].

Regarding the importance of having multiple antennas at the user side in order to increase the user's throughput, in the best of our knowledge, only one massive MIMO theoretical study considers such situation [43]. They conclude that multi-antenna users are beneficial in scenarios with small number of users.

1.5 Non-stationarities over the array

A unique characteristic of massive MIMO channels is the non-stationarities over the array. The large number of antennas can occupy tens of wavelengths, so different parts of the array see different environments. In other words, different antennas receive the signal from different scatterers, or the power of the signal from a scatterer varies along the array. The consequence is that the channel can not be considered wide sense stationary in the antenna domain. The traditional use of Toeplitz matrices to describe the fading and correlation of the channel like in [60] can not be applied to massive MIMO.

The non-stationarities over the array where first descrived in [53]. The results present large variations over the array of the small fading, channel gain and angular spectrum. The authors warn of its effects on channel modelling, simulations and theoretical analysis. Paper A shows the non-stationarities in terms of power variation across the array. This characteristic of massive MIMO could be detrimental for the communication since not all the BS antennas can exploit all the DoF of the channel. Nevertheless, with the right signal processing this characteristic could be exploited. For example, in very large aperture arrays, users can be served by sub-parts of the array, which can save energy by not using some radio frequency chains.

1.6 Channel hardenning

As a result of multipath propagation, the wireless communications experience variations in the power of the received signal. The phenomenon is known as fading. Low power of the signal, or deep fades, can occur sporadically, and it can harm the communication. In scattering rich environments, the fading occurs independently in the channel links, and some links can have a good signal power while others are in a deep fade. Diversity exploits the independence between links to combat fading [34]. However some environments can have correlated channel links that do not contribute to the use of diversity. The diversity order is the number of independent channel links.

Due to the law of large numbers the probability of having a small power

in the combination of received signals is reduced by increasing the number of independent channel links [59]. In massive MIMO, the large number of BS antennas helps to harvest these independent channel links, and therefore, the channel becomes less fluctuating. This effect is called "channel hardening" [31]. Papers C, and E study the channel hardening in measured channels.

The antenna array topology greatly influence the independence of the channel links which is crucial for the channel hardening. Unipolar antennas can have a large coherence distance (3λ to 30λ, where λ is the wave length) [52]. Arrays with antennas separated $\frac{\lambda}{2}$ can reduce the side lobes in the beam pattern, but the antennas are too close to capture diversity. A good compromise is to group the antennas separated $\frac{\lambda}{2}$ in sets, and separate the sets by a larger distance to gather more diversity [52]. This is the approach followed by the Very Large Aperture array presented in Paper A and used for a measured campaign analysed throughout this thesis.

1.7   Channel measurements

In the recent years massive MIMO has been extensively studied using theoretical channel models. These channels not always represent the reality in the proper way, especially for new systems like massive MIMO. For this reason it is necessary to have channel measurements to study practical implementations of massive MIMO, and also to develop more accurate channels models. In the following the existing massive MIMO measurement campaigns are reviewed in approximately chronological order, however sometimes the order is modified to group measurements with similarities.

The first report of massive MIMO channel measurements appear in [17], where a cylindrical array with 128 antenna ports is used in a residential environment. Several static positions are measured with two antennas mounted on a car, and later on the different positions are combined to emulate a multiuser environment. The publication studies the sum-rate of the system for several linear precoders, and it shows that the performance is similar to optimal precoders. A similar conclusion is presented in [32] where a semi-cylindrical array containing 112 elements is used at the BS side.

A prototype was designed to study the performance of massive MIMO using time division duplexing (TDD) [57, 58]. This test-bed uses 64 antennas at the BS and simultaneously serves 15 terminals. The results show the system capacity for several precoders. There is a clear improvement in capacity when the number of BS antennas increases, but a saturation effect appears close to 64 antennas. Increasing the number of users also increases the system capacity until the number of users is similar to the number of BS antennas, when the capacity decreases due to the high inter-user interference.

Due to the technical difficulties to perform simultaneous measurements with a large number of antenna ports, most of the massive MIMO measure-

ments use the virtual antennas technique. A single antenna measurement is performed for multiple positions of the antennas. Later, the measurements are combined to form a virtual antennas array. Although this technique simplifies the measurement's technical requirements, it has some limitations. A static environment, and fixed user positions, has to be guaranteed for all antenna positions, therefore it can only measure static users.

A clear example of virtual array measurement is reported in [53]. The 128 antennas virtual array is used to measure the massive MIMO channel in a courtyard. They observe angle-of-arrival variations across the array and near filed effects that can help to decorrelate the channel of different users. They present low correlation between users and hardening of channel's eigenvalues. They propose that an extension of COST2100 channel model could be used to model massive MIMO channels. Similar conclusions of non-stationarities in the angular and delay domains are presented in outdoor scenarios with a 64-antennas virtual array [13]. In the same measurements as [53], the linear precoders can avoid the inter-symbol interference (ISI) due to delay spread, better when increasing the number of BS antennas [54].

The two arrays used in [17] and [53] are compared in [24] where both the linear and cylindrical arrays are reported to reach above 80 % to 90 % of the ideal capacity performance. The same measurements are used to improve the sum-rate by selecting a subset of antennas when the number of RF chains is smaller than the number of antennas [18]. It shows that the average DPC capacity can be increased up to 50 % and 35 % for the cylindrical array and 15 % and 10 % for the linear array, with 20 and 40 RF chains respectively, when having 120 available antennas at the BS. An algorithm that choses the antennas with maximum receive power has similar performance to the convex optimization [20]. Other switch configurations can also be used, and the number of RF chains can be reduced without significant losses [21]. These measurements were also reported in [25] to show the deficiencies of the Kronecker and Toeplitz assumptions in the correlation of the channel matrix. Also analyzing the data from this measurement campaign, [19] observes the similitude, in terms of the channel matrix's singular value spread, between NLoS measured channels and Rayleigh channel models. The singular value spread is reduced by increasing the number of BS antennas, however in LoS channels the spread is significantly larger than Rayleigh models. Finally it reaffirms that in massive MIMO a large proportion of the DPC capacity can be achieved using linear precoders.

Some channel measurements have been performed in indoor scenarios with a 12×12 virtual rectangular array, where the power variations across the array can be about 4.5 dB [41]. They also show that the RMS delay spread is not following a Gaussian distribution like in outdoor scenarios. Finally they conclude that the capacity with equal power allocation saturates fast when increasing the number of antennas, but the DPC capacity has no saturation.

A major drawback of using virtual arrays is the need for a static environment, which prevents from measuring dynamic users. The measurement campaign at Aalborg University, first presented in Paper A and also studied in Paper B, C, D, E, F uses real arrays with 64 antennas measured quasi-simultaneously using a fast switching mechanism. This permits to have 8 dual-antenna dynamic users measured simultaneously. In addition this measurement campaign includes arrays in three different shapes. This is the first measurement with dual-antenna users, and with real arrays with multiple shapes in indoor environments.

Another measurement campaign comparing three different arrays both in indoor and outdoor scenarios is presented in [26]. They argue that the channel offers more diversity in the horizontal domain than the vertical domain, so the horizontal array has better decorrelation properties, followed by the planar array, and finally the vertical one.

A measurement campaign without virtual arrays, with dynamic users measured simultaneously is presented in [14]. The results show a small improvement by increasing the number of antennas from 64 to 128, however there is a benefit of using dual polarized antennas. It also reaffirms that linear precoders approaches DPC sum-rates, and it shows that with massive MIMO more users can be simultaneously scheduled.

Several measurement campaigns explored stadium locations since METIS defined them as new deployment scenarios in its vision on 5G [36]. For example, a study on the angular of departure is presented in [62] and the frequency correlation function is investigated in [46]. This latter observes different results for different methods and conclude that the hypothesis of uncorrelated scattering is not valid. The authors use the data from this measurement campaign together with the data of measurements in the same location but at a different frequency to argue that channel coefficients, Rice factor and rms delay spread are stationary at high frequencies, but not at low frequencies [45]. More measurements where performed at the same location but with an increased number of BS antennas [44]. This publication studies the large scale fading over the BS array, and it proposes to add to the massive MIMO modelling a matrix representing the large scale fading. It also explains that the components of this matrix can be derived geometrically according to the environment.

A massive MIMO measurement at three different frequencies, but at the same indoor location is presented in [39]. The measurements are obtained with a 64-antennas virtual array at 2 GHz, 4 GHz and 6 GHz. The publications compares pathloss, delay spread and coherence bandwidth for the three frequencies and it concludes that the channel parameters are independent from the carrier frequency.

The use of virtual antenna arrays is widly extended in massive MIMO measurements due to the technical difficulty to measure a large number of

channel links simultaneously. The results obtained using virtual arrays are usually assumed to be the same as if the antennas were real. However, only one publication compared virtual and real arrays [64], and it validated the use of virtual arrays. It concludes that the power delay profile and the angles of the main paths are similar in virtual arrays and arrays with antennas measured simultaneously.

The second measurement campaign at Aalborg University extends its system to include 128 BS antennas. It was first presented in C and later it was analysed in E. The location is outdoor to emulate large venues like outdoor concerts or other crowded events. There are two double-antenna users. The main characteristic that distinguishes this measurements from others is that the measurements are performed with specific distances between the users. These measurements are important in order to model the channel of two users consistently with their relative position.

More recent measurements exploit the antenna correlation at the BS in order to reduce the overhead of the channel estimation [15]. Short term and long term low-dimensional bases are used to represent the channel. The long term bases are valid for several seconds, while the short term bases become outdated after one coherence time. The publication studies a rank-p vector-scalar LMMSE channel estimator which performs close to a full rank estimator.

A massive MIMO test bed is presented in [65]. The system consists of 112 BS antennas and 12 user antennas. All the channel links are measured simultaneously. In [65] the user antennas are USRP that are placed in static positions. The indoor measurements show an increase of spectral efficiency when the number of BS antennas increases and the user antennas are placed in a line. When the user antennas are placed forming a circle, there is no improvement in the spectral efficiency beyond 64 BS antennas. The same result is observed for the number of transmitted data streams. The same measurements are analysed in another publication together with other indoor measurements with 22 user antennas [28]. The second measurement campaign uses a 4×32 patch antennas array. This publication reports the measure of a real-time uncoded capacity of $1.59\,\mathrm{Gbit\,s^{-1}}$ for 12 users, and it reports a successful transmission of 256QAM symbols to 22 users that would be equivalent to $2.91\,\mathrm{Gbit\,s^{-1}}$.

Distributed arrays is considered as an option to help decorrelating the users' spatial signatures [11]. Indoor measurements, as well as anechoic chamber measurements, were performed using two antenna arrays of 32 antennas each. The rectangular planar arrays where positioned together in the same plane, separated in the same plane, or in orthogonal planes. The results show that arrays in a same plane have bad performance separating users located in a line orthogonal to that plane. The reason is that the users have the same angle of arrival even if the distance to the arrays is different. To place

one of the arrays perpendicular to the other decorrelates the users better, because the users have different angles to one of the arrays. The improvement of distributed arrays is more visible in the anechoic chamber measurements because there are no scatters to help decorrelating the users.

An outdoor-to-indoor scenario is studied in [63]. The transmitter is on top of a building and the receiver is in the fourth floor of a higher building. The main goal of this publication is to study the delay spread using two different frequency bandwidths. The conclusion is that the delay spread is larger at 100 MHz than at 200 MHz.

A massive MIMO test bed with high user mobility is presented in [29]. The BS is equipped with 100 antennas and both low speed walking users, and cars up to $29 \, \mathrm{km \, h^{-1}}$ are measured. The singular value spread is higher in the high mobility channels, and it has more dispersion. The results also show the importance of placing the antennas in the horizontal domain instead of vertical one, due to the angular spread of the environment. However, antennas located in the vertical domain are necessary to reduce the inter-user interference.

An equation is derived to model the ratio between sum-rate capacity with completely orthogonal channels and sum-rate capacity with partially orthogonal channels [40]. The measurements use 64 virtual antennas in the horizontal domain or 32 virtual antennas in the vertical domain and include indoor and outdoor scenarios. The channels are measured with the sounder described in [42]. The results show that one parameter of the equation is constant for SNR above $-5 \, \mathrm{dB}$ and the other parameter depends on the scenario.

1.8 Channel modelling

The design of wireless communications techniques require accurate models of the propagation channel in order to validate their performance using simulations. The channel models present a trade-off between complexity and accuracy, so it is important that a model describes the properties that affect the performance of a communication technique, but it is not necessary to model the whole reality.

The main characteristic of MIMO channels is the use of the spatial domain for the transmission. Since the appearance of multi-antenna communication systems several system level channel models have been developed. Some examples are the 3GPP spatial channel model (SCM) [10], extended SCM (SCME) [3], Winner (WIM1) [2], Winner II (WIM2) [37], Winner+ (WIM+) [30] and QuaDRiGa [33]. Although each of these models represent an improvement respect to the previous models, they all fail to model accurately the characteristics of massive MIMO.

The main limitation of these models is threefold. First they do not consider spherical waves propagation. Second they do not account for non-

stationarities across the array. Finally they generate the channel of the users independently from their relative position.

Spherical waves is an important consideration for massive MIMO modelling, because the large aperture of the array makes the Rayleigh distance very large (i.e. it could be on the order of 1 km). Therefore the scatters at the BS side and the users are probably in the near field region of the array and the planar wave approximation does not hold any more.

Non-stationaities across the array as described in 1.5 is another important characteristic of massive MIMO channels. The large space occupied by the antennas makes different antennas to receive signals from different scatters, or from the same scatter but with large variations in power. This means that antennas placed in different parts of the array can experience different channel properties. In massive MIMO systems the channel can not be considered wide sense stationary in the antenna domain.

The benefits of massive MIMO rely on the asymptotic orthogonality of the channel vectors of different users. This is called favorable propagation as explained in 1.2. However if these users are close to each other their channel vectors can be highly correlated. Massive MIMO channels should model the users channels according to their relative position.

Paper G proposes a modification of Winner-type of channel models that overcomes these three limitations.

Recently, some modification to COST2100 channel model have been proposed [23]. COST2100 is based on clusters defined in the simulation environment, and not only descrived by their parameters like in Winner-type channel models [61]. The users can see the signal from a cluster if they are in its visibility region. In [23] the concept of cluster visibility regions is extended to the BS in order to adapt the COST2100 channel model to massive MIMO. This permits to model non-stationarities across the array, because different parts of the BS array are in different visibility region and they receive the signal from different clusters. [23] also modifies the power of a cluster inside the visibility region for a more accurate modelling. In addition, to avoid over-correlation of closely located users, a variation of the power of the multi-path components inside the cluster is also defined, so even user seeing the same clusters do not have identical channels [22]. The main drawback of COST2100 model is the difficult parametrization. The measured channels do not offer the characteristics of the clusters that are needed for the model [55].

The METIS project also describes the shortfalls of existing channel models and it develops three channel models [55]. The first one is map-based model, the second one is a stochastic model and the last one is a hybrid model. The map-based model supports spherical waves and large antenna array, so it could be used in massive MIMO system. However, map-based models can be computational expensive and memory demanding.

2 Aim of the Thesis

The objective of this thesis is to characterise and model the massive MIMO channel. The existing theoretical work on massive MIMO uses simplified mathematical models to draw conclusions on the performance of the systems. However, these simplified models can be very different from the real propagation channels. Some properties of the channels are not accounted in the most simplistic models, for example the correlation between users. Other properties have never been observed in previous systems, for example the non-stationarities across the arrays. For these reason the theoretical results on massive MIMO can be misleading, and it is necessary to study measured massive MIMO channels.

This thesis aims to study highly realistic massive MIMO scenarios. For this reason the measured environments are indoor locations similar to shopping malls or airport halls, and courtyards similar to open air concerts. These scenarios represent new hotspot deployments for the 5G, instead of the traditional cellular systems. The analysed measurements are performed in all the antennas quasi-simultaneously, which permits to have dynamic users. The users hold a mock-up handset so the effects of the handgrip are also accounted in the results.

A strong motivation for the thesis is to study the impact of the array aperture. The claimed benefits of massive MIMO rely on the excess of DoF in the system, and the aperture of the array has a big impact on it. For this reason we study linear arrays with well separated sets of antennas, uniform linear arrays, two dimensional compact arrays, as well as the impact of the antenna density in the array.

The focus of the thesis is not on the performance of massive MIMO in measured channels, but on the characteristics of the channels matrix that descrive the impact of the physical properties of the environment to the signal processing. For example, instead of studying the performance of a specific technique in order to exploit the diversity of the system, we study who the position of the users can affect the diversity. This result can be used by multiple transmission schemes.

The existing channel models fail to proper describe the characteristics of massive MIMO channels. Based on the results obtained analysing the measured channels, this thesis wants to adapt the existing channel models to better represent massive MIMO systems. The goal is not to create a new channel model, which would be difficult to implement to existing software used both in the industry and academy, but to adapt the existing models, so small modification in the existing software can yield more accurate results on the performance of massive MIMO.

3 Contribution

This thesis presents a characterisation of the massive MIMO channel based on measured data. The measurements are performed in highly realistic environments so the results are a good description of real massive MIMO implementations. The measurements are conducted in future scenarios for the 5G systems like shopping malls, outdoor concert venues, etc. The BS are mounted on the wall, and at the user side mock-up handsets are hold by real users with their own hand grip. All the channel links are measured quasi-simultaneously, what allows to have dynamic users.

The results presented in this thesis are not physical properties of the environment like, for example, the delay spread, but, instead, we present properties of the channel matrix that are determined by the physical environment and have an impact on the signal processing. For this reason the results have a larger range of applications compared to presenting the performance of massive MIMO using specific communications techniques. Some of the metrics studied are related with the DoF in the system, other metrics are related with properties of massive MIMO. Nevertheless, we also show some result of sum rate using specific precoding techniques.

This thesis brings insights on favorable propagation conditions. The orthogonality between the channel vectors of two users is studied for randomly located users, but also for specific distances between users. We observe a clear relationship between the distance between the users and the orthogonality of their channels. The multi-user multiplexing capabilities of massive MIMO are also studied, what shows the difficulties to multiplex closely spaced users, and the saturation effect when the number of users grows large. We also show the hardening of the channel and power non-stationarities over the array, which are new properties of massive MIMO systems. In addition the thesis present channel conditioning analysis for multi-antenna users. Massive MIMO can decorrelate the closely spaced antennas in the same handset. The transmission of multiple data streams to the same user permit to increase its throughput, and also increases the total sum rate of the system.

The aperture of the array plays a very important role in all the analysis of the measurements. The benefits of large aperture arrays are present throughout the thesis. We also show the importance of using horizontal arrays to gather more DoF in environments with horizontally distributed users.

Finally some modifications are proposed to be implemented in existing WINNER-type channel models, in order to adapt them to massive MIMO systems. The main modifications are: A method to ensure multi-user consistency and have orthogonality based on the distance between users, the generation of non-stationarities over the array, and finally the use of spherical waves.

4 Summary of Papers

4.1 Paper A

Towards Very Large Aperture Massive MIMO: a measurement based study
2014 IEEE Globecom Workshops (GC Wkshps) pp. 281.286, 2014

Motivation

Massive MIMO has been largely studied using simplified channel models. For further development of practical implementations it is necessary a deeper understanding of its channel characteristics. Some massive MIMO channel measurements have been conducted in residential scenarios, but not in indoor large venues, which are possible deployments in the future 5G. In addition the excess number of degrees of freedom that massive MIMO claims can be affected by the shape of the base station array and specially by its aperture.

Paper content

In this work, we provide an analysis of a highly realistic massive MIMO measured channel. The base station has 64 antenna elements, serving 8 dynamic users with 2 antennas each. The base station array can be configured into 3 shapes each one with a different aperture. We study the orthogonality between the channel vectors of the users, the degree of multi-user multiplexing, the MIMO capabilities of the two antennas in the same handset, and the non-stationarities across the base station.

Main results

The analysis of the measured channels confirms that massive MIMO achieves favorable propagation conditions. Although well separated users benefit from low channel vector correlation, the antennas in the same device and closely spaced users have higher correlation. The benefits of larger apertures in the base station array are clear, specially in scenarios with crowded users. We also observe that users in the same azimuth angle have orthogonal channel vectors when using very large aperture arrays, probably due to the spherical waves in the near field. The results show that 8 single-antenna users can be simultaneously multiplexed, however the degrees of freedom tend to saturate when increasing the number of users, specially for the 2 dimensional array. The large number of antennas in the base station can transmit independent data streams to the antennas in the same handset, even if they are closely spaced. Finally we show power non-stationarities across the array.

4.2 Paper B

Frequency Dependence of Measured Massive MIMO Channel Properties
IEEE 83rd Vehicular Technology Conference (VTC Spring) pp. 1-5, 2016

Motivation

Massive MIMO measurements are necessary in order to understand the characteristics of the channels and to permit a better implementation. Some measurements using virtual arrays can not have multiple realizations of the channel in the time domain, so they rely on frequency sub-bands for the statistics. The results observed in a sub-channel can be different in other sub-channels at different frequencies. To study the characteristics of the channel in multiple sub-bands can be beneficial for multi-carrier systems.

Paper content

This paper shows the characteristics of a measured massive MIMO channel in several sub-bands. The measurements analysed have 64 antennas at the base station and 8 dual-antenna users. The scenario is similar to an indoor shopping mall as a possible new deployment scenario for 5G. The measurements represent a very realistic implementation with moving users and handset mockups. The study includes results of the correlation between the channel vectors of the users and its standard deviations across the sub-bands. It also shows the mean and standard deviation of normalized sum of eigenvalues for single-antenna users representing the multi-user multiplexing of the system. Finally, it presents the MIMO capabilities of the 2-antennas handset in the form of condition number of the channel. The condition number is shown for multiple sub-bands, and with the mean and standard deviations when increasing the number of base station antennas.

Main results

This investigation concludes that the characteristics of the channel are similar for all the sub-bands used in these measurements. This result is observed in the three metrics studied. These metrics are the scalar product between the channel vectors, the NPCG (i.e. normalized sum of eigenvalues), and the condition number of the two antennas in the same handset. We also observe that the larger the aperture of the array the more similar are the properties of the channel. From the results we can observe that the user handgrip also helps to stabilize the characteristics of the channel across sub-bands. Finally the number of base station antennas is also reducing the standard deviation across sub-bands of the studied metrics.

4.3 Paper C

Massive MIMO Properties based on Measured Channels: Channel Hardening, User Decorrelation and Channel Sparcity

50th Asilomar Conference on Signals, Systems, and Computers, IEEE pp. 1804-1808, 2016

Motivation

Some signal processing methods for massive MIMO extensively exploit some properties of the channel that has not been deeply studied in measured channels. These properties are: Channel hardening, orthogonality of the channel vectors of users at specific distances between them, and dimension of the signal subspace. This work is motivated by the lack of study of the mentioned properties.

Paper content

This study is based on two massive MIMO measurement campaigns. The first one has 64 base station antennas and 8 dual-antenna users in an indoor scenario similar to a shopping mall. The second measurement campaign has 128 antennas at the base station and 2 dual-antenna users in an outdoor scenario that could be used as a concert venue. To study the channel hardening we look at the standard deviation over channel realizations of the average power across the array. The orthogonality of the channel vector of the users is computed for specific positions of the users. Finally we observe the eigenvalue profile for the channel of a single user, and the angle of arrival using a steering vector beam-sweeping.

Main results

First we observe that the average power of the channel across the array becomes more stable when the number of base station antennas increases. However the hardening is not as strong as in Gaussian channels due to the correlation between links. Increasing the aperture of the base station array increases the hardening effect. We also observe a clear relationship between the orthogonality of the channel vector of the users with the distance between these users in NLoS. The analysis of the eigenvalue profile shows a larger dimension of the signal subspace for NLoS channels compared to LoS. However, the smoothness in the profile does not reveal a clear number for the dimension of the subspace. The angle of arrival shows a rich scattering environment.

4.4 Paper D

Impact of Array Aperture in Massive MIMO: a Measurement based Study
Submitted to IEEE Transactions on Antennas and Propagation

Motivation

The motivation for this publication is to study the impact of the array aperture on the characteristics of the channel. Some results have been obtained for massive MIMO using simplified models, but these results can be far from the real implementation. This study aims to better understand the characteristics of the channel using highly realistic massive MIMO deployments. The studied scenarios are large indoor venues, which are the new deployment scenarios of 5G.

Paper content

This paper presents the analysis of an indoor measurement campaign. The measurements are recorded using 64 BS antennas and 8 users holding a 2-antennas mock-up handset. The users move to generate the small scale fading in the channel, and they are positioned well separated or close to each other, in LoS or NLoS. The study shows the orthogonality of the channel vector of the users, and its statistics over the users for several numbers of BS antennas. The results are compared for the different array apertures and scenarios. We also plot the degree of multi-user multiplexing when increasing the number of users in the system, and we show statistics over the users for the measured scenarios and arrays. Finally we investigate the condition number of the channel and we compare the results for the measured arrays and scenarios.

Main results

Focusing on the single-antenna users scenario we observe a decrease on the channel vector correlation logarithmical with the number of antennas (equivalent to the aperture of the array), which is similar to the Gaussian channel. The multi-user multiplexing capabilities are higher for well-separated users in LoS compared to NLoS, followed by grouped users in LoS and, again, followed by grouped users in NLoS. The aperture of the array is critical to decorrelate the antennas in the same handset. NLoS scenarios also help to improve the MIMO capabilities of the devices. In general the compact array shows worse properties than the linear arrays. Finally we observe larger variations of the results in the measured channels than in the Gaussian ones, probably because the users move in the near field and it can generate non-stationarities on the channels.

4.5 Paper E

An Experimental Study of Massive MIMO Properties in 5G Scenarios
Under major revision by IEEE Transactions on Antennas and Propagation

Motivation

The motivation for this publication is to study three main characteristics of massive MIMO that are used in some signal processing techniques, but they have never been deeply studied in measured channels. These characteristics are: channel hardening, multi-user consistency and dimension of the signal subspace. Two massive MIMO measurement campaigns are used to study these topics.

Paper content

This publication analyses two massive MIMO measurement campaigns. The first one uses 64 BS antennas and it serves 8 dual-antenna users. The scenario is a large indoor venue. The second measurement campaign uses 128 BS antennas serving 2 dual-antenna users. The measurements are recorded in an outdoor venue. The standard deviation of the average power across the arrays is used as a measure of the hardening of the channel. The results are presented for an increasing number of BS antennas (i.e. increasing the aperture of the array) and the different arrays and scenarios are also compared. The channel vector orthogonality is presented for specific distances between the users together with its impact to the matched filter capacity. Finally, to study the dimension of the subspace of the signal, we present the power profile of the eigenvalues for several measured scenarios, and the beamforming angle-of-arrival.

Main results

The results presented in this publication show the increase of the channel hardening effect when increasing the number of BS antennas. They also show that larger aperture arrays achieve larger hardening due to better separated antennas and gathering more diversity. The results also show that in NLoS scenarios the distance between the users is determinant for the channel vector orthogonality. In LoS scenarios it is the beampattern of the array which influences the channel vector orthogonality. Finally, the profile of eigenvalues does not show a clear subspace occupied by the signal, but the angle-of-arrival shows energy scattered in all directions.

4.6 Paper F

Experimental Study of the Benefits of a Second Antenna at the User Side in a Massive MIMO System
Accepted by IEEE Access

Motivation

This article is motivated by the lack of studies on massive MIMO with multiple antenna users. Since the beginning, massive MIMO has been described as a very large number of antennas at the base station serving multiple single-antenna users. However, the use of multiple antennas at the user handset opens the possibility for MIMO transmission to the individuals and therefore, increase the throughput of the system. This article wants to study if the short distance between antennas in the handset increases the correlation and it is difficult to transmit independent data streams to the antennas.

Paper content

This publication studies the benefits of a second antenna at the user handset. It uses a massive MIMO measurement that involves 64 BS antennas serving 8 dual-antenna users. The target scenarios are new 5G deployments like large indoor venues (i.e. shopping malls, airport halls, etc.). The publication analyses the single user systems, to avoid the effect of the inter-user interference, and the system load. The impact of the correlation between the channels of the two antennas on the capacity is studied. The impact of the number of BS antennas is also studied, as well as the differences between the measured scenarios (i.e. LoS, NLoS, spread users, grouped users, etc.). Multi-user systems are studied to compare the linear precoders like zero-forcing for single-antenna users and block diagonalization for double antenna users with the DPC capacity.

Main results

The results confirm the benefits of adding a second antenna to the handset of the user. Larger number of BS antennas increases the orthogonality of the user antennas and the measured channels become more similar to the Gaussian channels. The allocation of power to both antennas in the handset varies in each channel realization due to the fading characteristics of the channel, but increasing the number of BS antennas increases the number of realizations with power in both antennas. Multi-user systems are also benefited by double-antenna users, but the load of the system can be harmful. Increasing the number of BS antennas makes throughput using linear precoders closer to DPC capacity.

4.7 Paper G

Geometry-Based Stochastic Channel Models for 5G: Extending Key Features for Massive MIMO
2016 IEEE 27th Annual International Symposium on Personal, Indoor, and Mobile Radio Communications (PIMRC)

Motivation

The existing system level channel models fail to represent the characteristics of massive MIMO channels. The results observed in measured channels need to be properly modelled in order to have reliable simulations and performance evaluation of massive MIMO systems. Instead of creating new models it is interesting to adapt the existing ones because they are used in numerous applications in the industry and academia, and it would be too costly to replace them for completely new ones.

Paper content

This paper proposes three modifications for WINNER-type channel models to adapt them to massive MIMO systems. There are three basic characteristics of massive MIMO that need to be implemented. The first one is multi-user consistency, which allows to generate the channel of the users with correlation according to their relative position. The second is the non-stationarities across the base station array, so different parts of the array see different clusters. The third is the spherical wave modelling, since the users and scatterers might be in the near field region of the array.

Main results

This publication describes three modifications to overcome three limitations of WINNER-type channel models to model massive MIMO channels. First, we introduce the concept of aura. This aura is a circular region surrounding the users and its intersection defines the number of common clusters between users. The radius of the aura is defined by the stationarity interval. With this implementation, the channel vector orthogonality is determined by the distance between users. To ensure non-stationnarities across the array, this is divided into smaller sub-arrays. Each sub-array is treated like an individual users and independent clusters are generated for each one of them. Common clusters between the different parts of the array is achieved by overlapping the auras of the sub-arrays. Finally we define the focal point of the cluster at the transmit side in order to generate the spherical waves.

5 Discussion

The idea of large number of BS antennas apeared since the consolidation of MIMO technologies in the beginnings of 2000s decade. For example there were some publications mentioning the central limit theorem for MIMO channels with a large number of BS antennas [31], or stating that it is always advantageous to increase the number of BS antennas, even when the reverse SINR is low and the channel estimate poor [47]. Nevertheless, massive MIMO movement is considered to start with the seminal work of Marzetta in 2010 [48]. In this publication he describe a cellular system with BS comprising a very large number of antennas serving several single antenna users in the same time-frequency recourse.

Shortly after this publication [48], and after some other theoretical works on massive MIMO [56], the first channel measurements were performed [17, 32, 57, 58]. The measured channels used in this thesis were also among the first massive MIMO measurement campaigns, and they had three unique characteristics. The first one is its ability to measure quasi-simultaneously all the BS antennas and multiple user. Some of the previous campaigns measured a single user in multiple locations and they combined the channel to create a multi-user channel. Some other campaigns used virtual arrays to measure the large number of BS antennas. The second unique characteristic is the high reality of the implementation, which included 8 real users holding a mock-up handset, and moving in a specific area. The final unique characteristics was the large indoor location, which corresponds to an idea of hotspot deployment in crowded scenarios like shopping malls. Later on these scenarios where defined in the METIS deliverable as new 5G scenarios [36] and more measurement campaigns where performed in such locations.

Another key characteristic of this thesis is its focus on the aperture of the BS array and its shape. The aperture of the array is a limiting factor of the DoF in the channel and massive MIMO uses the excess of DoF to obtain its benefits. Therefore, the aperture of the array has an impact on the performance of massive MIMO.

The results presented in this thesis have an impact on the study of the massive MIMO characteristics as well as on its practical implementation. Contrary to theoretical studies using over-simplified channel models, this study gives an insight on massive MIMO channel characteristics in real environments that have an impact on the signal processing and communication techniques. It also helps to better understand the channel and to make a better implementation of the technology. These results can also be used to improve the massive MIMO channel modelling.

6   Conclusion

This thesis responds to the need of better understanding the massive MIMO propagation channel. Theoretical analysis using simplified channel models proved the remarkable benefits of massive MIMO. However, the models used for the theoretical work can be over-simplified and the results might not be close to the reality. A deeper knowledge on the characteristics of the channel is necessary for a further development and implementation.

This thesis presents the analysis of highly realistic massive MIMO measured channels, in order to describe its characteristics. Two measurement campaigns are used. The first measured channels use 64 antennas at the BS and 8 dual-antenna users. The second measurement campaign has 128 antennas at the BS and 2 users using dual-antenna mockup handsets. The users are dynamic and their handgrip is reflected on the channel. All the users are measured simultaneously and the BS antennas are measured quasi-simultaneously using a fast switching mechanism. The scenarios measured correspond to the new deployment scenarios of 5G like shopping malls and outdoor venues.

The aperture of the BS array and its shape are important factor studied in this thesis. They can impact the DoF of the channel and it determines the performance of massive MIMO. The results show comparisons of 3 array shapes in indoor scenarios: A very large aperture array with well separated sets of 8 antennas (with an aperture of 6 m), a large aperture uniform linear array (with an aperture of 2 m), and a compact 2-dimension array (with 25 cm x 28 cm sides).

The results show the importance of the aperture of the array in order to gather DoF of the system. This is specially visible in crowded scenarios. The aperture of the array is also important to make orthogonal the channel vectors of antennas in the same handset. Even if the 2 antennas in the same handset are so close to each other, the large number of BS antennas in massive MIMO can exploit the MIMO properties of the channel. In the results we also observe the favorable propagation conditions of massive MIMO. In particular we show the scalar product between channel vector for specific distances between the users, both in LoS and NLoS scenarios. In addition, we observe the benefits of adding a second antenna to the user's handset. We also show power non-stationarities across the array and the channel hardening effect.

Finally, this thesis proposes three modifications of WINNER-type channel models to adapt them to massive MIMO channels. The modifications allow to generate similar channels for users that are close to each other (i.e. multi-user consistency), generate non-stationarities across the array, and model spherical waves at the BS.

References

[1] J. B. Andersen, "Array gain and capacity for known random channels with multiple element arrays at both ends," *IEEE Journal on Selected Areas in Communications*, vol. 18, no. 11, pp. 2172–2178, 2000.

[2] D. S. Baum, H. El-Sallabi, T. Jämsä, J. Meinilä, P. Kyösti, X. Zhao, and D. Laselva, "IST-2003-507581 WINNER D5. 4 v. 1.4 Final Report on Link Level and System Level Channel Models," Tech. Rep., 2005.

[3] D. Baum, J. Hansen, and J. Salo, "An interim channel model for beyond-3G systems: extending the 3GPP spatial channel model (SCM)," in *2005 IEEE 61st Vehicular Technology Conference*, vol. 5. IEEE, 2005, pp. 3132–3136.

[4] S. Biswas, C. Masouros, and T. Ratnarajah, "On the energy efficiency of massive MIMO with space-constrained 2D antenna arrays," in *2016 IEEE International Conference on Communications, ICC 2016*. IEEE, 2016, pp. 1–6.

[5] ——, "Performance analysis of large multiuser MIMO systems with space-constrained 2-D antenna arrays," *IEEE Transactions on Wireless Communications*, vol. 15, no. 5, pp. 3492–3505, 2016.

[6] E. Bjornson, J. Hoydis, M. Kountouris, and M. Debbah, "Massive MIMO systems with non-ideal hardware: Energy efficiency, estimation, and capacity limits," *IEEE Transactions on Information Theory*, vol. 60, no. 11, pp. 7112–7139, 2014.

[7] E. Björnson, M. Kountouris, M. Bengtsson, and B. Ottersten, "Receive Combining vs. Multi-Stream Multiplexing in Downlink Systems with Multi-Antenna Users," *IEEE Transactions on Signal Processing*, vol. 61, no. 13, pp. 3431–3446, 2013.

[8] E. Björnson, E. G. Larsson, and T. L. Marzetta, "Massive MIMO: Ten myths and one critical question," *IEEE Communications Magazine*, vol. 54, no. 2, pp. 114–123, 2016.

[9] F. Boccardi, R. Heath, A. Lozano, T. L. Marzetta, and P. Popovski, "Five disruptive technology directions for 5G," *IEEE Communications Magazine*, vol. 52, no. 2, pp. 74–80, 2014.

[10] G. Calcev, D. Chizhik, B. Göransson, S. Howard, H. Huang, A. Kogiantis, A. F. Molisch, A. L. Moustakas, D. Reed, and H. Xu, "A wideband spatial channel model for system-wide simulations," *IEEE Transactions on Vehicular Technology*, vol. 56, no. 2, pp. 389–403, 2007.

[11] C. M. Chen, V. Volskiy, A. Chiumento, L. Van Der Perre, G. A. Vandenbosch, and S. Pollin, "Exploration of User Separation Capabilities by Distributed Large Antenna Arrays," in *2016 IEEE Globecom Workshops (GC Wkshps)*. IEEE, 2016, pp. 1–6.

[12] P. Eggers, "Dual directional channel formalisms and descriptions relevant for Tx-Rx diversity and MIMO," EURO-COST, 2003. COST 273 – TD (03) 044, Tech. Rep., 2003.

[13] D. Fei, R. He, B. Ai, B. Zhang, K. Guan, and Z. Zhong, "Massive MIMO Channel Measurements and Analysis at 3.33 GHz," in *2015 10th International Conference on Communications and Networking in China (ChinaCom)*. IEEE, 2015, pp. 194–198.

References

[14] J. Flordelis, X. Gao, G. Dahman, F. Rusek, O. Edfors, and F. Tufvesson, "Spatial separation of closely-spaced users in measured massive multi-user MIMO channels," in *IEEE International Conference on Communications*.   IEEE, 2015, pp. 1441–1446.

[15] J. Flordelis, S. Hu, F. Rusek, O. Edfors, G. Dahman, X. Gao, and F. Tufvesson, "Exploiting antenna correlation in measured massive MIMO channels," in *2016 IEEE 27th Annual International Symposium on Personal, Indoor, and Mobile Radio Communications (PIMRC)*.   IEEE, 2016, pp. 1–6.

[16] G. J. Foschini, "Layered space-time architecture for wireless communication in a fading environment when using multi-element antennas," *Bell Labs Technical Journal*, vol. 1, no. 2, pp. 41–59, 1996.

[17] X. Gao, O. Edfors, F. Rusek, and F. Tufvesson, "Linear Pre-Coding Performance in Measured Very-Large MIMO Channels," in *Vehicular Technology Conference (VTC Fall), 2011 IEEE*.   IEEE, 2011, pp. 1–5.

[18] X. Gao, O. Edfors, J. Liu, and F. Tufvesson, "Antenna selection in measured massive MIMO channels using convex optimization," in *2013 IEEE Globecom Workshops (GC Wkshps)*.   IEEE, 2013, pp. 129–134.

[19] X. Gao, O. Edfors, F. Rusek, and F. Tufvesson, "Massive MIMO Performance Evaluation Based on Measured Propagation Data," *IEEE Transactions on Wireless Communications*, vol. 14, no. 7, pp. 3899–3911, 2015.

[20] X. Gao, O. Edfors, F. Tufvesson, and E. G. Larsson, "Massive MIMO in Real Propagation Environments: Do All Antennas Contribute Equally?" *IEEE Transactions on Communications*, vol. 63, no. 11, pp. 3917–3928, 2015.

[21] ——, "Multi-Switch for Antenna Selection in Massive MIMO," in *2015 IEEE Global Communications Conference (GLOBECOM)*.   IEEE, 2015, pp. 1–6.

[22] X. Gao, J. Flordelis, G. Dahman, F. Tufvesson, and O. Edfors, "Massive MIMO Channel Modeling - Extension of the COST 2100 Model," Tech. Rep., 2015.

[23] X. Gao, F. Tufvesson, and O. Edfors, "Massive MIMO channels - Measurements and models," in *2013 Asilomar Conference on Signals, Systems and Computers*, 2013, pp. 280–284.

[24] X. Gao, F. Tufvesson, O. Edfors, and F. Rusek, "Measured propagation characteristics for very-large MIMO at 2.6 GHz," in *2012 Conference Record of the Forty Sixth Asilomar Conference on Signals, Systems and Computers (ASILOMAR)*.   IEEE, 2012, pp. 295–299.

[25] X. Gao, M. Zhu, F. Rusek, F. Tufvesson, and O. Edfors, "Large antenna array and propagation environment interaction," in *2014 48th Asilomar Conference on Signals, Systems and Computers*.   IEEE, 2014, pp. 666–670.

[26] M. Gauger, J. Hoydis, C. Hoek, H. Schlesinger, A. Pascht, and S. ten Brink, "Channel Measurements with Different Antenna Array Geometries for Massive MIMO Systems," in *SCC 2015; 10th International ITG Conference on Systems, Communications and Coding*.   IEEE, 2015, pp. 1–6.

[27] D. Gesbert, M. Kountouris, R. W. Heath, C. B. Chae, and T. Sälzer, "Shifting the MIMO Paradigm," *IEEE Signal Processing Magazine*, vol. 24, no. 5, pp. 36–46, 2007.

References

[28] P. Harris, W. B. Hasan, S. Malkowsky, J. Vieira, S. Zhang, M. Beach, L. Liu, E. Mellios, A. Nix, S. Armour, A. Doufexi, K. Nieman, and N. Kundargi, "Serving 22 Users in Real-Time with a 128-Antenna Massive MIMO Testbed," in *2016 IEEE International Workshop on Signal Processing Systems (SiPS)*. IEEE, 2016, pp. 266–272.

[29] P. Harris, S. Malkowsky, J. Vieira, E. Bengtsson, F. Tufvesson, W. B. Hasan, L. Liu, M. Beach, S. Armour, and O. Edfors, "Performance Characterization of a Real-Time Massive MIMO System With LOS Mobile Channels," *IEEE Journal on Selected Areas in Communications*, vol. 35, no. 6, pp. 1244–1253, 2017.

[30] P. Heino, J. Meinilä, P. Kyösti, L. Hentilä, T. Jämsä, E. Suilkkanen, E. Kunnari, and M. Narandžić, "D5.3: WINNER+ Final Channel Models," Tech. Rep., 2010.

[31] B. M. Hochwald, T. L. Marzetta, and V. Tarokh, "Multiple-antenna channel hardening and its implications for rate feedback and scheduling," *IEEE Transactions on Information Theory*, vol. 50, no. 9, pp. 1893–1909, 2004.

[32] J. Hoydis, C. Hoek, T. Wild, and S. ten Brink, "Channel measurements for large antenna arrays," in *2012 International Symposium on Wireless Communication Systems (ISWCS)*. IEEE, 2012, pp. 811–815.

[33] S. Jaeckel, L. Raschkowski, K. Borner, and L. Thiele, "QuaDRiGa: A 3-D multi-cell channel model with time evolution for enabling virtual field trials," *IEEE Transactions on Antennas and Propagation*, vol. 62, no. 6, pp. 3242–3256, 2014.

[34] W. C. Jakes, *Microwave Mobile Communications*, W. C. Jakes, Ed. New York: Wiley, 1974.

[35] J. S. Jiang and M. A. Ingram, "Spherical-wave model for short-range MIMO," *IEEE Transactions on Communications*, vol. 53, no. 9, pp. 1534–1541, 2005.

[36] K. Kusume and M. Fallgren, "Updated scenarios , requirements and KPIs for 5G mobile and wireless system with recommendations for future investigations (Deliverable D1.5)," METIS, Tech. Rep., 2015.

[37] P. Kyösti, J. Meinilä, L. Hentilä, X. Zhao, T. Jämsä, C. Schneider, M. Narandzi, M. Milojevi, A. Hong, J. Ylitalo, V.-M. Holappa, M. Alatossava, R. Bultitude, Y. D. Jong, and T. Rautiainen, "IST-4-027756 WINNER II D1. 2 V1. 2 WINNER II Channel Models," Tech. Rep., 2007.

[38] E. G. Larsson, O. Edfors, F. Tufvesson, and T. L. Marzetta, "Massive MIMO for Next Generation Wireless Systems," *IEEE Communications Magazine*, vol. 52, no. 2, pp. 186–195, 2014.

[39] J. Li, B. Ai, R. He, K. Guan, Q. Wang, D. Fei, Z. Zhong, Z. Zhao, D. Miao, and H. Guan, "Measurement-Based Characterizations of Indoor Massive MIMO Channels at 2 GHz, 4 GHz, and 6 GHz Frequency Bands," in *2016 IEEE 83rd Vehicular Technology Conference (VTC Spring)*. IEEE, 2016, pp. 1–5.

[40] J. Li and Y. Zhao, "Measurement-Based Asymptotic User Orthogonality Analysis and Modelling for Massive MIMO," *IEEE Communications Letters*, vol. PP, no. 99, pp. 1–1, 2017.

[41] J. Li, Y. Zhao, and Z. Tan, "Indoor Channel Measurements and Analysis of a Large-Scale Antenna System at 5.6 GHz," in *2014 IEEE/CIC International Conference on Communications in China (ICCC)*. IEEE, 2014, pp. 281–285.

References

[42] J. Li, Y. Zhao, C. Tao, and B. Ai, "System Design and Calibration for Wideband Channel Sounding With Multiple Frequency Bands," *IEEE Access*, vol. 5, pp. 781–793, 2017.

[43] X. Li, E. Björnson, S. Zhou, and J. Wang, "Massive MIMO with Multi Antenna Users: When are Additional User Antennas Beneficial?" in *23rd International Conference on Telecommunications (ICT)*. IEEE, 2016, pp. 1–6.

[44] L. Liu, D. W. Matolak, C. Tao, Y. Lu, B. Ai, and H. Chen, "Geometry based large scale attenuation over linear massive MIMO systems," in *2016 10th European Conference on Antennas and Propagation (EuCAP)*. IEEE, 2016, pp. 1–5.

[45] L. Liu, C. Tao, D. W. Matolak, Y. Lu, B. Ai, and H. Chen, "Stationarity Investigation of a LOS Massive MIMO Channel in Stadium Scenarios," in *2015 IEEE 82nd Vehicular Technology Conference (VTC2015-Fall)*. IEEE, 2015, pp. 1–5.

[46] Y. Lu, C. Tao, L. Liu, W. Li, J. Xiao, and P. Liu, "Frequency correlation investigation of massive MIMO channels in a stadium at 4.45 GHz," in *2015 17th International Conference on Advanced Communication Technology (ICACT)*. IEEE, 2015, pp. 271–274.

[47] T. L. Marzetta, "How Much Training is Required for Multiuser Mimo?" in *2006 Fortieth Asilomar Conference on Signals, Systems and Computers*, 2006, pp. 359–363.

[48] ——, "Noncooperative cellular wireless with unlimited numbers of base station antennas," *IEEE Transactions on Wireless Communications*, vol. 9, no. 11, pp. 3590–3600, 2010.

[49] C. Masouros and M. Matthaiou, "Space-constrained massive MIMO: Hitting the wall of favorable propagation," *IEEE Communications Letters*, vol. 19, no. 5, pp. 771–774, 2015.

[50] H. Q. Ngo, E. Larsson, and T. Marzetta, "Aspects of Favorable Propagation in Massive MIMO," in *Signal Processing Conference (EUSIPCO), 2014 Proceedings of the 22nd European*, no. 2. IEEE, 2014, pp. 76–80.

[51] H. Q. Ngo, E. G. Larsson, and T. L. Marzetta, "Energy and spectral efficiency of very large multiuser MIMO systems," *IEEE Transactions on Communications*, vol. 61, no. 4, pp. 1436–1449, 2013.

[52] A. Paulraj, R. Nabar, and D. Gore, *Introduction to Space-Time Wireless Communications*, 1st ed. New York, NY, USA: Cambridge University Press, 2008.

[53] S. Payami and F. Tufvesson, "Channel measurements and analysis for very large array systems at 2.6 GHz," in *2012 6th European Conference on Antennas and Propagation (EUCAP)*. IEEE, 2012, pp. 433–437.

[54] ——, "Delay spread properties in a measured massive MIMO system at 2.6 GHz," in *IEEE International Symposium on Personal, Indoor and Mobile Radio Communications, PIMRC*. IEEE, 2013, pp. 53–57.

[55] L. Raschkowski, P. Kyösti, K. Kusume, and T. Jämsä, "METIS D1.4: METIS Channel Models," Tech. Rep., 2015.

[56] F. Rusek, D. Persson, B. K. Lau, E. G. Larsson, T. L. Marzetta, O. Edfors, and F. Tufvesson, "Scaling Up MIMO: Opportunities and Challenges with Very Large Arrays," *IEEE Signal Processing Magazine*, vol. 13, no. 1, pp. 40–60, 2013.

References

[57] C. Shepard, H. Yu, N. Anand, E. Li, T. L. Marzetta, R. Yang, and L. Zhong, "Argos: practical many-antenna base stations," in *Proceedings of the 18th annual international conference on Mobile computing and networking - Mobicom '12*.   ACM, 2012, pp. 53—64.

[58] C. W. Shepard, "Argos: Practical base stations for large-scale beamforming," Master of Science Thesis, Rice University, 2012.

[59] D. Tse and P. Viswanath, *Fundamentals of Wireless Communication*, 1st ed.   Cambridge University Press, 2005.

[60] A. van Zelst and J. S. Hammerschmidt, "A single coefficient spatial correlation model for multiple-input multiple-output (MIMO) radio channels," in *27th General Assembly of the International Union of Radio Science (URSI)*, no. 1, 2002, pp. 1–4.

[61] R. Verdone and A. Zanella, *Pervasive Mobile and Ambient Wireless Communications (COST Action 2100)*.   Springer, 2013.

[62] L. Wenjuan, L. Liu, T. Cheng, L. Yanping, X. Jingcheng, and L. Pengyu, "Channel measurements and Angle Estimation for Massive MIMO Systems in a Stadium," in *2015 17th International Conference on Advanced Communication Technology (ICACT)*.   IEEE, 2015, pp. 105–108.

[63] C. Xu, J. Zhang, Q. Zheng, H. Yu, and L. Tian, "Measurement-based Delay Spread Analysis of Wideband Massive MIMO System at 3.5 GHz," in *2017 IEEE International Conference on Computational Electromagnetics (ICCEM)*.   IEEE, 2017, pp. 246–248.

[64] H. Yu, Q. Zheng, Z. Zheng, L. Tian, and Y. Wut, "The Rationality Analysis of Massive MIMO Virtual Measurement at 3.5 GHz," in *CIC International Conference on Communications in China (ICCC Workshops)*.   IEEE, 2016, pp. 1–5.

[65] S. Zhang, P. Harris, A. Doufexi, A. Nix, and M. Beach, "Massive MIMO real-time channel measurements and theoretic TDD downlink throughput predictions," in *2016 IEEE 27th Annual International Symposium on Personal, Indoor, and Mobile Radio Communications (PIMRC)*.   IEEE, 2016, pp. 1–6.

References

Part II

Papers

Paper A

Towards Very Large Aperture Massive MIMO: a
measurement based study

Àlex Oliveras Martínez, Elisabeth De Carvalho, Jesper Ødum
Nielsen

Abstract

Massive MIMO is a new technique for wireless communications that claims to offer very high system throughput and energy efficiency in multi-user scenarios. The cost is to add a very large number of antennas at the base station. Theoretical research has probed these benefits, but very few measurements have showed the potential of Massive MIMO in practice. We investigate the properties of measured Massive MIMO channels in a large indoor venue. We describe a measurement campaign using 3 arrays having different shape and aperture, with 64 antennas and 8 users with 2 antennas each. We focus on the impact of the array aperture which is the main limiting factor in the degrees of freedom available in the multiple antenna channel. We find that performance is improved as the aperture increases, with an impact mostly visible in crowded scenarios where the users are closely spaced. We also test MIMO capability within a same user device with user proximity effect. We see a good channel resolvability with confirmation of the strong effect of the user hand grip. At last, we highlight that propagation conditions where line-of-sight is dominant can be favorable.

1   Introduction

In the seminal work of Marzetta [1], a massive MIMO (Multiple Input Multiple Output) system refers to a multi-user MIMO communication system where a base station comprises a very large number of antennas, much larger than the number of served users. In this under-determined multi-user system, the extra spatial Degrees of Freedom (DoF) are exploited to make the multi-antenna multi-user MIMO channel asymptotically orthogonal. In addition, relying on the knowledge of the channel, a proper processing at the Base Station (BS) averages out the fading at the receivers in the downlink direction and at the BS in the uplink direction. Based on those features, enabled by the extra DoF, massive MIMO is recognized as a promising technology for very high system throughput and energy efficiency.

In massive MIMO systems, the spatial DoFs available in the multi-antenna multi-user channel play a central role. With an independent and identically distributed (i.i.d.) modelling of fading, the number of DoF is simply defined and limited by the number of antennas. This simple modelling provides an inappropriate account of the DoF limitation though. For a given propagation environment, the array physical characteristics, its physical size and geometry, define the number of DoF as it defines the angular resolvability. This can be easily understood in a line-of-sight environment, where users can be separated if they are further apart than the resolution unit. In a scattering environment, the array dimension defines the degree of resolvability of the scattering clusters and hence the DoF (see e.g. [2]). In this paper, *array aper-*

ture refers to the dimension of the arrays. We have two types of array, a linear array and a square array: the array aperture is the length of a linear array and the length of the side of a square array.

Increasing the number of antennas within a fixed array aperture is useful to grab all the available DoF up to the limit imposed by the aperture. After this limit is exceeded, increasing the number of antennas does not bring improvement. There is another important point that advocates for very large aperture arrays: as pointed out in [3] [4] an increased aperture implies an extended vision range of the environment. The more the array can capture of his environment, the more diversity it can capture, implying more DoF.

The importance of the aperture to achieve the theoretical performance of massive MIMO systems is the motivation for a series of channel measurements performed at Aalborg University where the primary focus is on the impact of the array aperture. The measurements presented in this paper targets a deployment of massive arrays that differs from the current mainstream of a cellular deployment where the massive BS is placed outdoors. In general, we address a deployment in large venues, possibly indoors, where massive arrays with a Very Large Aperture (VLA) are designed as an integral part of a new large infrastructure. Referring to the 5G scenarios defined within the EU project METIS [5], VLA arrays can be deployed along walls or ceiling of a shopping mall or airport, around the structure of a football stadium or along the facade of a building. Such scenarios benefit from line-of-sight propagation with the potential of very high rank point-to-point MIMO channels [6] and acute discrimination between users, especially in crowd scenarios. They also benefit from rich scattering as the arrays see a wide range of diverse scatterers. Our vision is that the theoretical benefits described in [1] can be achieved in those large infrastructure deployment, while cellular deployment with BS located in high towers would benefit from the capability of massive MIMO for sharp beams. Our measurement campaign provides a first positive echo to this vision.

To this date, still very few measurement campaigns with published results exist. There are 5 of them [3] [4] [7] [8] [9]. All target outdoor scenarios at frequency 2.6 GHz. Following the first publications on massive MIMO, the major stress of those measurements is set on the impact of number of antennas, not relating it directly to array aperture. Only in [3] [4] can we find a comparison between two different aperture arrays where the larger aperture array was found to have better performance. In [7] [8], the orthogonality between the channels of 2 users (the normalized scalar product) has been measured to increase with the number of BS antennas. All the existing measurement campaigns confirm the promises held by the theoretical studies. However, as pointed out in [7] [8], a saturation is observed creating a gap with the performance of i.i.d. channels, likely coming from the limitation of the DoF. All those campaigns face the problems induced by the large num-

ber of antennas and the impossibility to achieve simultaneous measurements with the current technology. The solution adopted is to create a virtual massive array and/or virtual multi-user set-up. Measurements are performed with a set of small number of antennas and users, which are moved for a subsequent measurement. This methodology creates heavy constraints of the measurement protocols imposing the environment to remain static within a whole measurement interval.

Our measurement campaign involves 64 antennas that are rearranged in 3 different geometrical forms (see fig. A.1). In the first array, the antennas, separated by half the wavelength, are placed within a square. We refer to this array as "Compact 2D". It corresponds to a common view on the design of massive arrays, where the massive array is as compact as possible. In the "Large Aperture array", the 64 antennas are spread along a line of 2 meters. In the "Very Large Aperture array", the antennas are spread along a line of 6 meters. Note that one advantage of the compact 2D array is to offer beamforming capabilities in 2 dimensions: this capability will be tested against the one-dimensional beamforming (in Bohagen2007) offered by the linear arrays. The distinctive features of our measurements can be described as follows: First, we have a multi-user set-up where 8 users transmit simultaneously to the massive BS. Second, we test MIMO capabilities within the same device with and without user proximity effects: the 8 users hold devices with 2 antennas. Last, we perform quasi-simultaneous measurements: the set-up includes 16 fully parallel transmitters (8 mobile units with 2 antennas) and 8 fully parallel receive units. At the BS, the received signals from 8 antenna elements are measured simultaneously. Using fast switching, the parallel system is extended to allow measurements with 64 element BS arrays.

Our general conclusion is that performance is better as the array aperture increases. More specifically, our main findings are summarized as follows:

- Inter-user link orthogonality: the impact of the aperture is mainly visible when the users are closely grouped. As the number of users increases, the very large array is able to hold performance that is closed to the i.i.d. channel.

- Intra-user link orthogonality (MIMO capability): we see a good channel resolvability that is better for the very large array. Furthermore, our measurements confirm the strong effect of the user hand grip.

- Power variations across the array: the largest variations are seen for the Very Large Aperture array. However, even for the Compact 2D array, we can see power variations larger than 10dB.
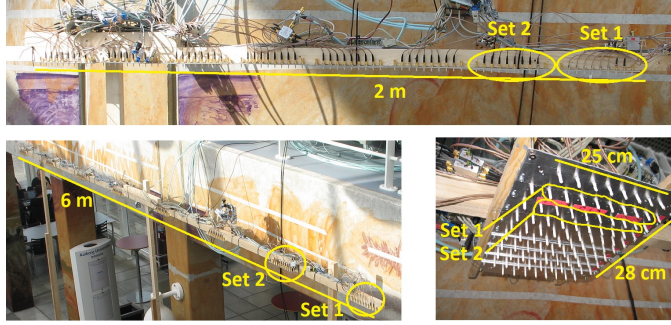
Fig. A.1: Three array shapes are tested with different aperture: Very Large Aperture at the bottom-left, Large Aperture at the top and Compact 2D at the bottom right.
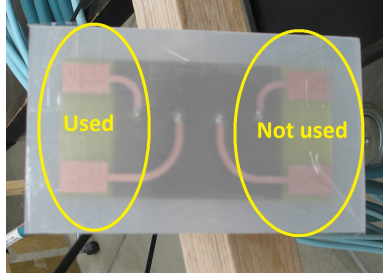
Fig. A.2: Handset with four antennas. Only two are used

2 Measurement setup

The measurements campaign was performed in one of the canteens at Aalborg University. This location can be considered as a large indoor venue and has a similar structure as a shopping mall: a big open space with high ceiling, stairs (to go to an upper level), and some small areas on the side with a lower ceiling (see fig. A.3).

2.1 Three array shapes with different aperture

We use a total of 64 monopole elements. For practical reasons, the 64 elements are grouped in sets of 8 elements. The distance between elements in the same set is $\lambda/2$ at 5.8 GHz. Each set has 2 dummy elements at the ends to provide balanced properties among the active elements (load, coupling, correlation). Those sets are arranged in 3 different array shapes, pictured in fig. A.1: 1) a square Compact 2D array of 25cmx28cm, where the sets are placed in a square, 2) a Large Aperture linear array of 2 meter long where the sets are placed near to each other along a line, 3) a Very Large Aperture

Fig. A.3: Top-left, Spread users LoS. Top-right, spread users NLoS. Bottom-left, Free space in front the stairs. Bottom-right, Grouped users LoS.

linear array of 6 meter long, where the sets are placed further away. The array is placed along a wall of the room, parallel to the stairs.

2.2   Multi-user Scenarios

A total of 8 handsets transmit to the massive array (Fig. A.2). Eight users hold the handsets as if in data mode in one or both hands. The device is located at a few centimeters from the body: see figure A.3. The users move randomly in an area of 1 square meter. Our original intent in having this small mobility area was to measure small scale fading. However, after analyzing the data, we found that power fluctuations originating from the user movement were larger than expected for the measurements to reflect small scale fading. As a result, we decided to normalize the channel as described in (A.1), where the channel at each measurement is normalized to the same value. The devices are also tested in free space (no user proximity effect) and also moved within a 1 square meter area.

Six scenarios are tested, each one with specific propagation properties, with LoS (Line of Sight) and NLoS (without LoS) and with a specific distribution of the users: see fig. A.3 and fig. A.4.

- **Spread LoS Parallel**: the users face the array holding the devices so that the two-antenna array is parallel to the BS array. Four users are in a line parallel to the BS array between the stairs and the BS array and four of them in a line behind the stairs. The distance between users is
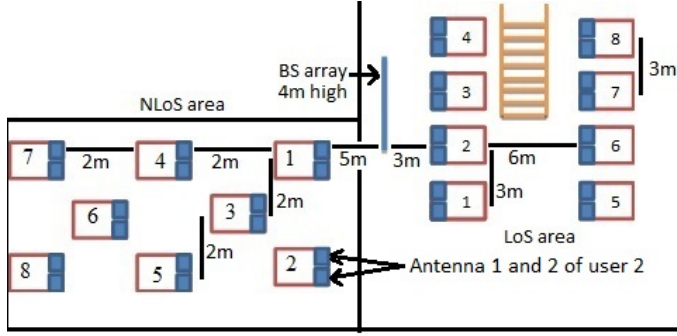
Fig. A.4: Floor map with location of BS array, LoS area, NLoS area and user numbering.

3m and the distance from the users to the array varies from 5m to 12m.

- **Spread LoS Perpendicular**: the distribution of users is the same but the users do not face the array but rather look in a direction parallel to the array. The two-antenna array in the handsets and the BS array are perpendicular. In pure LoS conditions, the two-antenna in the array cannot be likely resolved. The purpose of this scenario is to test whether this is the case or whether scattering is rich enough to allow discrimination between the two antennas.

- **Grouped LoS**: the users are behind the stairs, all in a small area of 1.5mx6m, shoulders to shoulders and moving away from each other. The distance to the array varies from 10m to 12m.

- **Free Space in front the stairs**: the 8 handsets are fastened to a table and the table was moved randomly within a small area. The table is placed between the stairs and the BS array.

- **Free Space behind the stairs**: the same as before but the table is placed behind the stairs.

- **Spread NLoS**: the users are in non LoS conditions, in the lateral room with a distance between users of 2m and a distance to the BS array from 5m to 11m.

Figure. A.4 provides an illustrative floor map of the large room where the measurement were conducted. The stairs are in orange, the BS array is in blue. The 8 users (with 2 antennas each) are depicted in LoS and NLoS conditions. To ease the analysis in section 3, we associate a user number to its geographical position. In the scenarios Grouped LoS and Free space, the relative position of the users (and their numbers) is the same but the distance between them is reduced.

2.3 Equipment and measurement conditions

A correlation based channel sounder is used to make the measurements. The carrier frequency is 5.8 GHz and the bandwidth about 100 MHz. There are 16 fully parallel transmitters (the 8 devices with the 2 antennas), and 8 fully parallel receivers. A fast switching mechanism between the receive sets (8 time switch) allow for a capture of the complete 64×16 MIMO channel in 655μs. For each deployment of the BS array and scenario, 1200 realizations of the channel were recorded in 20s, while the users move inside the 1 square meter area. The measurements are calibrated up to the antenna connectors, i.e. the antennas are considered part of the channel. Therefore, any mutual coupling and non-ideal characteristics of the arrays are included, as they would be in an actual system. Our analysis is based on narrow band channel data obtained via Fourier transforms of the wideband measurements. The statistics are taken over the 1200 measurements.

3 Numerical analysis of the measurements

In this section we focus on the analysis of the results obtained in the measurement campaign. The notations are as follows: the number of users is $K = 8$, the number of antennas for each user is $N = 2$, the number of base station antennas is $M = 64$, and the number of channel realizations is $R = 1200$. In this paper, we report results for the most significant scenarios.

The results obtained are compared with the i.i.d. Gaussian channel, to provide a comparison between the real measurements and the theoretical results. At the same time the three different arrays are evaluated and compared to each other to show the effect of the aperture on the channel performance.

To analyze the results, the communication system considered is a single cell MU-MIMO (Multi-user MIMO) system with K users, having N antennas each one, and a base station with M antennas serving the users. We denote $\mathbf{H}_r \in \mathbb{C}^{M \times KN}$ the matrix corresponding to realization r of the channel. Later some subsets of this matrix will be considered. Notice that $M > (KN)$. We denote $\mathbf{h}_{kr}^{(n)} \in \mathbb{C}^{M \times 1}$ as the channel vector from antenna $n \in \{1, 2\}$ in the handset of user k to the BS array. In matrix $\mathbf{H}_r$, the two user channel vectors are placed in two consecutive columns. The system has a power gain control so all the users receive the same power regardless their distance to the base station. The power of channel vector $\mathbf{h}_{kr}^{(n)}$ is normalized:

$$\bar{\mathbf{h}}_{kr}^{(n)} = \frac{\mathbf{h}_{kr}^{(n)}}{\left\| \mathbf{h}_{kr}^{(n)} \right\|} \sqrt{M}. \tag{A.1}$$

In this way it is fair to compare users in different location and the results will

be determined by the channel conditions and not by the path loss of the user. We denote $\bar{\mathbf{H}}_r \in \mathbb{C}^{M \times KN}$ as the channel matrix made out of the normalized vectors in (A.1). Several figures of merit are obtained from the channel matrix giving a basis to understand the channel.

3.1 Overview of the Correlation Properties

A first step to analyze the behavior of the channel is to look at the correlation between channel vectors, encompassed in the following matrix:

$$\mathbf{S} = \frac{1}{R} \sum_{r=1}^{R} \bar{\mathbf{H}}_r^H \bar{\mathbf{H}}_r \tag{A.2}$$

The elements of matrix S are pictured in fig. A.5 and fig. A.6. The 2x2 blocks along the diagonal represent the correlation between the channels for the same device. The off-diagonal blocks represent the correlation between the channels of different devices. We notice a significant difference in the behavior of the intra-user and inter-user channels. This is the reason why we later detail the performance separately for those two kinds of channels. Matrix $\mathbf{S}$ is shown for two scenarios: "Grouped User in LoS" and "Free space". Both scenarios illustrate a crowd scenario with devices closer to each other in the "Free space" case. Furthermore, by comparing both scenarios, user proximity effects can be assessed. In the figures, the two antennas associated with each user are denoted **a** and **b**, respectively.

Inter-user properties: the Very Large Aperture array clearly performs the best and the Compact 2D array clearly performs the worse. While the Very Large Aperture and Large Aperture arrays can satisfactorily discriminate all the users in the grouped LoS scenario, correlation among users appear for the Compact 2D array. The correlations appear not only for users in the same line, but also for users behind each other (5,1 or 6,2). As the devices become more packed (free space), performance degrades for all arrays with the apparition of correlated users. For the Large Aperture array, strong correlations appear for some pairs of users (1,5 and 2,6 and 3,7 and 4,8) that are behind each other. So we deduce that the Large Aperture array loses its resolution in the elevation angle. Finally in the Compact 2D array the correlation is large even for neighboring users (specially the ones further away from the base station). Channels with low correlation can be seen for users that are far from each other (1,4 and 1,8 and 4,5 and 5,8).

Intra-user properties: It is expected that the channel correlation properties within a same device are worse than across devices as the antenna are close by. In the free space scenario, the Very Large Aperture array performs remarkably better than the other arrays. Comparing now with the "Grouped LoS" scenario, we can notice the large impact of user proximity effects which can equalize the performance among arrays.
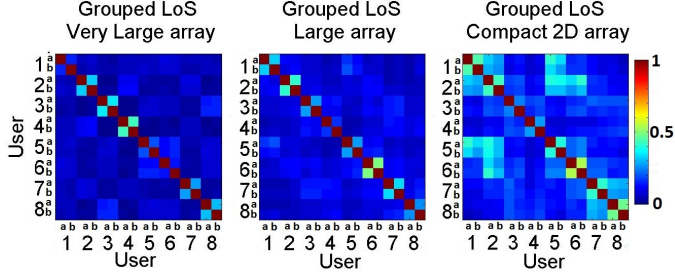
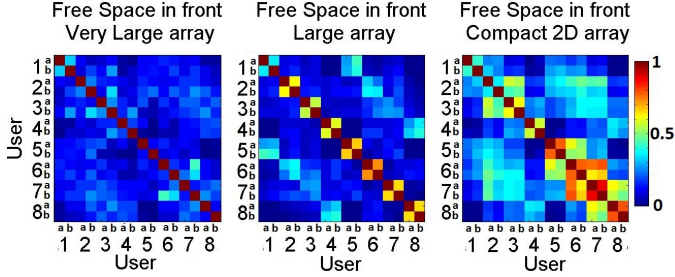**Fig. A.5:** Correlation matrix for the scenario: Grouped users in LoS

**Fig. A.6:** Correlation matrix for the scenario: Free space in front of the stairs

3.2 Inter-user properties

Here the inter-user channel properties are considered. The goal is to explore what happens when the number of users in the system increases. We call the number of users in the system C and we increase C from 1 to K. We collect all the combinations of C channels from C different users (only one channel per user out of the two channels is selected). We form a new channel matrix for realization r denoted generically as $\mathbf{G}_r$ and take statistics on our metric over the different user combinations and channel realizations.

The metric adopted here is the sum of the eigenvalues normalized by largest eigenvalue (NPCG, Normalized Parallel Channel Gain). Denoting $\lambda_{i,r}$ as the ith eigenvalue of the matrix $\mathbf{G}_r^H \mathbf{G}_r$, then the metric is defined as:

$$\mathrm{NPCG} = \frac{1}{\lambda_{\mathrm{max},r}} \sum_{i=1}^{C} \lambda_{i,r}. \tag{A.3}$$

$\lambda_{\mathrm{max},r}$ is the largest eigenvalue. This metric is preferred to the condition number of the channel as the latter gives only information on the ratio between the larger and the smaller eigenvalue, whereas metric (A.3) reflects the behavior of all the eigenvalues. Notice that, for a channel that is very well conditioned with equal eigenvalues, NPCG $= C$ and for a channel that is poorly conditioned NPCG $= 1$.
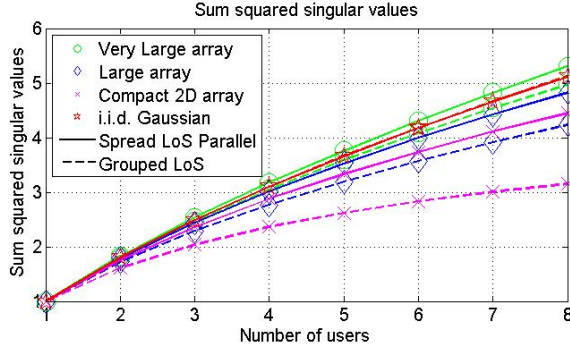
Fig. A.7: Normalized sum of eigenvalues w.r.t. increasing number of users in the Spread LoS with users antennas parallel to the BS array and grouped LoS.

In the same figure, fig. A.7 two scenarios are represented, 'Spread LoS' with their two antennas parallel to the BS array and 'Grouped LoS'. Comparing both scenarios, it is obvious that the more spread the users, the better. For all the number of users and all the arrays the channel of grouped users has worse conditioning. The limitation of the Compact 2D array in the DoF available to 8 users is particularly visible in the grouped LoS scenario. Note that the Very Large Aperture array in the spread LoS scenario gives performance slightly better than the i.i.d. Gaussian case. This can happen in LoS conditions depending on the location of the users.

In the next figure, fig. A.8, two scenarios are plotted. One is the 'Spread NLoS' and the other is the 'Free space behind the stairs' (the scenario with minimal inter-device distance). The three arrays have a worse channel conditioning than the previous scenario. For the Compact 2D array adding new users can hardly increase the metric showing again a limitation in the DoF. Two effects can be observed. On one hand the effect of NLoS propagation and on the other hand the effect of closely spaced devices. In both cases the Very Large Aperture array and the Large Aperture array have a similar behavior. It appears that the scattering is rich enough so that increasing the aperture from large to very large does not bring improvement in the NLoS scenario. At last, we show the results for the free space scenario, where we can see an overall degradation of the performance.

3.3   Intra-user properties

To evaluate the MIMO channel properties within a same device, we go back to the conventional condition number as we have only 2 antennas. The condition number indicates how spread the eigenvalues of the channel are. It is defined as $CN = 10 \log_{10}(\frac{\lambda_{\max}}{\lambda_{\min}})$ where $\lambda_{\max}$ and $\lambda_{\min}$ are the maximum and minimum eigenvalues of the MIMO channel matrix. Statistics on the
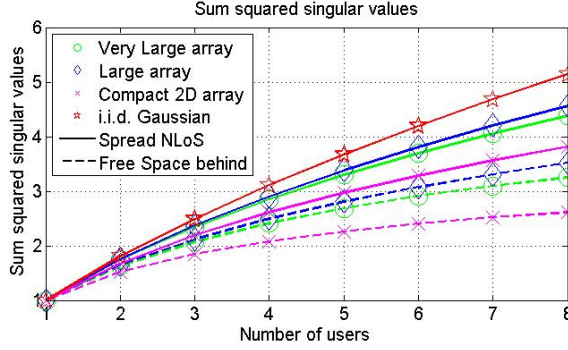
Fig. A.8: Normalized sum of eigenvalues w.r.t. increasing number of users in the Spread NLoS and Free space in front of the stairs scenarios.

condition number are taken over the R realizations of the channel.

Fig. A.9 and Fig. A.10 shows the cumulative distribution function (CDF) of the condition number. First, it can be noticed that there is a significant gap between the i.i.d. case and the measured cases, mostly due to user proximity effect and small spacing between the antennas. In general, the Very Large Aperture array still performs the best with slopes that are steeper than the other arrays. As the aperture increases, the number of DoF increases and the distribution of the eigenvalues tend to a deterministic quantity. This is in line with a similar effect in i.i.d. channels when the number of antennas (and hence DoF) increases.

Fig. A.9 accounts for the 'Spread User' scenarios, where the array formed by the antennas at the device is parallel or perpendicular to the BS array. We do not observe a clear tendency in the comparison between both scenarios, while the scenario with perpendicular arrays performs much worse in pure LoS than the scenario with parallel arrays. This might indicate that scattering is rich enough to enable MIMO capabilities in both cases. This observation is actually positive: it makes the access robust to device orientation as the devices will have a random orientation relative to the BS in general.

Looking at the fig. A.10, where the users are 'Spread NLoS' and in 'Free space in front of the stairs', we observe that the Very Large Aperture array remains robust towards both scenario conditions. Both large and compact arrays also give robust performance in the NLoS scenarios brought by a rich scattering environment. Poor performance is observed in the LoS free space scenario. More analysis is needed to fully understand this case. Our interpretation is that performance tend to depend on location in LoS, suggesting a more favorable location relative to the Very Large aperture array compared to the other arrays.
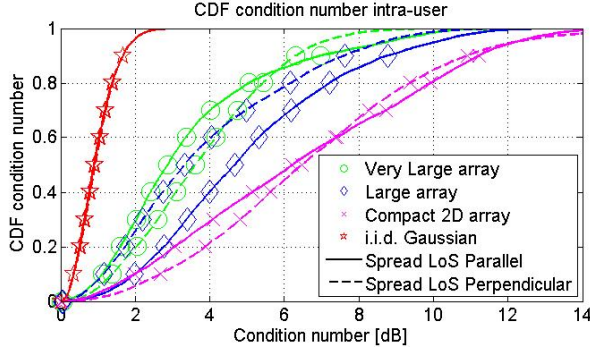
Fig. A.9: Intra-user condition number in the Spread LoS with users antennas parallel and per-pendicular to the BS array
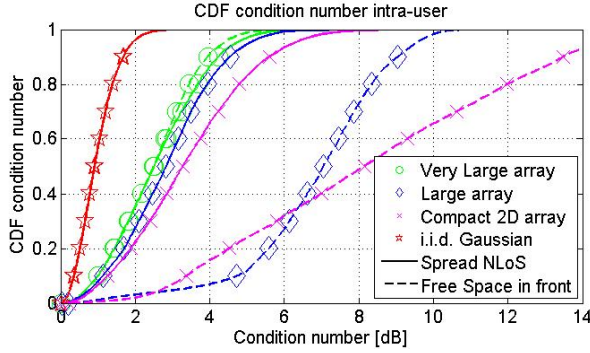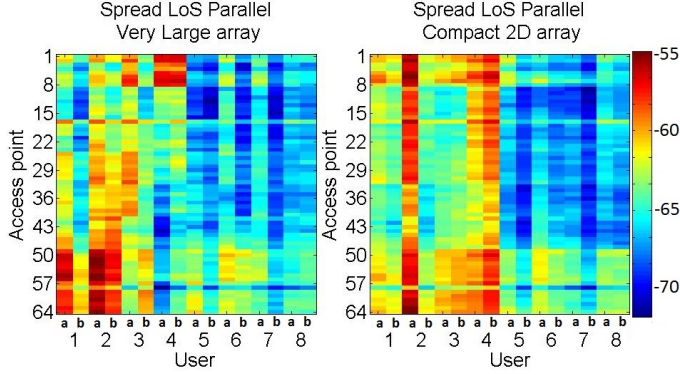

Fig. A.10: Intra-user condition number in the Spread NLoS and Free space in front of the stairs scenarios

3.4 Power Variations across the Array

As mentioned in [3] [4] [8] where measurements involving a large aperture massive array have been performed, channel characteristics become non-stationary across the array, such as the received power or the direction of arrivals. In general, the environment that is observed is different from one part of the array to another.

In this section, to illustrate this phenomenon, we examine the variations of the received power across the array for one scenario (i.e. 'Spread LoS') and two arrays, the very large and the compact one, shown in fig. A.11. The x axis represents each user (2 antennas per user), and the y axis represents the received power averaged over the 1200 measurements at each of the 64 BS antennas. Several observations can be made. First, obviously, the users that are further away from the array have a smaller received power. Second, as the aperture increases, so does the impact of path loss variations across the

Fig. A.11: Average power variations across the Very Large and the Compact 2D array for the "Spread user in LoS" scenario.

array. This is more visible for users that are closer to the array in front of the stairs. Third, the power variations depend on the environment: users 7 and 8 are positioned behind the stairs that have a shadowing effect and make the receive power uniform compared to other users. At last, the power variations are smaller in the Compact 2D array case compared with the Very Large Aperture one. However, even for this small aperture, significant variations of 10dB order can be observed.

The property of non-stationarity across a large aperture array is a new feature that gives a distinctive edge to the type of communication system studied in this paper. It impacts the performance of the system but also the multi-user access methods which could be beneficial in terms of multi-user diversity.

4   Conclusion and Future Work

The presented investigation describes a measurement campaign involving a massive array with 64 antennas and 8 users with MIMO capabilities in a large indoor environment. The main purpose is to investigate on the impact of the massive array aperture. Three different shape and aperture of the base station array were tested as well as different propagation conditions (LoS and NLoS), user device distribution (spread and grouped) and user proximity effect. The measurements confirm that the aperture is important to create the spatial DoF that brings the benefits promised by the theoretical studies on massive MIMO. We found that the array with the largest aperture perform the best with performance close to the i.i.d. channel. The channel tends to be better conditioned bringing very good discrimination among users but also between antennas of a same device, where the user proximity effect still has a

major effect. Building on this experience drawn from this first measurement campaign, we are planning a new campaign involving a much larger number of antennas in a larger venue as well in outdoor conditions.

References

[1] T. L. Marzetta, "Noncooperative cellular wireless with unlimited numbers of base station antennas," *IEEE Transactions on Wireless Communications*, vol. 9, no. 11, pp. 3590–3600, 2010.

[2] A. Poon, R. Brodersen, and D. Tse, "Degrees of Freedom in Multiple Antenna Channels: A Signal Space Approach," *IEEE Transactions on Information Theory*, vol. 51, no. 2, pp. 523–536, 2005.

[3] X. Gao, F. Tufvesson, O. Edfors, and F. Rusek, "Measured propagation characteristics for very-large MIMO at 2.6 GHz," in *2012 Conference Record of the Forty Sixth Asilomar Conference on Signals, Systems and Computers (ASILOMAR)*. IEEE, 2012, pp. 295–299.

[4] X. Gao, O. Edfors, F. Rusek, and F. Tufvesson, "Massive MIMO in real propagation environments." in *arXiv preprint arXiv:1403.3376*. arXiv, 2014, pp. 1–6.

[5] K. Kusume and M. Fallgren, "Updated scenarios , requirements and KPIs for 5G mobile and wireless system with recommendations for future investigations (Deliverable D1.5)," METIS, Tech. Rep., 2015.

[6] F. Bøhagen, P. Orten, and G. E. Øien, "Design of optimal high-rank line-of-sight MIMO channels," *IEEE Transactions on Wireless Communications*, vol. 6, no. 4, pp. 1420–1424, 2007.

[7] X. Gao, O. Edfors, F. Rusek, and F. Tufvesson, "Linear Pre-Coding Performance in Measured Very-Large MIMO Channels," in *Vehicular Technology Conference (VTC Fall), 2011 IEEE*. IEEE, 2011, pp. 1–5.

[8] J. Hoydis, C. Hoek, T. Wild, and S. ten Brink, "Channel measurements for large antenna arrays," in *2012 International Symposium on Wireless Communication Systems (ISWCS)*. IEEE, 2012, pp. 811–815.

[9] S. Payami and F. Tufvesson, "Channel measurements and analysis for very large array systems at 2.6 GHz," in *2012 6th European Conference on Antennas and Propagation (EUCAP)*. IEEE, 2012, pp. 433–437.

Paper B

Frequency Dependence of Measured Massive MIMO Channel Properties

Àlex Oliveras Martínez, Elisabeth De Carvalho,
Jesper Ødum Nielsen, and Lishuai Jing

1. Introduction

Abstract

A multi-user massive MIMO measurement campaign is conducted to study the channel propagation characteristics (e.g. user correlation, sum of eigenvalues and condition number), focusing on the stability over frequencies and the impact of the array aperture. We use 3 arrays with 64 antennas (6m linear array, 2m linear array and 25cm by 28cm squared 2D array) serving 8 users holding a handset with 2 antennas. The study of the measurements shows that the propagation characteristics of the channel are stable for all the measured frequencies. We also observe that user proximity and user handgrip reduce the dispersion of the studied properties of the channel across frequencies, and in such cases the larger the aperture of the array is, the less dispersed the properties are. Increasing the number of base station antennas improves the propagation characteristics of the channel and stabilizes the properties in the frequency domain.

1 Introduction

Massive MIMO is seen as one of the most promising technologies for 5G [1]. Marzetta describes it in his seminal work as a multi-user system in which a base station comprises a much larger number of antennas than the number of users, improving the performance of the conventional MIMO systems [2]. In certain propagation conditions it can achieve large gains in capacity, reliability and energy efficiency [3], [4]. Some channel propagation characteristics are favorable for massive MIMO systems [5].

In the literature, only a few measurements are carried out to study the channel propagation characteristics of massive MIMO [6], [7], [8], [9], [10], [11], [12]. Most of the existing measurement campaigns use virtual antennas. In this technique a single antenna is moved along a trajectory to measure the channel at several locations creating a virtual array. Due to the limitations of this technique (i.e. not simultaneous measurements) it is not realistic to measure dynamic users. Even if users remain static, a long time is needed to perform the measurements, which makes it arguable to consider a static environment. From the existing literature only [11] uses a large number of elements (i.e. 64 antennas) and measures all the channel links quasi simultaneously. It is also the only measurements performed in large indoor scenarios, similar to shopping malls, airports' halls, which are considered by the authors to be the future scenarios where massive MIMO will be deployed.

In this contribution we use measured massive MIMO channels to study the channel propagation characteristics (e.g. user correlation, sum of eigenvalues and condition number) at several frequencies. We compare the results at each frequency to study their variation. Our goal is to investigate if the results presented in [11] can be extended to a larger range of frequencies, and

therefore useful in multicarrier systems. To the authors knowledge this is the first analysis of wideband massive MIMO channels. It distinguishes itself from other measurement based studies because it does not use virtual antennas. The data used for the study is obtained in a measurement campaign described in [11].

2 Measurements

2.1 Location

We conducted a large indoor measurement campaign at Aalborg University, see Fig. B.1 and Fig. B.2. The considered environment is similar to a shopping mall which has a large open space in the center with high ceiling (used for line-of-sight (LoS) measurements) and a smaller lateral space with low ceiling (used for non-line-of-sight (NLoS) measurements). There is a staircase going from the center of the open space to an upper level.

2.2 Base station array

64 monopole antenna elements are used at the base station. The monopoles are grouped in sets of 8 elements separated by $\lambda/2$ (where λ is the wavelength) and 2 dummy monopoles are placed at the edges so that active elements have similar surroundings. The sets are grouped in 3 ways to form arrays with different aperture. The first array, referred to as Very Large Aperture (VLA), is 6 m long, and it is constructed by grouping the sets longitudinally with a separation of 50 cm between them. The second array is a 2 m uniform linear array, named as Large Aperture (LA). To build this array we place the sets of antennas longitudinally next to each other. The third array is a compact 2D array (C2D), with dimensions 25 cm by 28 cm. This array has the antennas sets stacked on top of each other, see Fig. B.3. The base stations (BS) arrays are placed in the lateral wall in the large space at 4 meters height. The arrays are parallel to the staircase.

2.3 Users and handsets

In the measurements the users hold a mockup handset to simulate a scenario in which 8 users are simultaneously connected to a base station (BS). They hold the mockup simulating the use of data capabilities of a phone (i.e. the mockup is placed in front of the thorax and the flat surface of the handset pointing to the face). The handsets have four patch antennas (one at each corner), but only the two antennas in the top are used, see Fig. B.4. The users move randomly inside a square of $1\,\mathrm{m}^2$ area to generate small scale fading but without changing the large scale properties of the channel. To study the

effect of user proximity, we consider two handgrip cases. In the hand free case, handsets are attached to a table, and this is moved in a small area. In a more realistic case the users are allowed to grab the mockup according to their preferences.

2.4 Scenarios

We name scenarios according to the dispositions of the users.

1. Spread LoS Parallel: The users are in the large space, four users in front of the stairs and four behind the stairs. The users are facing the BS array (i.e. the two antennas of the handset form an array parallel to the BS array). See Fig. B.1 top-left and Fig. B.2.

2. Spread NLoS: The users are placed in the lateral space. The handset arrays are parallel to the BS array. See Fig. B.1 top-right and Fig. B.2.

3. Grouped LoS: The users are in the large room behind the stairs. They start right next to each other, then they walk away from each other during the measurements, increasing the distance between them. The handset arrays are parallel to the BS array. See Fig. B.1 bottom-right.

4. Free Space in front the stairs: In this scenario there are no users. The eight handsets are attached to a table, in two rows of four handsets. The table is placed in front of the stairs in the large room. There is a person sitting on the floor and moving the table to generate the fading. See Fig. B.1 bottom-left.

2.5 Channel sounder

A MIMO channel sounder is used at $5.8\,\text{GHz}$ central frequency with $100\,\text{MHz}$ bandwidth. It is partly parallel and has a fast switching mechanism to measure 64x16 channels semi-simultaneously (i.e. $655\,\mu s$), so we can consider the channel to be static during the measurement interval. 1200 time-domain samples of the channel are recorded in $20\,\text{s}$.

3 Data analysis

The channel impulse responses are obtained from the sounder. We apply a Fast Fourier Transform to generate the channel matrices.

We denote $\mathbf{h}_{krf}^{(n)} \in \mathbb{C}^{M\times 1}$ as the channel vector from antenna $n \in \{a,b\}$ in the handset of user $k \in \{1,...,8\}$ to the BS array in the realization $r \in \{1,...,1200\}$ and frequency index $f \in \{1,...,50\}$, with $M = 64$ denoting the number of base station antennas. The sub-channel bandwidth is $2\,\text{MHz}$. In
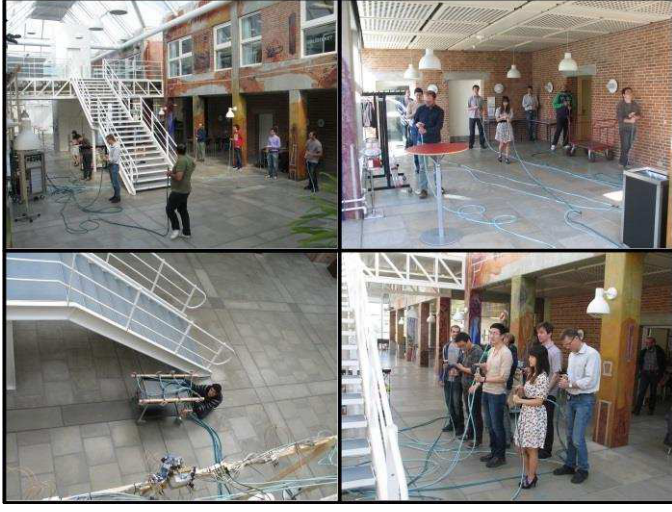
Fig. B.1: Top-left, Spread users LoS parallel. Top-right, Spread users NLoS. Bottom-left, Free space in front of the stairs. Bottom-right, Grouped users LoS
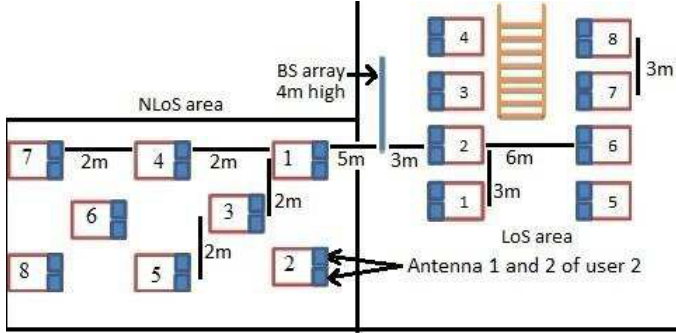
Fig. B.2: Floor map with location of BS array, LoS area, NLoS area and user numbering

matrix $\mathbf{H}_{krf} \in \mathbb{C}^{M \times N}$ the two user channel vectors of user k at realization r and frequency index f are placed in two consecutive columns, with $N = 2$ denoting the number of antennas in a single device. The matrix $\mathbf{H}_{rf} \in \mathbb{C}^{M \times KN}$ (where $K = 8$ is the number of users) contains each user matrix $\mathbf{H}_{krf}$ in a consecutive column.

By normalizing the channel power we create a virtual power gain control so all the users receive the same power regardless their distance to the base
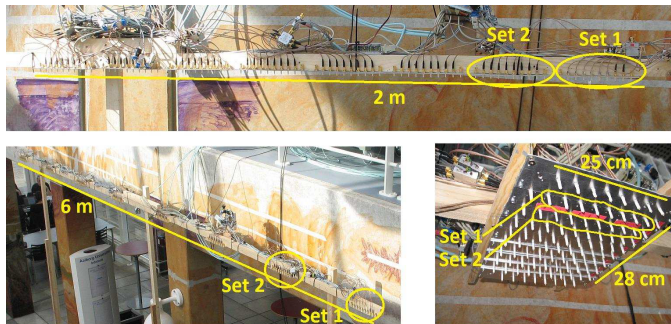
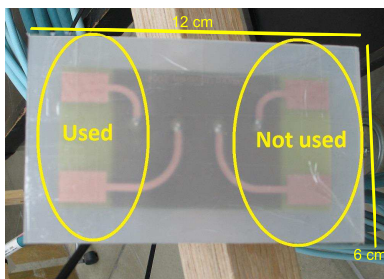**Fig. B.3:** Bottom-left: VLA, Top: LA and Bottom-right: C2D

Fig. B.4: Handset with four antennas. Only two are used

station. The normalized channel vector is

$$\bar{\mathbf{h}}_{krf}^{(n)} = \frac{\mathbf{h}_{krf}^{(n)}}{\left\| \mathbf{h}_{krf}^{(n)} \right\|} \sqrt{M} \tag{B.1}$$

with $\|\ \|$ denoting the euclidean norm. With this normalization, the results will be determined by the channel eigenvalue distribution and not by the power imbalance between users due to different locations or different antenna efficiencies.

4   Results

4.1   Orthogonality properties

The orthogonality of the channel vectors is a key factor to achieve the expected performance of massive MIMO. In order to study the channel properties of massive MIMO we analyze the scalar product between the spatial signatures (i.e. channel vectors) of all the possible pairs of antennas.

We compute the orthogonality matrix between channel vectors of the normalized channel and we average the result for all the channel realizations. The sub-index k_1 and k_2 are the two users, and the supra-index are the antennas of the users (n_1 and n_2 respectively). The scalar product calculated at frequency index f, reads

$$s_{k_1 k_2, f}^{(n_1 n_2)} = \frac{1}{R} \sum_{r=1}^{R} \frac{|(\mathbf{h}_{k_1 r f}^{(n_1)})^\dagger \mathbf{h}_{k_2 r f}^{(n_2)}|}{\left\| \mathbf{h}_{k_1 r f}^{(n_1)} \right\| \left\| \mathbf{h}_{k_2 r f}^{(n_2)} \right\|}, \tag{B.2}$$

where R is the number of channel realizations. The complete orthogonality matrix $\mathbf{S}_f$ (with dimensions (8x2)by(8x2)) is created using these scalar products as its entries.

In Fig. B.5, we give insights on $\mathbf{S}_f$ selecting the Free space in front of the stairs scenario at the center frequency. The axis show the number of each user, but notice that each user has two antennas. The sixteen values in the diagonal represent the auto-scalar-product of the 16 antennas at the user side. The eight 2x2 blocks in the diagonal are the cross-scalar-product between antennas in the same device (there are 8 devices). The other values are the cross-scalar-product between antennas in different devices. In Fig. B.5 we can see that the LA array has not enough resolution to separate the two antennas from the same user handset (i.e. 2x2 squares in the diagonal) since the scalar product coefficients are large. On the other hand the VLA has enough spatial resolution to make the intra-user channels orthogonal. The C2D array has the worst performance of the 3 arrays.

In this work we investigate the statistics of the spatial domain orthogonality along the frequencies. We compute the standard deviation (std.) for each entry of the matrix $\mathbf{S}_f$ over all the frequencies:

$$std_{k_1 k_2}^{(n_1 n_2)} = \sqrt{\frac{1}{N-1} \sum_{f=1}^{N} |s_{k_1 k_2, f}^{(n_1 n_2)} - \mu_{k_1 k_2}^{(n_1 n_2)}|^2}, \tag{B.3}$$

where $N = 50$ is the number of studied frequencies and μ is the mean scalar product over the frequencies.

This metric shows how the scalar product for each pair of user antennas varies in the frequency domain. The larger the standard deviation (std.), the more disperse is the scalar product over frequencies and vice versa. The std. is presented in linear scale. Notice that the matrix diagonal has 0 standard deviation because the scalar product has always the same value (i.e. maximum scalar product 1).

To investigate the user proximity on the channel properties, in Fig. B.6, we study the Free space scenario as a benchmark to compare the scenarios with users (i.e. Fig. B.7). We observe a larger std. in the Free space scenario compared with other scenarios. As in this scenario there are no users, we can
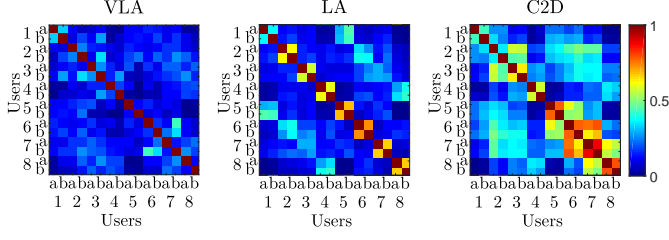
Fig. B.5: Correlation matrix at the center frequency for the scenario: Free space in front of the stairs
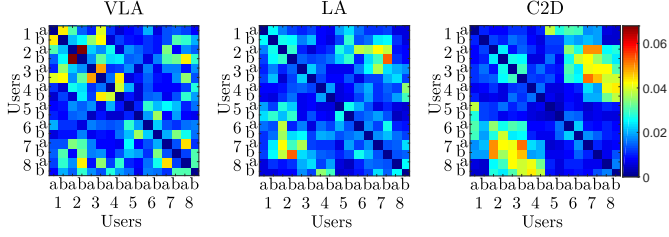
Fig. B.6: Std of the correlation matrix for the scenario: Free space in front
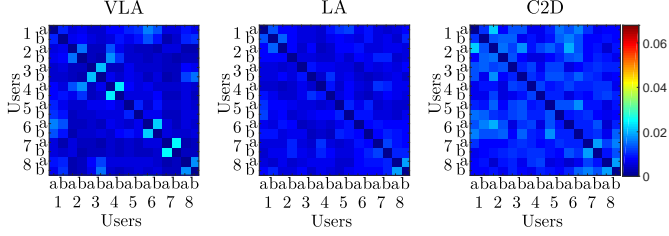

Fig. B.7: Std of the correlation matrix for the scenario: Grouped users in LoS

say that the absence of user destabilizes the orthogonality for all the frequencies. This may be because the users introduce scattering and the scattering averages the properties of the channels.

In Fig. B.7 (i.e. Grouped LoS scenario) we see that the std. averaged over all the pairs of antennas is different for the linear arrays and the compact array. The linear arrays have less std. than the compact array. We conclude that having larger aperture arrays makes the orthogonality between user channel vectors more stable in the frequency domain. It is also noticeable that the VLA has some pairs of antennas with a slightly higher std. (e.g. user 1 antenna *a* with user 6 antenna *a*). When the array is very large the location of the antennas plays an important role to determine its orthogonality. Small variations on the antenna location can make large variations in the scalar product of the channels.

4.2 Inter-user properties

Massive MIMO is intended to serve a large number of users simultaneously, therefore we investigate the effect of increasing the number of users in the system. We study the inter-user channel properties. We consider single antenna users and we sum the eigenvalues of the channel matrix when increasing the number of users in the system. This metric is called Normalized Parallel Channel Gain (NPCG), and it is closely related to the sum capacity of the channel. Denoting λ_{irf} as the ith eigenvalue of the matrix $\bar{\mathbf{H}}_{rf}^{H}\bar{\mathbf{H}}_{rf}$ at realization r and frequency index f, then the metric is defined as:

$$\text{NPCG}_{rf} = \frac{1}{\lambda_{\max,rf}} \sum_{i=1}^{C} \lambda_{irf}, \tag{B.4}$$

where $\lambda_{\max,rf}$ is the largest eigenvalue and C is the number of users that increases from 1 to 8.

This metric is similar to the condition number. We compute the NPCG instead of the condition number because in systems with more than two eigenvalues, the condition number hides information (showing only the variation between the maximum and minimum eigenvalues), but the NPCG adds the contribution of all the eigenvalues. Notice that the best channel with equal eigenvalues would have a NPCG equal to the number of single antenna users.

Fig. B.8 shows the mean and standard deviation of the NPCG over all the frequencies for each number of users in the Grouped LoS scenario. The mean values have the same trend seen in [11] for the central frequency. The VLA gives the highest NPCG. It is followed by the LA, and the C2D is the worst array. We observe that the standard deviation is relatively small for all the arrays. The different frequencies infer small variations on the NPCG of the channel. Another remarkable property is that increasing the number of users in the system increases the standard deviation slightly. This may be because having more users in the system makes the spatial signatures to occupy more dimensions of the channel subspace and it is more difficult to have each spatial signature orthogonal to the others. So a small change in the user position makes the channel vector correlated with other user's channel vectors. This effect is accentuated when the users are close to each other.

4.3 Intra-user properties

Massive MIMO can create very narrow beams due to its large aperture arrays. We study the channel properties between the antennas in the same device to analyze the spatial resolution of the beams. In this case we calculate the condition number because there are only two antennas in the devices and the channel matrix has only two eigenvalues. The condition number can
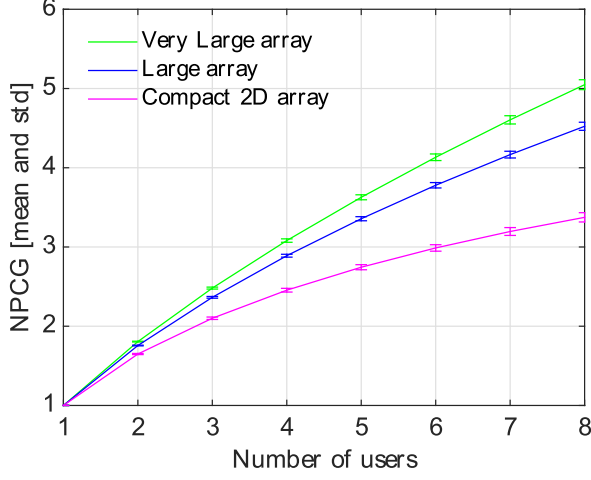
Fig. B.8: Mean and Std over frequency of the sum of squared singular values for the scenario: Grouped users in LoS

therefore reveal the channel properties. The condition number is computed as,

$$\text{CN}_{krf} = 10 \log_{10}\left(\frac{\lambda_{\text{max},krf}}{\lambda_{\text{min},krf}}\right), \tag{B.5}$$

where $\lambda_{\text{max},krf}$ and $\lambda_{\text{min},krf}$ are the maximum and minimum eigenvalues of the MIMO channel matrix $\bar{\mathbf{H}}_{krf}^{H}\bar{\mathbf{H}}_{krf}$. k is the user, r is the time snapshot and f is the frequency index.

Statistics of the condition number are taken over all the users and realizations of the channel. The mean and standard deviation of the condition number are plotted for each frequency in Fig. B.9 for the VLA in the Free space in front of the stairs scenario, and Fig. B.10 for the VLA in the Spread NLoS scenario.

Comparing the results in Fig. B.9 and Fig. B.10 we show that the channel properties in the scenarios with users and NLoS are more stable than in the scenarios without users. The user proximity, the handgrip and the NLoS scatterers introduce multiple paths in the channel, leading to an average of the channel making the channel condition less disperse over frequencies. In the Free space scenario, the channel is dominated by the LoS path, leading to more responsiveness to frequency variations. This result has also been observed in all the other parameters analyzed in this paper. From these figures we can also observe that the std. remain practically constant for all the frequencies. This means that the variation of the condition number over
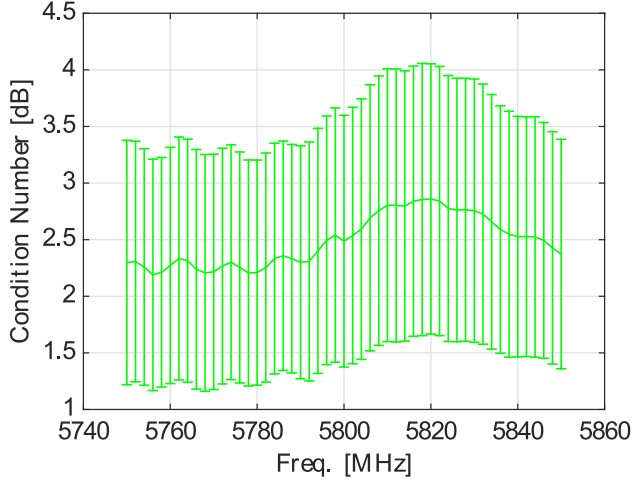
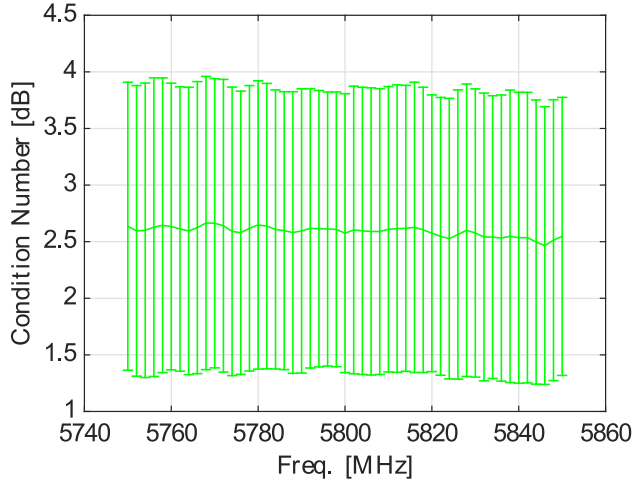**Fig. B.9:** Mean and Std of condition number for the scenario: Free space in front of the stairs, VLA

the time domain (closely related with the outage probability) is the same for all the frequencies.

Next we study the impact of the number of antennas on the condition number. Fig. B.11 shows the statistics of the condition number as the number of base station antennas increases from 2 to 64. We select the antennas from the beginning of the array (i.e. the antennas near to the bridge), and the antennas are taken in a consecutive order. We take the average over all the frequencies for both the mean and the std. and we plot the curves for the three arrays together in the scenario Spread LoS. We observe from Fig. B.11 that the VLA always has the minimum mean and std. of the condition number. In second position we can find the LA, and the worse array is the C2D. Increasing the number of antennas improves the channel properties because the mean and std. of the condition number decreases.

5   Summary

In this work the channel properties in the frequency domain of a wide-band massive MIMO system are analyzed. The orthogonality properties are studied using the scalar product, the inter-user properties are analyzed using the NPCG and the intra-user properties are analyzed using the condition number. In scenarios with users the studied channel characteristics are less disperse than scenarios with no users. In this case, it is also possible to see that the larger the aperture of the array, the more stable the properties of the chan-

Fig. B.10: Mean and Std of condition number for the scenario: Spread NLoS, VLA
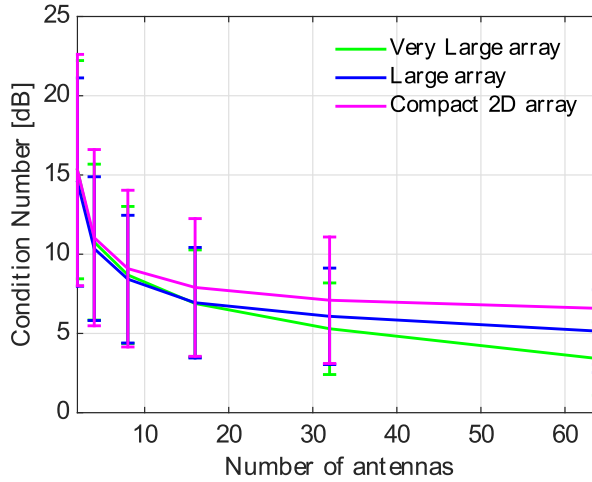
Fig. B.11: Mean and Std of condition number averaged for all the frequencies for the scenario: Spread LoS Parallel

nel across different frequencies. It is advantageous to use a large number of antennas at the base station, because the channel condition number becomes smaller and it becomes more stable across the investigated frequencies.

References

[1] F. Boccardi, R. Heath, A. Lozano, T. L. Marzetta, and P. Popovski, "Five disruptive technology directions for 5G," *IEEE Communications Magazine*, vol. 52, no. 2, pp. 74–80, 2014.

[2] T. L. Marzetta, "Noncooperative cellular wireless with unlimited numbers of base station antennas," *IEEE Transactions on Wireless Communications*, vol. 9, no. 11, pp. 3590–3600, 2010.

[3] H. Q. Ngo, E. G. Larsson, and T. L. Marzetta, "Energy and spectral efficiency of very large multiuser MIMO systems," *IEEE Transactions on Communications*, vol. 61, no. 4, pp. 1436–1449, 2013.

[4] F. Rusek, D. Persson, B. K. Lau, E. G. Larsson, T. L. Marzetta, O. Edfors, and F. Tufvesson, "Scaling Up MIMO: Opportunities and Challenges with Very Large Arrays," *IEEE Signal Processing Magazine*, vol. 13, no. 1, pp. 40–60, 2013.

[5] H. Q. Ngo, E. Larsson, and T. Marzetta, "Aspects of Favorable Propagation in Massive MIMO," in *Signal Processing Conference (EUSIPCO), 2014 Proceedings of the 22nd European*, no. 2.   IEEE, 2014, pp. 76–80.

[6] X. Gao, F. Tufvesson, O. Edfors, and F. Rusek, "Measured propagation characteristics for very-large MIMO at 2.6 GHz," in *2012 Conference Record of the Forty Sixth Asilomar Conference on Signals, Systems and Computers (ASILOMAR)*.   IEEE, 2012, pp. 295–299.

[7] X. Gao, O. Edfors, F. Rusek, and F. Tufvesson, "Massive MIMO in real propagation environments." in *arXiv preprint arXiv:1403.3376*.   arXiv, 2014, pp. 1–6.

[8] ——, "Linear Pre-Coding Performance in Measured Very-Large MIMO Channels," in *Vehicular Technology Conference (VTC Fall), 2011 IEEE*. IEEE, 2011, pp. 1–5.

[9] J. Hoydis, C. Hoek, T. Wild, and S. ten Brink, "Channel measurements for large antenna arrays," in *2012 International Symposium on Wireless Communication Systems (ISWCS)*.   IEEE, 2012, pp. 811–815.

[10] S. Payami and F. Tufvesson, "Channel measurements and analysis for very large array systems at 2.6 GHz," in *2012 6th European Conference on Antennas and Propagation (EUCAP)*.   IEEE, 2012, pp. 433–437.

[11] À. Oliveras Martínez, E. D. Carvalho, and J. Ø. Nielsen, "Towards Very Large Aperture Massive MIMO: a measurement based study," in *Globecom Workshops (GC Wkshps), 2014*.   IEEE, 2014, pp. 281–286.

[12] J. Flordelis, X. Gao, G. Dahman, F. Rusek, O. Edfors, and F. Tufvesson, "Spatial separation of closely-spaced users in measured massive multi-user MIMO channels," in *IEEE International Conference on Communications*. IEEE, 2015, pp. 1441–1446.

References

Paper C

Massive MIMO Properties based on Measured Channels: Channel Hardening, User Decorrelation and Channel Sparsity

Àlex Oliveras Martínez, Elisabeth De Carvalho, Jesper Ødum Nielsen

Abstract

Three prominent features of massive MIMO are studied using channel measurements. Those features are extensively exploited in signal processing methods for massive MIMO and have been only partially, or not at all, validated. First, channel hardening is characterized as a function of the number of antennas. Second, user decorrelation is evaluated as a function of the distance between users. At last, the channel angular spread, proposed as a basis for pilot contamination and frequency division duplexing operation, is assessed. The whole study is based on two measurement campaigns involving a base station with 64 antennas and 128 antennas.

1   Introduction

A massive MIMO system is a multi-user wireless system where the base station is equipped with a very large number of antennas. It is one of the key technologies intended for 5G wireless systems [1] as it brings large improvements in throughput and energy efficiency [2–4]. Those improvements are due to the increase in spatial degrees of freedom brought by the larger dimension of the arrays along with the larger number of antennas. Those augmented degrees of freedom lead to the remarkable properties of massive MIMO, not only boosting performance but also simplifying the multi-user processing.

One property of massive MIMO is its ability for channel hardening. A proper transmit or receive multi-antenna processing at the base station (BS) enables the formation of beams that are statistically stable: the resulting equivalent channel becomes asymptotically deterministic, depending only on large scale fading parameters.

Another property is the asymptotic decorrelation of the users as the number of antennas becomes large, meaning that their channel vectors become asymptotically orthogonal. Asymptotic user decorrelation combined with increased beamforming gain to each user explain the high throughput that can be achieved by massive MIMO. Channel hardening entails a simplification in the decoding at the user as well as in the resource allocation and user scheduling as the equivalent channels are slowly varying.

At last, as massive MIMO defines a larger number of angular degrees of freedom, propagation environments could exist where the propagation paths to a given device occupy a small number of angular degrees of freedom, meaning that their (cumulative) angular spread is small. This property is used in [5] as a basis for frequency division duplexing operation in massive MIMO and as a user discrimination method to suppress pilot contamination in [6].

Due to the lack of channel measurements, the properties of massive MIMO

are still largely unverified. In this paper, based on two measurement campaigns, we study the three aforementioned properties of the massive MIMO channel: 1) channel hardening, 2) user decorrelation, 3) channel low angular spread. One major technical obstacle in performing channel measurements for massive MIMO comes from the difficulty of measuring the many channel links involved in massive MIMO. Most of the existing campaigns assume a quasi-static environment where one antenna or a group of antennas is moved at each measurement to form a virtual array. For example, moving 7 antennas to form a 112 antenna array [7], or moving a single antenna to create a 128 antenna array [8]. Only [9–11] propose campaigns where the multiple links are measured within a short duration based on a switching mechanism at the BS. Most of the existing studies focus on evaluating the performance of linear precoders in massive MIMO conditions [12, 13]. And some others study the impact of the array shape [10, 14].

We use the data from two measurement campaigns. The first measurements took place in a large indoor environment, with a 64-antenna BS and had as main purpose to study the impact of the massive array dimension. The second measurement campaign was outdoors and had as main purpose the study of the inter-user properties. The main conclusions of our study are as follows:

- Channel hardening: in both indoor and outdoor, strong line-of-sight (LOS) or non-line-of-sight (NLOS) with poor scattering environment, we observe a channel hardening increase as the number of antennas increases. Channel hardening can be significantly weaker in measurements compared to the Gaussian channel. In an indoor environment, the arrays with largest aperture tend to bring the strongest channel hardening.

- User decorrelation: in an outdoor environment, we test the user correlation according to the inter-user distance. In LOS, the full size array (128 antennas) is able to separate the users irrespective of the inter-user distance, so that the correlation only depends on the array radiation pattern. With a reduced sized array, a stronger correlation is observed when the users are in close proximity. In NLOS, a strong correlation is observed with closely spaced users, even with the full array size: this suggests that the users share paths or clusters that cannot be discriminated by the BS array. In general, the array size and number of antennas decrease the inter-user correlation.

- Channel low angular spread: this property is tested in an indoor environment where rich scattering is expected. We verify that the channel tends to occupy a large portion of the angular space.

2 Measurements

The massive MIMO features are tested based on two measurement campaigns conducted at Aalborg University. One was indoors with 64 antennas at the BS and is called "indoor-64". The other one was outdoors with 128 antennas at the BS and is called "outdoor-128".

2.1 Measurement campaign indoor-64

The first campaign was performed in a large indoor venue with a base station with 64 antennas and 8 users each with a 2-antenna MIMO terminal. The 64 antennas are grouped in sets of 8 antennas. Rearranging the antenna sets, three different arrays were created: a very large aperture array (6 m long), a large array (2 m long) and a compact 2D array (25 cm×28 cm). Different user configurations are tested including spread users (denoted as S-LoS∥, S-LoS⊥, S-NLoS), closely spaced users (denoted as G-LoS, G-NLoS), in both LOS and NLOS scenarios. During one measurement, the users move randomly in a $1\,\mathrm{m}^2$ area to generate small-scale changes in the channel. More details can be found in [10].

2.2 Measurement campaign outdoor-128

The second campaign was carried out in a large courtyard at Aalborg University. A base station array consisting of 128 monopoles was used. The antennas are arranged in 8 sets of 16 elements separated by $\lambda/2$. Two dummy monopoles are added at the ends of each set so that all the active elements have similar properties. The sets are separated by approximately 34 cm to form a 6 m array. The array was placed on the outside wall of a building at approximately 4 m from the ground. The array can be seen in Fig. C.1.

The base station serves 2 users holding a mockup handset with 2 antennas. The handsets are the same as in indoor-64 and can be seen in [10]. The handsets were attached to the top of a stick. The users move the handset in a small area of about 10 cm by 10 cm to create small-scale channel changes, while they keep the lower end of the stick fixed in marked positions on the ground to control the approximate position. Fig. C.2 shows the two users during a measurement. Two scenarios were tested: LOS (i.e. in the courtyard, 30 m in front of the array) and NLOS (outside the field, behind a group of trees. At 60 m from the BS). The LOS channel was measured at 10 positions, and the NLOS channel was measured at 21 positions. In LOS the users increased their relative distance along a line parallel to the array. In NLOS the users followed orthogonal and crossing trajectories. The setup of the scenarios can be seen in Fig. C.3.

Fig. C.1: Base station array formed by 8 sets (sub-arrays) with 16 elements.

2.3 Channel sounder and normalization

The measurements were made with a correlation based channel sounder operating at 5.8 GHz and with a bandwidth of 100 MHz. The sounder measures a 8x16 MIMO channel fully in parallel in indoor-64 and 8x4 in outdoor-128, which is further extended by connecting the elements of each antenna set via a fast switch. During the measurements the 64x16 and 128x4 massive MIMO channels are sampled at a rate of 60 Hz during 20 s, for a total of 1200 channel realizations.

We use the Fourier Transform of the channel impulse responses obtained from the sounder and use the narrow band channel at the central frequency for analysis. We denote $\mathbf{h}_k(r) \in \mathbb{C}^{M \times 1}$ as the channel vector from user $k \in \{1, ..., 8\}$ in indoor-64 and $k \in \{1, 2\}$ in outdoor-128 to the BS array for channel realization $r \in \{1, ..., R\}$, where $R = 1200$ is the total number of channel realizations. $M = 64$ in indoor-64 and $M = 128$ in outdoor-128, is the number of BS elements. $h_{mk}(r)$ is the mth entry of the vector, corresponding to the mth element of the BS array.

The channel vectors are normalized as follows:

$$\overline{\mathbf{h}}_k(r) = \frac{\mathbf{h}_k(r)}{\sqrt{\sum_{r=1}^{R} \|\mathbf{h}_k(r)\|^2}} \sqrt{MR} \tag{C.1}$$

where $\|\cdot\|$ is the euclidean norm. This normalization creates a virtual power gain control that removes the user power imbalance but we keeps the differences among BS elements. We note that the average value of each channel coefficient is equal to 1.

3 Channel hardening

Firstly we analyze the channel hardening property of the massive MIMO system in our measurements as a function of the number of antennas at the BS. The metric of interest is the sum of the channel power over the antennas for one given snapshot. This corresponds to a post-processing by matched filtering. We show the standard deviation of the sum power.

For a selected subset of M' antennas, we compute the sum power for user

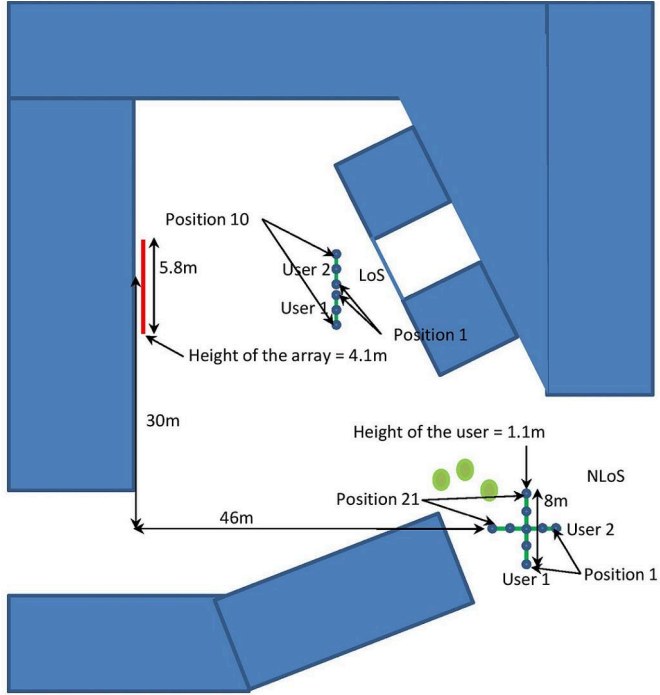**Fig. C.2:** 2 users in a NLOS scenario holding a 2 antennas mockup.

Fig. C.3: Floor map of the courtyard. Showing the positions of the users in orthogonal lines. Each lines has 21 positions.

k and snapshot r as:

$$\overline{P}_k(r) = \frac{1}{M'} \sum_{m=1}^{M'} |h_{mk}(r)|^2 \qquad (C.2)$$

71

The standard deviation is computed over the R realizations of the channel as

$$Std_k = \sqrt{\frac{1}{R}\sum_{r=1}^{R}(\overline{P}_k(r) - \mu)^2} \qquad \text{(C.3)}$$

where $\mu = \frac{1}{R}\sum_{r=1}^{R}\overline{P}_k(r)$ is the mean power over the snapshots.

Fig. C.4 shows the results for user 2 in the LOS and NLOS scenario of outdoor-128. The antennas are chosen in a consecutive order from the first antenna in the left side of the array. We compare the results with an independent identically distributed Gaussian random channel with same average power (named Gaussian in the figure). We observe that the variation of the average channel energy decreases when increasing the number of base station antennas. Those measurements show clearly a channel hardening in measured massive MIMO channels, but the measured hardening is not as strong as in the Gaussian channel.

We observe similar results in the LOS and NLOS scenarios. These results are similar for other users, user's antennas, and positions. In LOS, for a given snapshot, the power of each link is approximately the same across the antenna array. The sum power variations are due to the user's movement across the snapshots of one measurement.

In NLOS the standard deviation is consistently larger than the LOS case, i.e., the hardening is less than in the LOS environment. This is possible since not only the LOS component is reduced but also the distribution of the other components arriving via scattering is changed. Although the LOS component is blocked in the measured NLOS scenario, the main part of the energy is still expected from a few directions with relatively strong components, and thus not like the ideal Gaussian channel.

One way to define the hardening is as the ratio of the standard deviation obtained with 128 elements to the standard deviation obtained with a single antenna. With this definition the hardening for the simulated Gaussian case is about 60 dB while it is about 48 dB for the measured NLOS and LOS channels. While the difference between the simulated and measured channels is about 12 dB, the observed hardening is still very significant.

Fig. C.5 shows the same metric in indoor-64 for one of the users in a group of spread users in LOS of the array. The channel hardening effect is also confirmed in this measurement campaign and is due to combination of LOS and rich scattering. We see a hardening effect as the number of antennas increases. With a number of 64 antennas, the difference in the standard deviation can still be significant compared to the Gaussian case, especially for the compact 2D array. The results can vary for different users or scenarios, but statistics over all the users show that the very large array brings more hardening than the large array which in turn is better than the compact 2D array.

As a conclusion, from our measurements, we have observed a channel
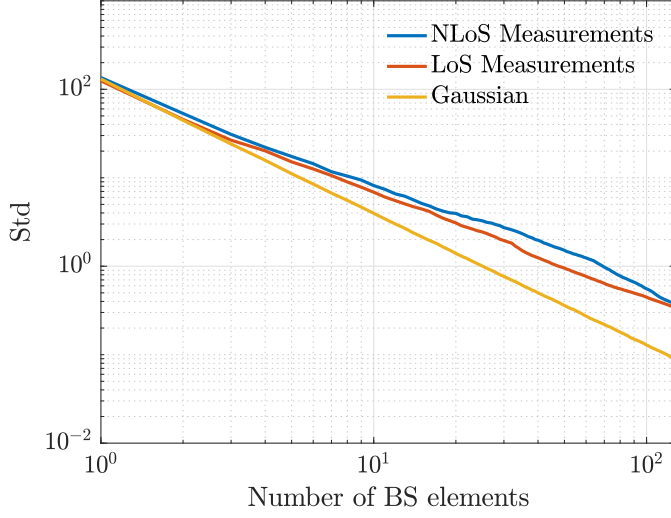
Fig. C.4: Variation in mean channel vector energy when increasing the base station antennas. User 1 antenna b
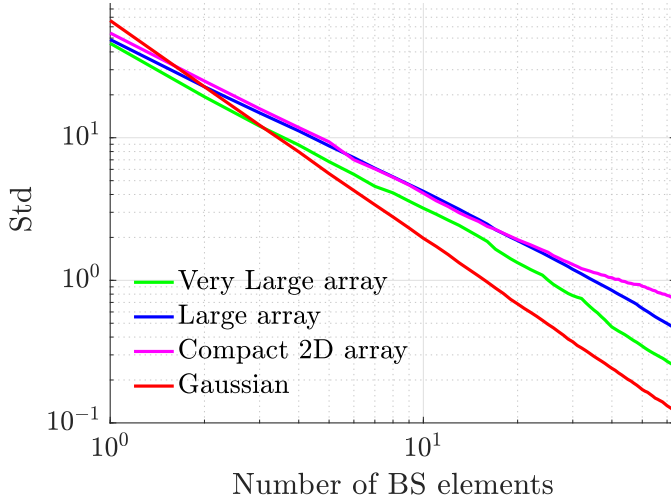
Fig. C.5: Variation in mean channel vector energy when increasing the base station antennas. Spread LOS parallel scenario

hardening as the number of antennas increases. The hardening slope is weaker than in the Gaussian channel case and can result in a significant gap in the sum power standard deviation. In an indoor environment, the array aperture is seen as an important factor in determining the hardening level.

4   User decorrelation

We focus on the scalar product of the channel vectors of 2 users with specific separation, defined for snapshot r as

$$SP(r) = \frac{\left|\overline{\mathbf{h}}_1(r)^H \overline{\mathbf{h}}_2(r)\right|}{\left\|\overline{\mathbf{h}}_1(r)\right\| \left\|\overline{\mathbf{h}}_2(r)\right\|} \tag{C.4}$$

where $|\cdot|$ is the absolute value, and the superscript H denotes the conjugate transpose. We show the average value of $SP(r)$ over the different snapshots of a same measurement.

Fig. C.6 shows the result in the NLOS scenario for different numbers of antennas. The antennas are chosen in a consecutive order from the first antenna in the left side of the array. Looking at the maximum number of base station antennas (i.e. 128 antennas) we observe that the closer the users are, the larger the scalar product is. The decorrelation distance can be obtained for a target correlation. For a correlation of 0.25, the decorrelation distance is approximately 65 cm (12 times the wavelength). For a smaller number of base station antennas we observe a larger correlation. When the users are well separated even a small number of antennas can separate the users. When the users are very close, their channels are very correlated regardless of the number of base station antennas. The reason is that the closer the users, the more similar the surroundings and the scatterers the signal propagates through, and, thus, their channels are more correlated.

Fig. C.7 shows the results in the LOS scenario for different numbers of antenna. We observe that only the full array size with 128 antennas is able to separate the 2 users when they are closely spaced, while the other array sizes show an increase in the correlation. Furthermore, for larger inter-user distance, the correlation appears to follow the radiation pattern of the array where grating lobes are visible.

As a conclusion, we observe a clear decrease of the correlation brought by an increased number of antennas. In LOS, correlation appears almost constant as the inter-user distance varies for the full size array because it is able to separate the users even very closely spaced. In NLOS, when the users are close to each other, even the full size array leaves a high inter-user correlation, implying that the users share path or clusters that cannot be distinguished by the array.

5   Channel Angular Spread

Finally, we study the channel angular spread of the massive MIMO channel for indoor-64. We base this study on the covariance matrix of the vectorial
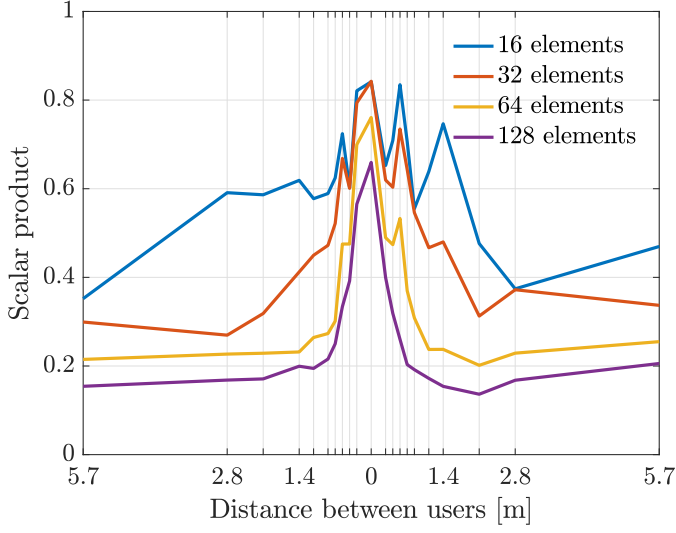
Fig. C.6: Channel vector scalar product between user 1 and user 2, NLOS scenario, increasing number of base station antennas
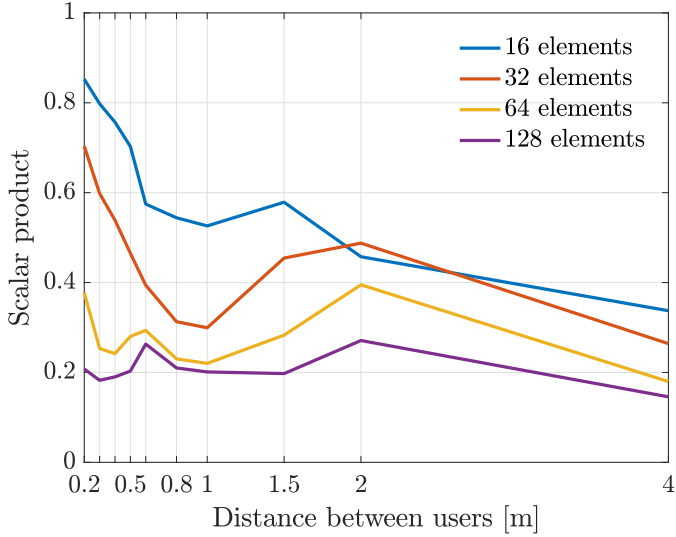
Fig. C.7: Channel vector scalar product between user 1 and user 2, LOS scenario

received signals at the BS when the user moves locally, i.e during a measurement segment. For user k, the covariance matrix is defined as:

$$\mathbf{C}_k = \frac{1}{R} \sum_{r=1}^{R} \mathbf{h}_k(r)\mathbf{h}_k(r)^H \tag{C.5}$$

75

Fig. C.8: Normalized eigenvalues profile, User 1, C2D, LOS and NLOS scenarios in indoor-64
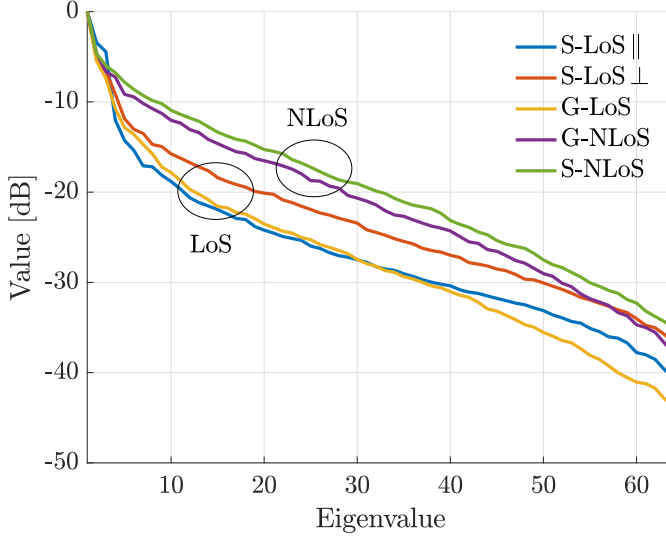
The covariance matrix gives a description of the angular space occupied by the user during this movement. In particular, if the angular spread of the channel is limited, then a large portion of the eigenvalues of the covariance matrix will be very small compared to the largest one.

Fig. C.8 shows the value of all the eigenvalues for one given user and the smallest array (C2D), for the LOS and NLOS scenarios in indoor-64. From the figure we observe that the NLOS scenarios gives larger eigenvalues than the LOS scenario. This is expected since the NLOS scenarios involve more scattering so that the user occupies a larger angular space. The eigenvalue profile is similar to the profile obtained with simulated channels (Winner cluster-based channels) where the paths occupy the whole angular space.

As a complement to the eigenvalue profile of the covariance, Fig. C.9 shows the angular distribution of the channel. For each array subset of 8 antennas, the angular power distribution (i.e. the power after receive processing by the steering vectors obtained by sweeping the angular space) is shown for each snapshot. Clearly, the figure shows a rich-scattering environment, confirming the eigenvalue profile observed in Fig. C.8.

As a conclusion, as it can be expected in an indoor rich scattering environment, the measurements confirm that channel tends to occupy a large portion of the angular space.
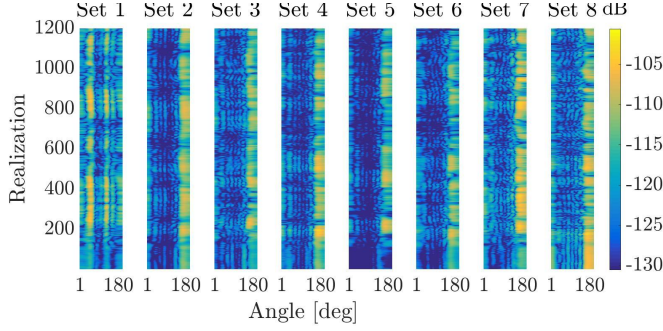
Fig. C.9: Minimum number of eigenvalues that has at least half of the total power, User 1, S-LoS ⊥

6 Conclusion

Two measurement campaigns are used to investigate three prominent properties of massive MIMO channels: channel hardening, user decorrelation and channel angular spread. The first measurement campaign involves a 64-antenna base station and the second ones involves a 128-antenna base station. The measurements show a channel hardening for both LOS and NLOS scenario brought by massive MIMO, but that can be significantly weaker than in the Gaussian channel case. Correlation properties are different in both LOS and NLOS. In LOS, correlation is determined by the angular resolution of the array and its ability to separate the users spatially. In NLOS, the measurements suggest common paths or clusters that cannot be resolved by the array, when the users are in close proximity. Finally, in a rich indoor scattering environment, the channel appears to occupy a large part of the angular space defined by the massive array.

References

[1] A. Osseiran, J. F. Monserrat, and P. Marsch, *5G Mobile and Wireless Communications Technology*, 1st ed. Cambridge University Press, 2016.

[2] T. L. Marzetta, "Noncooperative cellular wireless with unlimited numbers of base station antennas," *IEEE Transactions on Wireless Communications*, vol. 9, no. 11, pp. 3590–3600, 2010.

[3] F. Rusek, D. Persson, B. K. Lau, E. G. Larsson, T. L. Marzetta, O. Edfors, and F. Tufvesson, "Scaling Up MIMO: Opportunities and Challenges with Very Large Arrays," *IEEE Signal Processing Magazine*, vol. 13, no. 1, pp. 40–60, 2013.

[4] E. G. Larsson, O. Edfors, F. Tufvesson, and T. L. Marzetta, "Massive MIMO for Next Generation Wireless Systems," *IEEE Communications Magazine*, vol. 52, no. 2, pp. 186–195, 2014.

[5] A. Adhikary, J. Nam, J.-Y. Ahn, and G. Caire, "Joint Spatial Division and Multiplexing," *IEEE Transactions on information theory*, vol. 59, no. 10, pp. 6441–6463, 2013.

[6] H. Yin, L. Cottatellucci, D. Gesbert, R. R. Muller, and G. He, "Pilot decontamination using combined angular and amplitude based projections in massive MIMO systems," in *2015 IEEE 16th International Workshop on Signal Processing Advances in Wireless Communications (SPAWC)*. IEEE, 2015, pp. 216–220.

[7] J. Hoydis, C. Hoek, T. Wild, and S. ten Brink, "Channel measurements for large antenna arrays," in *2012 International Symposium on Wireless Communication Systems (ISWCS)*. IEEE, 2012, pp. 811–815.

[8] S. Payami and F. Tufvesson, "Channel measurements and analysis for very large array systems at 2.6 GHz," in *2012 6th European Conference on Antennas and Propagation (EUCAP)*. IEEE, 2012, pp. 433–437.

[9] X. Gao, O. Edfors, F. Rusek, and F. Tufvesson, "Linear Pre-Coding Performance in Measured Very-Large MIMO Channels," in *Vehicular Technology Conference (VTC Fall), 2011 IEEE*. IEEE, 2011, pp. 1–5.

[10] À. Oliveras Martínez, E. D. Carvalho, and J. Ø. Nielsen, "Towards Very Large Aperture Massive MIMO: a measurement based study," in *Globecom Workshops (GC Wkshps), 2014*. IEEE, 2014, pp. 281–286.

[11] J. Flordelis, X. Gao, G. Dahman, F. Rusek, O. Edfors, and F. Tufvesson, "Spatial separation of closely-spaced users in measured massive multiuser MIMO channels," in *IEEE International Conference on Communications*. IEEE, 2015, pp. 1441–1446.

[12] X. Gao, F. Tufvesson, O. Edfors, and F. Rusek, "Measured propagation characteristics for very-large MIMO at 2.6 GHz," in *2012 Conference Record of the Forty Sixth Asilomar Conference on Signals, Systems and Computers (ASILOMAR)*. IEEE, 2012, pp. 295–299.

[13] X. Gao, O. Edfors, F. Rusek, and F. Tufvesson, "Massive MIMO Performance Evaluation Based on Measured Propagation Data," *IEEE Transactions on Wireless Communications*, vol. 14, no. 7, pp. 3899–3911, 2015.

[14] M. Gauger, J. Hoydis, C. Hoek, H. Schlesinger, A. Pascht, and S. ten Brink, "Channel Measurements with Different Antenna Array Geometries for Massive MIMO Systems," in *SCC 2015; 10th International ITG Conference on Systems, Communications and Coding*. IEEE, 2015, pp. 1–6.

Paper D

Impact of Array Aperture in Massive MIMO: a Measurement based Study

Àlex Oliveras Martínez, Elisabeth De Carvalho, and Jesper Ødum Nielsen

Abstract

*A multi-user massive MIMO measurement campaign is conducted to study the channel propagation characteristics, focusing on the impact of the array aperture which is a limiting factor on degrees of freedom available in the multiple antenna channel. We use **3** arrays with **64** antennas (**6m** linear, **2m** linear and **25**cm by **28**cm squared) serving **8** users each holding a handset with **2** antennas. The scenarios include LoS or NLoS with spread or grouped users, as well as without users. We observe the benefits of using a very large aperture of the array gathering more degrees of freedom. Spread users perform better than group ones, and in LoS they perform better than in NLoS. We also assess the performance of very large aperture arrays serving crowded scenarios and resolving antennas in the same user device. The MIMO capabilities of the handset are better exploited in NLoS and grouped users due to the larger degree of scattering. We observe the improvement brought by increasing the number of antennas, but at a slower pace for the compact array.*

1 Introduction

In a massive MIMO (Multiple-Input Multiple-Output) system [1], one base station (BS) equipped with a very large number of antenna elements serves simultaneously multiple users. When the number of BS antennas is much larger than the number of served users, extra spatial degrees of freedom (DoF) appear in this over-determined system. Those extra DoF bring key enhancements in the properties of the multi-user massive MIMO channel, as they allow an averaging of random quantities, such as fast fading, receive noise, inter-user interference, and ultimately make them deterministic. Massive MIMO brings the promise of huge gains in throughput and energy efficiency [2, 3] propelling it as a primary candidate technology for 5G wireless systems [4–7].

The spatial DoFs, or rank of the multi-user MIMO channel, play a central role in characterizing the performance of a massive MIMO system. The conventional assumption of an independent and identically distributed (i.i.d.) Gaussian channel implies that the DoFs are solely limited by the number of antennas. In reality, the DoFs are limited by the size of the BS array, the aperture [8], or the propagation environment. In line-of-sight (LoS) propagation, it is obvious as the beamwidth is determined by the array aperture. In an environment with scattering, the performance is in addition governed by the size of the scattering clusters and how they are seen from the BS array and the user terminals. Increasing the number of antennas in the array increases the spatial sampling of the signal and may yield more DoF, but the DoF are limited by the aperture of the array and the spatial Nyquist sampling theorem.

The role played by the array aperture motivates the measurement campaign presented in this publication and first introduced in [9]. These measurements support a deployment of massive MIMO systems where the arrays are very large and integrated into building infrastructure, contrasting with the deployment of BS arrays that are as compact as possible. The stadium scenario defined in the project METIS [10] is a representative example where a massive array is deployed around the structure of the stadium. Other deployments include hotspots with high density of users such as an open air festival or shopping malls.

Several publications exist on channel measurements for massive MIMO systems. In [11] 7 real antennas are rotated to create a cylindrical array with 112 virtual antennas, while [12, 13] use a cylindrical array with 128 real antennas. In the work [14] a linear array with 128 virtual antennas is used, and the same array is used again in [15], and [16, 17] compare the two arrays used in the previously mentioned [12, 15]. All of the previously described measurements are conducted at 2.6 GHz in outdoor locations. Another early implementation of massive MIMO with 64 antennas is [18]. More recently 2 measurements with 64 and 128 virtual antennas have been reported [19, 20]. They mostly focus on the impact of the number of antennas and all concur on the benefits of increasing the number of antennas to improve the user channel orthogonality and multi-user MIMO channel conditioning. [14, 16, 17] address non stationarity in terms of power angular spectrum.

One common feature standing out from all these publications is the technical difficulty in measuring simultaneously a large number of links. The vast majority of the measurement campaigns rely on a setting where the massive array is virtual: one antenna or a subset of antennas are measured and then moved to a new location for a subsequent measurement. The scope of such an approach is quite limited since it assumes a completely static channel between the individual measurements, and can not capture dynamic channels.

Our measurements are conducted at 5.8 GHz and the results can be applied to the sub-6 GHz in legacy systems, as concluded in [21]. The large frequency under 6 GHz allows us to have smaller antennas and larger electrical apertures in less space. Three arrays with 64 antennas and different size and shape are tested: 2 linear arrays of length 6m and 2m, respectively, and a 25cm by 28cm square array. These arrays serve eight users, each holding a handset with two antennas. The scenarios include line of sight (LoS), non LoS (NLoS), users that are closely spaced or spread, devices with or without user proximity. The measurements build on a unique feature of the Aalborg University channel sounder, i.e. its ability to measure simultaneously 8×16 links. In the current work this system is extended into a system measuring 64×16 MIMO channels quasi-simultaneously during 655 µs. This allows measurements of dynamic channels, such as when users are holding the handsets and moving in realistic scenarios.

The goal of this study is to give an insight on the physical properties of the massive MIMO channel, independently from the transmission technique. We do not show results on sum-rate or throughput to avoid limiting our contribution to a specific precoder. Instead we show results that can be used both in channel modelling and analysing specific systems.

1.1 Contributions

The data obtained from this measurement campaign was first analyzed in [9] where the metrics shown in this manuscript were exemplified with some limited scenarios. In this paper, we focus on extracting statistical results over the dynamics of the channel, the position of the users, the type of array and scenario. In addition, unlike in [9], we study the impact of an increase number of antennas in each type of arrays and corresponding scaling law.

The main contributions and finding in this paper are summarized as follows:

- Considering single antenna users and inter-user properties: the channel vector scalar product decreases logarithmically with the number of antennas (equivalently increased aperture) at a rate similar to the Gaussian channel. There is an offset with the Gaussian channel that depends on the spatial degrees of freedom defined by the propagation characteristics relative to the array aperture. The multi-user MIMO channel is best conditioned when the users are well separated in LoS compared to in NLoS, which is again better than when users are in a group in LoS, finally followed by grouped users in NLoS.

- Considering MIMO properties of 2-antenna users: the MIMO properties improve when the massive array aperture increases. The channel vector scalar product decreases at a rate that is slower than for the Gaussian channel and with an offset that is larger than for the inter-user channel. In general, the more compact array shows markedly worse properties than the larger aperture arrays with same number of antennas. Although LoS conditions are favourable in massive MIMO, we observed that MIMO properties in a single device are better in NLoS scenarios and in the case where the users are grouped as larger scattering is involved. Non-stationarity properties could also be observed as the antennas added to the arrays do not have the same impact in the improvement of the MIMO properties.

- We found that the three studied metrics have larger standard deviations among the measured channels, compared to the Gaussian channel. This might be due to the fact that the user movements happen in the near field and results in larger variations of the metrics, possibly non-stationarities.
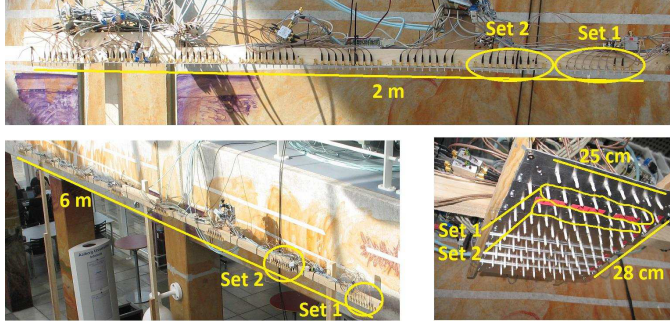
Fig. D.1: Arrays with 64 antennas with three configurations. Bottom-left: VLA, Top: LA and Bottom-right: C2D

2 Measurements and Data

In the following we briefly outline the measurement campaign. For more details refer to [9].

2.1 Three massive array shapes

Three BS arrays are tested, all consisting of 64 monopole elements. The monopoles are arranged in eight linear arrays, named sets in the following, each with eight elements separated by $\lambda/2$.

The array sets are grouped in three dispositions, see Fig. D.1:

VLA: The very large aperture array is a linear 6 m long array where the antenna sets are placed longitudinally with a separation of 50 cm.

LA: The large aperture array is a linear 2 m long array where the antenna sets are placed longitudinally with no separation.

C2D: The compact 2D array has dimensions 25 cm by 28 cm where the antenna sets are placed next to each other, along the long edges.

2.2 Eight handsets with two antennas

The measurements involve eight mock-up handsets with four antennas. However, only two elements of each handset are used in order to have more users and study crowded scenarios. The total of 16 channels from the user side are measured simultaneously. Eight users hold the handsets in front of them imitating "data mode" as if using a smartphone for browsing. They are allowed to have their own hand-grip to make the measurements more realistic.

Fig. D.2: Several distributions of the users, spread or grouped, in LoS or NLoS, or without users. Top-left, S-LoS ∥. Top-right, S-NLoS. Bottom-left, F-InFront. Bottom-right, G-LoS

	LoS	NLoS
Spread Users	**(S-LoS ∥)** **(S-LoS ⊥)**	**(S-NLoS)**
Grouped users	**(G-LoS)**	**(G-NLoS)**
Free Space	**(F-InFront)** **(F-Behind)**	

Table D.1: Scenario reference table.

2.3 Seven scenarios

In the following *scenarios* denotes the dispositions of the users or handsets. Seven scenarios are tested, each one with specific propagation properties, with LoS and NLoS and with a specific distribution of the devices, see Fig. D.2. Table D.1 summarizes the scenarios.

1. **Spread LoS Parallel** (**S-LoS ∥**): The users are in the large space, four in front of the stairs and four behind the stairs. The two rows of users are separated by 6 m and the users in the same row are separated by 3 m. The users face the BS array (i.e. the two antennas of the handset form an array approximately parallel to the BS array). See Fig. D.2 top-left.

2. **Spread LoS Perpendicular** (**S-LoS ⊥**): The users are in the same position as in the previous scenario but turned 90° to their right. The two antennas of the handset form an array approximately perpendicular to the BS array.

3. **Spread NLoS** (**S-NLoS**): The users are located in the lateral space, with 2m distances between them. The handset arrays are parallel to the BS array. See Fig. D.2 top-right.

4. **Grouped LoS** (**G-LoS**): The users are in the large space behind the stairs. They start the measurements packed next to each other in two rows of four users, and they walk away from each other during the measurements, increasing the distance between them. The handset arrays are parallel to the BS array. See Fig. D.2 bottom-right.

5. **Grouped NLoS** (**G-NLoS**): This scenario is similar to the previous scenario. The users are located in the lateral space with NLoS propagation.

6. **Free Space in front stairs** (**F-InFront**): There are no users. The handsets are attached to a table, in two rows of four handsets. The table is placed in front of the stairs in the large space. There is a person sitting on the floor and moving the table to generate the fading. See Fig. D.2 bottom-left.

7. **Free Space behind stairs** (**F-Behind**): This is the same as the previous scenario but the table is placed behind the stairs.

2.4   Channel sounder: quasi-simultaneous measurements

The measurements were made with a correlation based channel sounder operating at 5.8 GHz and with a bandwidth of about 100 MHz. The sounder measures a 8×16 MIMO channel fully in parallel, which is further extended by connecting the elements of each antenna set via a fast switch, so that the 64 elements are multiplexed onto the 8 parallel channels of the channel sounder. During the measurements the users move randomly in a $1\,\mathrm{m}^2$ area while the massive MIMO channel is sampled at a rate of 60 Hz during 20 s, for a total of 1200 channel realizations in the measurement run.

2.5   Narrowband channel and Normalization

We focus on the analysis of a narrow band channel obtained via Fourier transform of the measurements' impulse responses. We denote $\mathbf{h}_k^{(n)}(r) \in \mathbb{C}^{M \times 1}$ as the channel vector from antenna $n \in \{a, b\}$ in the handset of user $k \in \{1, ..., 8\}$ to the BS array at channel realization $r \in \{1, ..., R\}$, where $R = 1200$. $M = 64$ is the number of BS elements. $h_{mk}^{(n)}(r)$ is the mth entry of the vector, corresponding to the mth element of the BS array. We call $\mathbf{H}(r) \in \mathbb{C}^{M \times KN}$ the full 64×16 channel matrix. $K = 8$ is the number of users and $N = 2$ is the number of antennas per user. The two channel vectors of user k at realization r are placed in two consecutive columns of $\mathbf{H}(r)$.

Normalizing the channel we create a virtual power gain control, where the received energy from each user is normalized as:

$$\overline{\mathbf{h}}_k^{(n)}(r) = \frac{\mathbf{h}_k^{(n)}(r)}{\sqrt{\sum\limits_{r=1}^{R} \sum\limits_{n=1}^{N} \left\| \mathbf{h}_k^{(n)}(r) \right\|^2}} \sqrt{MRN} \tag{D.1}$$

where $\|\cdot\|$ is the Euclidean norm, and N is the number of antennas per user.

With this normalization, we remove the user power imbalance but we keep the differences among BS elements, channel realizations, and handset antennas' power imbalance. We denote $\overline{\mathbf{H}}(r) \in \mathbb{C}^{M \times KN}$ as the channel matrix made out of the normalized vectors in (D.1).

3   Scalar product map of the three arrays

In theory, massive MIMO owes in large part its superior performance to the asymptotic orthogonality of the channel vectors. In our case, this means that the instantaneous channel matrix $\overline{\mathbf{H}}(r)$ should verify for each of the measurements:

$$\mathbf{G}(r) = \frac{1}{M} \overline{\mathbf{H}}(r)^H \overline{\mathbf{H}}(r) \approx \mathbf{I} \tag{D.2}$$

where $(\cdot)^H$ is the conjugate transpose operator and $\mathbf{I}$ is the identity matrix. To account for the orthogonality properties of the measured channels, we compute the following matrix:

$$\overline{\mathbf{G}} = \frac{1}{R} \sum_{r=1}^{R} \bar{\mathbf{G}}(r) \tag{D.3}$$

in which element (i, j) of $\bar{\mathbf{G}}(r)$ is $\frac{\left| \mathbf{h}_i(r) \mathbf{h}_j(r) \right|}{\|\mathbf{h}_i(r)\| \|\mathbf{h}_j(r)\|}$, where $\mathbf{h}_i$ is the ith column of $\mathbf{H}(r)$. $\overline{\mathbf{G}}$ is the average of the absolute value of the pairwise scalar product between channel vectors. For simplicity, we refer to this quantity as the mean scalar product.

Fig. D.3 displays examples of the elements of $\overline{\mathbf{G}}$. The 2x2 blocks along the diagonal represent the mean scalar product between the channels for the same device. The off-diagonal blocks represent the mean scalar product between the channels of different devices. We notice a significant difference in the behavior of the intra-user and inter-user channels. This is the reason why we later detail the performance separately for those two kinds of channels.

3.1   Inter-user scalar product

Fig. D.3 displays the channel scalar products in scenario F-InFront using all the 64 base station antennas. We examine first the mean value of the off-block
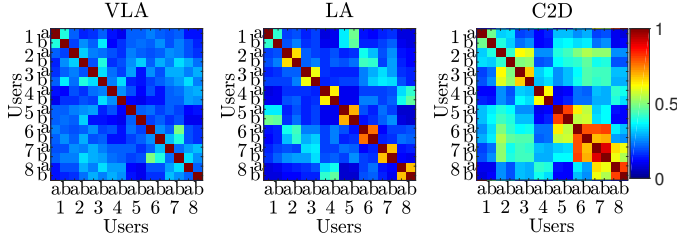
Fig. D.3: Scalar product between user's channel vectors comparing three base station arrays. Scenario: F-InFront

diagonal terms of $\overline{\mathbf{G}}$, i.e. the terms accounting for inter-user scalar products. The VLA and LA have comparable values of 0.22 and 0.20, respectively, while C2D achieves a larger value of 0.34. A more significant difference between the arrays can be seen when looking at individual devices and their respective position. In the LA matrix, two block lines parallel to the main diagonal are visible. Those entries correspond to the antennas in the same azimuth angle but different elevation angle, as seen from the BS array. The value of the mean scalar product (0.33 for LA and 0.25 for VLA) indicates that the LA provides worse resolution than the VLA in the elevation domain. This property comes from the location of the devices in the near-field of the linear arrays. The C2D array performs the worst. Compared to LA, the zone of large scalar products is extended to devices in the same vicinity (e.g. device 6 and 7). Only very separated devices (i.e. 4 and 5, 1 and 4, or 1 and 8) achieve a low mean scalar product.

Fig. D.4 shows the statistics of the 112 inter-user combinations with a varying number of base station antennas and the three arrays in the G-LoS scenario. The resulting array is chosen to be as compact as possible, so the aperture of the array increases when the number of antennas increases. For the linear arrays the antennas are consecutively added starting from the antenna closer to the bridge. For the C2D array consecutive rows of antennas are added starting from the bottom right (see Fig. D.1). The results for an i.i.d. Gaussian channel are used for comparison purposes and are labeled as 'G'. The boxplot shows the quartiles, whiskers and outliers. It divides the data in 4 regions each one containing 25 % of the results (i.e. 25th, 50th and 75th percentiles), the whiskers contain the values 1.5 times the inter-quartile range, above or below the 75th and 25th percentiles, and the rest of the data are outliers (i.e. crosses in red). In this specific scenario we observe lower correlations for larger aperture arrays. This result holds regardless the number of elements in the base station array. However, in some other scenarios the LA has better performance than the VLA. This will be analyzed in 3.2 and can be observed in the solid lines in Fig. D.5. For the Gaussian channel, according to the central limit theorem, the scalar product decreases as the

3. Scalar product map of the three arrays
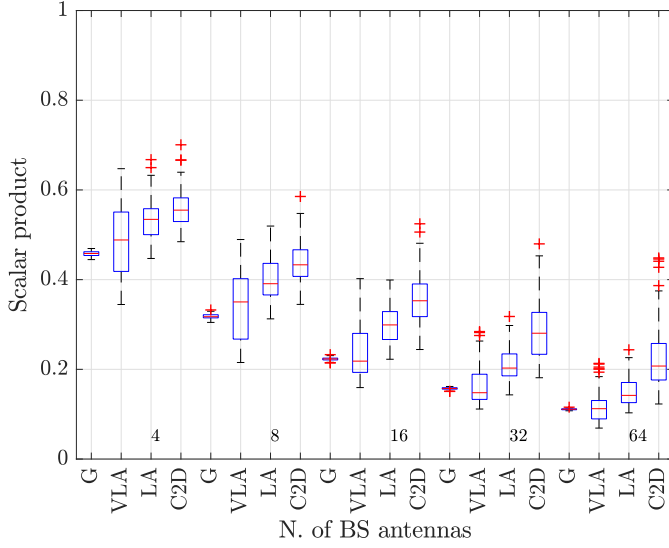
Fig. D.4: Boxplot with statistics over users' combinations of the inter-user scalar product increasing the number of base station elements. Scenario: G-LoS
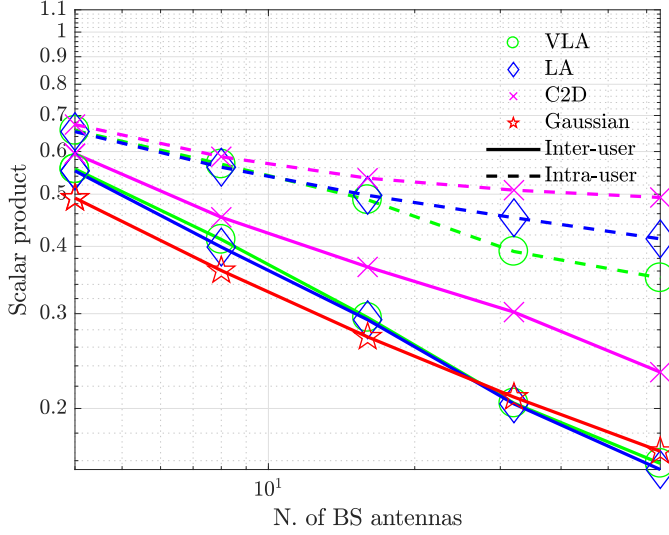
Fig. D.5: Mean of the scalar product for each array increasing the number of base station elements with both axis in log scale, averaged over all the scenarios

inverse of the number of antennas. For the VLA and the LA, performance is close to the Gaussian case. For C2D, we still observe a logarithmic scaling with the number of antennas but with a significant offset. Similar plots to
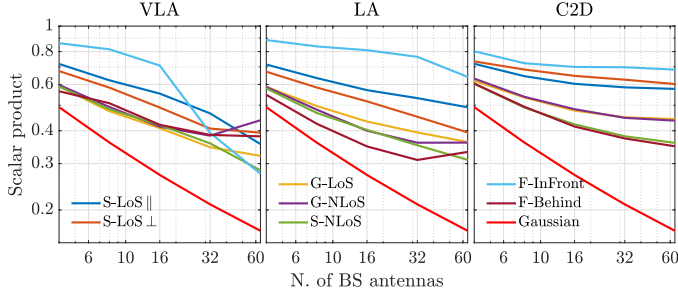
Fig. D.6: Mean of the intra-user scalar product for each array and each scenario increasing the number of base station elements

Fig. D.4 are made for all scenarios, and in the results for the scenarios not shown here, there is a slightly better performance in LoS scenarios compared to NLoS, but the latter have less dispersion. We observe a lower dispersion of the results for the Gaussian channel compared to the measured channels.
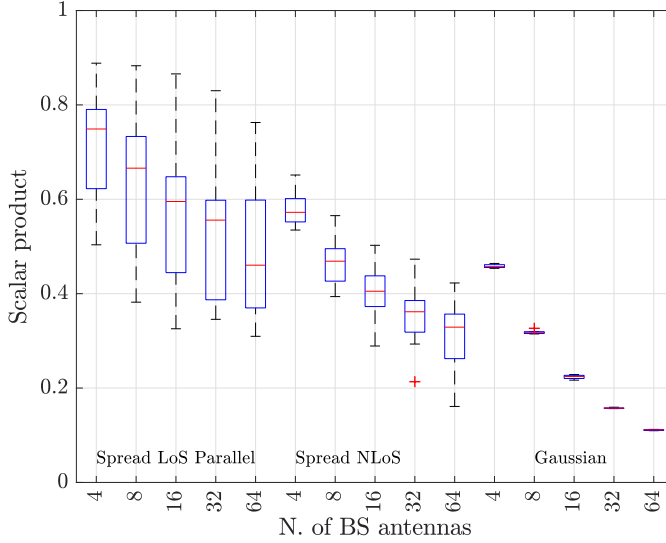
3.2 Intra-user scalar product: MIMO capability of the devices

Looking again at the specific scenario of Fig. D.3 but focusing on the intra-user entries (the block diagonal), we see that such closely spaced antennas (by half the wavelength) are more correlated in the LA than in the VLA (mean scalar product of 0.64 for LA compared with 0.27 of VLA). The C2D array has an intra-device mean scalar product of 0.68, not much higher than the LA array. These results show the improvement brought by increasing the aperture of the array to transmit to the two antennas in the same device simultaneously. The impact of the array is similar to the inter-user cases, where VLA usually, but not always, is the best, followed by LA and finally C2D. The results for different arrays and scenarios can be compared in Fig. D.6.

Fig. D.7 shows the statistics of the 8 intra-user combinations with several numbers of base station antennas and two scenarios for the LA array. The results for an i.i.d. Gaussian channel are used for comparison purposes. Even if the scalar product is larger in the intra-user case compared with the inter-user case, there is also an improvement from increasing the number of base station antennas. The reduction in scalar product is similar to the Gaussian channel (0.29, 0.24, 0.35 when increasing from 4 to 64 BS antennas for S-LoS ∥, S-NLoS, and Gaussian channel respectively) but there is an offset due to the correlation between the user antennas. The amount of dispersion in the results is larger than in the Gaussian channel as well as larger than the inter-user case.

All the scenarios and arrays are compared in Fig. D.6. We observe that there is a tendency for the NLoS scenarios to have lower scalar product than

Fig. D.7: Boxplot with statistics over users' combinations of the intra-user scalar product. Array: LA

the LoS. As in the inter-user case, the VLA array tends to be the best, followed by the LA and the C2D, but some scenarios differ. The MIMO capabilities of the device benefit from the NLoS conditions of the channel. However, the aperture of the array still plays an important role. We also notice the importance of the position of the antennas. Different antennas contribute differently to the scalar product and the lines are not straight.

To compare the arrays, in Fig. D.5 we compute the mean scalar product for all channel realizations, users, and scenarios with both axes in log scale. The result shows that in the intra-user situation, when the aperture of the array increases more than 16 antennas the VLA is better than the LA and the LA is better than the C2D. The three curves have a slope that is less steep than the Gaussian channel due to the high correlation between antennas. In the inter-user situation, the LA is still better than the C2D, and even slightly better than the VLA. The linear arrays' curves have a slightly steeper curve than the Gaussian channel.

4 Properties of the singular eigenvalues

While the previous section gave an overview of the orthogonality properties of the three arrays in different scenarios, we now look at the properties of the singular values of the channel matrix, first for inter-user channels (one antenna per user device) and second for intra-user channels (device MIMO
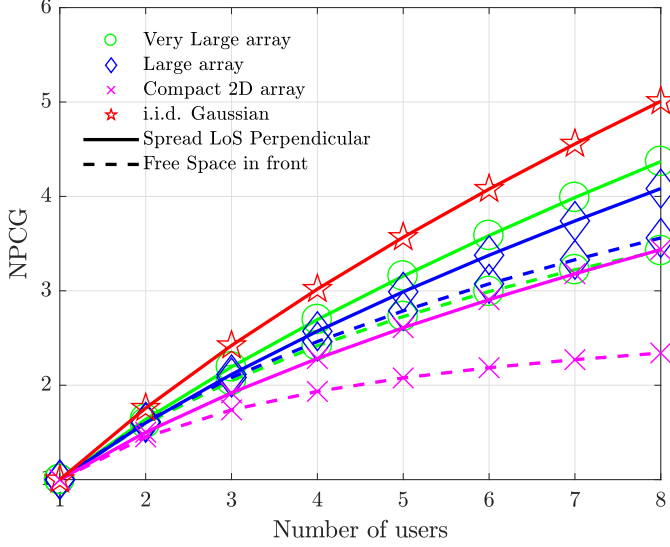
Fig. D.8: Average inter-user NPCG increasing the number of users. Scenarios: S-LoS$\perp$ and F-InFront

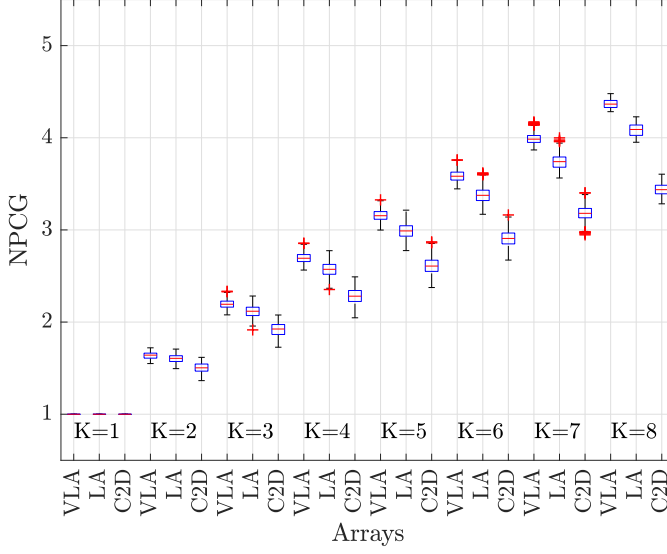channels).

4.1 Inter-user channel

The goal is to explore what happens when the number of users in the system increases. We call the number of users in the system C and we increase C from 1 to K. We collect all the combinations of C channels from C users (only one channel per user out of the two channels is selected). We form a new channel matrix for realization r denoted generically as $\mathbf{G}^{\text{Inter}}(r)$.

The metric adopted here is the sum of the eigenvalues normalized by largest eigenvalue (Normalized Parallel Channel Gain, NPCG). Denoting $\lambda_{i,r}$ as the ith eigenvalue of the matrix $\mathbf{G}^{\text{Inter}}(r)^H \mathbf{G}^{\text{Inter}}(r)$, then the metric is defined as:

$$\text{NPCG}(r) = \frac{1}{\lambda_{\max,r}} \sum_{i=1}^{C} \lambda_{i,r} \tag{D.4}$$

$\lambda_{\max,r}$ is the largest eigenvalue. We average the NPCG over r. This metric is preferred to the condition number of the channel as the latter gives only information on the ratio between the larger and the smaller eigenvalue, whereas metric (D.4) reflects the behavior of all the eigenvalues. Notice that, for a channel that is very well conditioned with equal eigenvalues, NPCG = C and for a channel that is poorly conditioned NPCG = 1.

Fig. D.9: Boxplot with statistics of the inter-user NPCG for different number of users (K). Scenario: S-LoS $\perp$

In Fig. D.8 we compare scenarios S-LoS $\perp$ and F-InFront. We show the average NPCG over the user and user element combinations and channel realizations (i.e. $\binom{K}{C}N^C R$ total combinations; this is 19200 for $C = 1$ and 2150400 for $C = 5$). The free space (F-InFront) generally gives worse performance than the spread users (S-LoS $\perp$), but the difference between scenarios depends on the array. The linear arrays give the smallest difference, followed by the C2D. For both scenarios, the linear arrays have the best performance. C2D array has the worst performance.

In Fig. D.9 we show a box plot with the statistics (i.e. quartiles, whiskers and outliers as explained in section 3) over the user and user element combinations for the S-LoS $\perp$ scenario. We observe that the results are very compact around the median, with small inter-quartile range and few outliers. This is valid for all the number of users. We observe similar results for the other scenarios.

In the following we study the impact of the number of antennas at the BS in 2 cases: 1) the number of antennas is increased as the array aperture increases (array expanding), 2) the number of antennas is increased as the array aperture is maintained (array densifying). In the first case, we expect performance improvement due to the increase of the spatial degrees of freedom. In the second case, we expect a conservation of the degrees of freedom available provided that the number of antennas are still larger than the DoF.

Fig. D.10 shows the NPCG in the G-LoS scenarios for all the arrays when
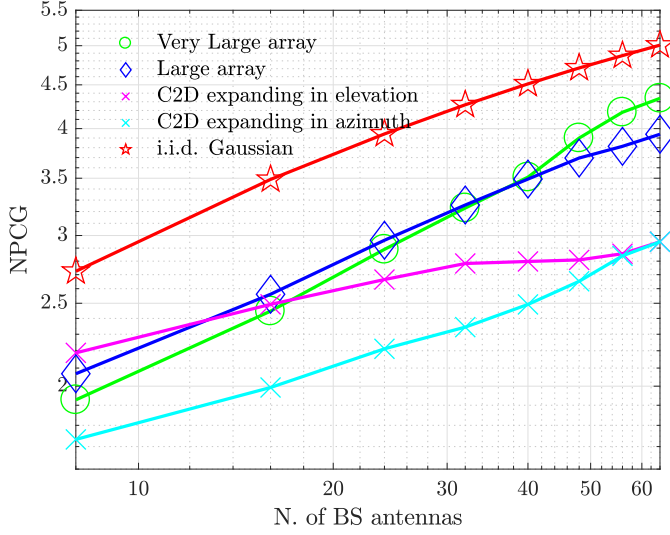
Fig. D.10: Average inter-user NPCG increasing the aperture of the array with K=8 users. Scenario: G-LoS

expanding the array. Both axis are in logarithmic scale. For the linear arrays the sets are expanded from the one nearer to the bridge to the one farther from the bridge. For the C2D array we test two options: 1) we add columns of antennas perpendicular to the wall, increasing the azimuth resolution. 2) we add rows of antennas parallel to the wall, increasing the elevation resolution. As expected, performance improves with the number of antennas. For the VLA the curve has two parts. With less than 40 antennas the behaviour is similar to LA, but the performance is boosted when adding more antennas. The reason may be that some of the users are behind the stairs so the first 40 are blocked by the bridge, while the rest of the antennas has a clear view of the users. The LA is shorter than the VLA and its antennas are always blocked by the bridge. Examining the C2D array curves, we observe that the most critical dimension is the azimuth dimension while increasing the elevation dimension brings only a small improvement. The reason is that the users are distributed in the azimuth domain (i.e. 4 columns), and not in the elevation domain (i.e. 2 rows). Also notice that when expanding in elevation the first 8 antennas already occupy the maximum aperture in the azimuth direction and therefore the captured degrees of freedom in that direction is high. As expected, increasing the aperture of the array captures more DoF of the channel and the performance is improved.

Fig. D.11 compares all the scenarios measured showing the NPCG metric when densifying the array (i.e. increasing the number of antennas for the same aperture). We observe that the S-LoS $\parallel$ is the scenario with maximum
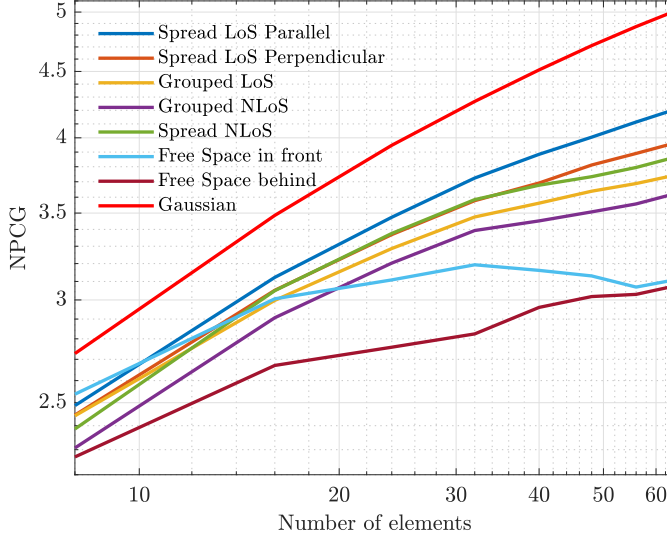
Fig. D.11: Average over channel realizations and arrays inter-user NPCG, densifying array. Scenarios: all.

degrees of freedom, followed by the other spread users scenarios, and then the grouped scenario in LoS and then grouped in NLoS. Finally the free space scenarios have the lowest NPCG. Both Spread LoS scenarios have the same position of the users, but the 90° shift of the users also implies a shift in the radiation pattern that can change the direct path and scatterers, and the DoF are reduced. In the free space scenarios the proximity of the antennas and the simultaneous movement results in highly correlated antennas, and their small contribution in the degrees of freedom can not compensate the energy added in the maximum eigenvalue, therefore the NPCG decreases.

4.2 Intra-user channel

To evaluate the MIMO channel properties within the same device, we go back to the conventional condition number as we have only 2 antennas. The condition number indicates how spread the eigenvalues of the channel are. It is defined as

$$\text{CN}(r) = \frac{\lambda_{\text{max},r}}{\lambda_{\text{min},r}} \tag{D.5}$$

where λ_{max} and λ_{min} are the maximum and minimum eigenvalues of the Gram matrix of the MIMO channel. Since the Gram matrix also represents the scalar product of the channel vectors, the CN and the scalar product are related metrics.

Fig. D.12 shows the cdf of the CN in scenarios S-LoS $\parallel$ and S-LoS $\perp$. The
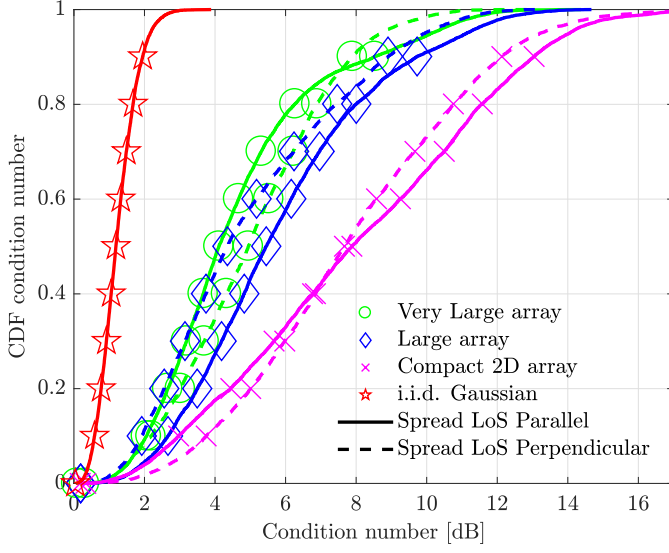
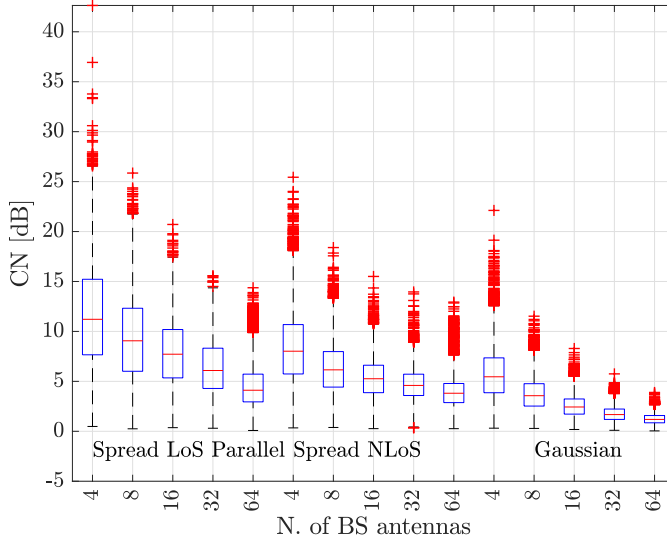**Fig. D.12:** CDF over realizations for the intra-user condition number. Scenarios: S-LoS∥ and S-LoS⊥
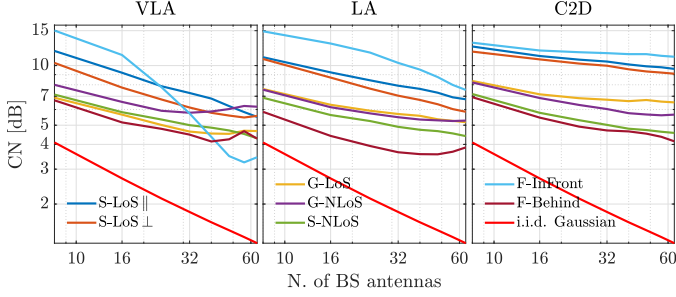
Fig. D.13: Average over users and realizations of the intra-user condition number increasing the number of base station elements with both axis in logarithmic scale.

VLA performs the best with a mean condition number of 4.1 dB and 4.9 dB for parallel and perpendicular devices respectively, followed by the LA (with a mean condition number of 5.4 dB and 4.3 dB for parallel and perpendicular devices respectively) and finally the C2D (with a mean condition number of 7.9 dB and 7.7 dB for parallel and perpendicular devices respectively). Neither of the arrays is able to approach the Gaussian channel that has a mean condition number of 1.2 dB. The orientation of the handset has no systematic impact on the orthogonality of the channel vectors.

Fig. D.13 shows the CN when expanding the array (i.e. choosing consecutive antennas from the right side of Fig. D.1), with both axis in logarithmic

Fig. D.14: Boxplot with statistics over users and channel realizations of the intra-user condition number, increasing the number of base station elements. Scenarios: S-LoS ∥ and S-NLoS. Array: VLA

scale. The gap between measurements and the Gaussian channels is due to the high correlation of the antennas in the measurements. We observe that adding more antennas improves the orthogonality of the channels at a lower rate than the Gaussian channel. Notice the similitude between Fig. D.13 and intra-user scalar product in Fig. D.6.

In Fig. D.14 we show the CN in a boxplot with the statistics (i.e. quartiles, whiskers and outliers as explained in section 3) over the K users and the R realizations. We compare two scenarios with spread users in LoS and NLoS. Observing the median we see a lower CN for the NLoS scenario compared with the LoS. We also see the benefit of increasing the number of base station antennas to decorrelate the channels of closely spaced user antennas. The length of the boxes shrinks when increasing the number of base station antennas which proves the channel hardening effect of massive MIMO. However, we also observe a high number of outliers in the higher end of the CN, which is due to the statistical distribution of the condition number as studied in [22].

5 Conclusion

The current work studies the propagation characteristics of measured multi-user massive MIMO channels, focusing on the effects of the array aperture.

The performance metrics used for comparisons are the mean scalar product, the Normalized Parallel Channel Gain (Normalized sum of eigenvalues), and the condition number.

We show a decrease in the scalar product between user's channel vectors when the number of base station antennas increases. For example, the median scalar product of the very large array in the grouped users in LoS decreases by 0.38 from 4 antennas to 64. The presented results confirm the better decorrelation properties of the large aperture arrays. The antennas in the same handset are easier to decorrelate in NLoS scenarios than in LoS.

Increasing the number of users in the system is more harmful in crowded scenarios than in spread users scenarios due to the limitation in DoF. There is a 0.24 NPCG difference between the spread users NLoS scenario and the grouped users NLoS averaging the three arrays with 64 antennas. The channel characteristics improve when increasing the number of antennas in the base station, but with a slower rate for the compact array. We also see a small dispersion of the results when considering all the combinations of users and their antennas.

Finally, the MIMO properties of the user handset are better with the very large array in most of the scenarios. For example the very large array has 1.3 dB better mean condition number than the large array in the spread users LoS parallel scenario. The close distance between antennas renders their channel correlated, far from the Gaussian channel. NLoS scenarios and grouped scenarios have larger scattering that permits to exploit the MIMO capabilities of the handset.

References

[1] T. L. Marzetta, "Noncooperative cellular wireless with unlimited numbers of base station antennas," *IEEE Transactions on Wireless Communications*, vol. 9, no. 11, pp. 3590–3600, 2010.

[2] F. Rusek, D. Persson, B. K. Lau, E. G. Larsson, T. L. Marzetta, O. Edfors, and F. Tufvesson, "Scaling Up MIMO: Opportunities and Challenges with Very Large Arrays," *IEEE Signal Processing Magazine*, vol. 13, no. 1, pp. 40–60, 2013.

[3] E. G. Larsson, O. Edfors, F. Tufvesson, and T. L. Marzetta, "Massive MIMO for Next Generation Wireless Systems," *IEEE Communications Magazine*, vol. 52, no. 2, pp. 186–195, 2014.

[4] B. Bangerter, S. Talwar, R. Arefi, and K. Stewart, "Networks and devices for the 5G era," *IEEE Communications Magazine*, vol. 52, no. 2, pp. 90–96, 2014.

[5] I. Chih-Lin, C. Rowell, S. Han, Z. Xu, G. Li, and Z. Pan, "Toward green and soft: A 5G perspective," *IEEE Communications Magazine*, vol. 52, no. 2, pp. 66–73, 2014.

[6] C. X. Wang, F. Haider, X. Gao, X. H. You, Y. Yang, D. Yuan, e.-H. M. Aggoune, H. Haas, S. Fletcher, and E. Hepsaydir, "Cellular architecture and key technologies for 5G wireless communication networks," *IEEE Communications Magazine*, vol. 52, no. 2, pp. 122–130, 2014.

[7] F. Boccardi, R. Heath, A. Lozano, T. L. Marzetta, and P. Popovski, "Five disruptive technology directions for 5G," *IEEE Communications Magazine*, vol. 52, no. 2, pp. 74–80, 2014.

[8] A. Poon, R. Brodersen, and D. Tse, "Degrees of Freedom in Multiple Antenna Channels: A Signal Space Approach," *IEEE Transactions on Information Theory*, vol. 51, no. 2, pp. 523–536, 2005.

[9] À. Oliveras Martínez, E. D. Carvalho, and J. Ø. Nielsen, "Towards Very Large Aperture Massive MIMO: a measurement based study," in *Globecom Workshops (GC Wkshps), 2014*. IEEE, 2014, pp. 281–286.

[10] K. Kusume and M. Fallgren, "Updated scenarios , requirements and KPIs for 5G mobile and wireless system with recommendations for future investigations (Deliverable D1.5)," METIS, Tech. Rep., 2015.

[11] J. Hoydis, C. Hoek, T. Wild, and S. ten Brink, "Channel measurements for large antenna arrays," in *2012 International Symposium on Wireless Communication Systems (ISWCS)*. IEEE, 2012, pp. 811–815.

[12] X. Gao, O. Edfors, F. Rusek, and F. Tufvesson, "Linear Pre-Coding Performance in Measured Very-Large MIMO Channels," in *Vehicular Technology Conference (VTC Fall), 2011 IEEE*. IEEE, 2011, pp. 1–5.

[13] J. Flordelis, X. Gao, G. Dahman, F. Rusek, O. Edfors, and F. Tufvesson, "Spatial separation of closely-spaced users in measured massive multi-user MIMO channels," in *IEEE International Conference on Communications*. IEEE, 2015, pp. 1441–1446.

[14] S. Payami and F. Tufvesson, "Channel measurements and analysis for very large array systems at 2.6 GHz," in *2012 6th European Conference on Antennas and Propagation (EUCAP)*. IEEE, 2012, pp. 433–437.

[15] X. Gao, F. Tufvesson, and O. Edfors, "Massive MIMO channels - Measurements and models," in *2013 Asilomar Conference on Signals, Systems and Computers*, 2013, pp. 280–284.

[16] X. Gao, F. Tufvesson, O. Edfors, and F. Rusek, "Measured propagation characteristics for very-large MIMO at 2.6 GHz," in *2012 Conference Record of the Forty Sixth Asilomar Conference on Signals, Systems and Computers (ASILOMAR)*. IEEE, 2012, pp. 295–299.

[17] X. Gao, O. Edfors, F. Rusek, and F. Tufvesson, "Massive MIMO Performance Evaluation Based on Measured Propagation Data," *IEEE Transactions on Wireless Communications*, vol. 14, no. 7, pp. 3899–3911, 2015.

[18] C. Shepard, H. Yu, N. Anand, E. Li, T. L. Marzetta, R. Yang, and L. Zhong, "Argos: practical many-antenna base stations," in *Proceedings of the 18th annual international conference on Mobile computing and networking - Mobicom '12*. ACM, 2012, pp. 53—-64.

[19] D. Fei, R. He, B. Ai, B. Zhang, K. Guan, and Z. Zhong, "Massive MIMO Channel Measurements and Analysis at 3.33 GHz," in *2015 10th International Conference on Communications and Networking in China (ChinaCom)*. IEEE, 2015, pp. 194–198.

[20] L. Wenjuan, L. Liu, T. Cheng, L. Yanping, X. Jingcheng, and L. Pengyu, "Channel measurements and Angle Estimation for Massive MIMO Systems in a Stadium," in *2015 17th International Conference on Advanced Communication Technology (ICACT)*. IEEE, 2015, pp. 105–108.

[21] J. Li, B. Ai, R. He, K. Guan, Q. Wang, D. Fei, Z. Zhong, Z. Zhao, D. Miao, and H. Guan, "Measurement-Based Characterizations of Indoor Massive MIMO Channels at 2 GHz, 4 GHz, and 6 GHz Frequency Bands," in *2016 IEEE 83rd Vehicular Technology Conference (VTC Spring)*. IEEE, 2016, pp. 1–5.

[22] M. Matthaiou, M. R. McKay, P. J. Smith, and J. A. Nossek, "On the condition number distribution of complex wishart matrices," *IEEE Transactions on Communications*, vol. 58, no. 6, pp. 1705–1717, 2010.

Paper E

An Experimental Study of Massive MIMO Properties
in 5G Scenarios

Àlex Oliveras Martínez, Jesper Ødum Nielsen,
Elisabeth De Carvalho, and Petar Popovski

Abstract

Three main characteristics of massive multiple-input-multiple-output (MIMO) are studied. The wide-spread use of these characteristics and their lack of validation motivates this study based in measurements. First we study the channel hardening when the number of antennas in the base station (BS) increases. Second we focus on the channel vector orthogonality between two users. Third we investigate the rank of the spatial covariance matrix. The data used for this research has been obtained in two measurement campaigns with all real antennas (i.e. neither virtual arrays nor virtual users). The first one has 64 BS elements arranged in 3 configurations, and it serves 8 users with 2 antennas each. The second campaign has 128 BS elements, serving 2 users with 2 antennas each. Both campaigns include line-of-sight (LoS) and non-line-of-sight (NLoS) scenarios, designed according to the future 5G deployment scenarios. We show the rate of channel hardening when the number of BS elements increases. We evaluate the sum-rate of two users at specific distances between them. We observe the large angular spread occupied by the user.

1 Introduction

The current growth in the number of mobile phones and other connected devices demands high data throughputs. The existing cellular systems fall behind the needed performance. Next generation wireless solutions will need to meet the increasing demand of capacity, reliability and energy efficiency. Massive MIMO tackles these requirements, thus, in the recent years, has attracted a lot of attention as an enabling technology for the next generations of communications systems (e.g. 5G [1]). The seminal work of Marzetta [2] describes it as a BS comprising a very large number of elements serving a much smaller number of single antenna terminals in the same time-frequency resource.

The benefits of massive MIMO have been extensively studied in theoretical channels but also in measurements. However, due to the difficulties to measure such a large number of antennas simultaneously, most of the measurements utilize virtual antennas to create the BS array [3–9]. However, some papers study measurements with real arrays [10–12] and some studies compare virtual and real arrays [13, 14]. Simulatenous user measurements are reported in [12]. Some papers describe outdoor scenarios [3–7, 11–14], some indoor scenarios [8, 9, 11]and some outdoor-indoor [10]. Most of the measurements have 64 antenna ports [6, 8, 11] or 128 [3, 5, 10, 12–14], with the exception of [4] that has 112, [7] that has 256 and [9] that has 400.

There are three determining topics for massive MIMO performance that have only been derived from simplified theoretical models. Here we would like to verify them experimentally:

Channel hardening

The superior number of BS elements with respect to users leaves degrees of freedom unused. The excess of degrees of freedom can be used to reduce fast fading and average out noise due to the law of large numbers. This effect is called channel hardening because the channel becomes more stable. This may not happen (or happen to less degree) in measured channels because the channels are not independent as needed for the law of large numbers to be effective.

Users' channel vector orthogonality

When the number of BS elements grows large the channel vector of two users becomes asymptotically orthogonal. This result allows to eliminate the inter-user (or intra-cell) interference. But the orthogonality between users' channel vectors strongly depends on their relative position. Two users close to each other, are inside the same radiation pattern beam (in LoS) or they see the same scatterers (in NLoS). As a result their channel vectors can be similar, and the orthogonality is affected.

Rank of the spatial covariance matrix

Some methods for multicell pilot contamination avoidance, channel estimation [15] and FDD transmission [16] assume low rank of the covariance matrix because the large aperture of the array in massive MIMO achieves very narrow beams and in absence of scatterers these narrow beams render a sparse covariance channel matrix. This is different from the rank of the instantaneous multi-user channel matrix that has been studied in other measurements [17]. However, studies on direction of arrivals can be found which are related to rank of the spatial covariance matrix [3, 6].

These three properties are studied from a channel characterisation perspective instead of a massive MIMO performance perspective. These allows us to abstract from specific transmission techniques and we can present general properties of the channel useful in a broader range of applications.

The following study uses the data of two measurement campaigns to analyze the three previously mentioned topics. Both measurements are conducted at 5.8 GHz. The first one has 64 BS real elements reconfigurable into three array shapes: A very long aperture (6 m) array, a long aperture (2 m) array, and a rectangular (25 cm by 28 cm) array. This array serves 8 users with 2 antennas each. Line-of-Sight (LoS) and Non-Line-of-Sight (NLoS) scenarios are measured. We focus on indoor scenarios where moving users hold a handset mockup. The second campaign has 128 real BS elements serving 2 users with 2 antennas each. The scenario is outdoors and includes both LoS and NLoS. The data of the measurements was first analyzed in [17–19]. The

location of the measurements is carefully chosen, envisioning new scenarios for the 5G wireless systems (i.e. large indoor spaces such as shopping malls, large venues, sport stadiums, etc. See [1] Chapter 2). Such scenarios can integrate very large BS arrays into their structures. We focus on such scenarios because their high user density represents a challenge for the next generation of wireless systems.

The previously published results revealed the orthogonality of arbitrarily located users, the degrees of freedom in the form of normalized sum of eigenvalues, the condition number of the channel matrix and power non-stationarities across the array [17, 18].

In this publication the analysis of the data from these campaigns shows us the hardening of the channel when the number of BS antennas increases. We see that larger apertures induce more hardening. However, the hardening is less than in the Gaussian channels. The Gaussian channel is defined for the rest of the paper as a channel with independent identically distributed complex Gaussian entries with zero mean and unit variance. We also observe that the correlation between users is tightly related to their relative position in NLoS and strongly depends on the radiation pattern in LoS. Finally we show the rank of the spatial covariance matrix and its impact on the channel hardening. In [19] these metrics were presented only in specific scenarios and users, while in this publication these results are presented with the statistics over all the scenarios and arrays used in the measurements. In addition we present the impact of the users' distance-specific correlation to the matched filter sum rate and we compare it with a simulated channel. We also show the beamforming angle of arrival averaged over channel realizations for several scenarios and users.

2 Measurement campaigns

2.1 5G scenarios

The first measurement campaign uses 64 BS elements and we call it 64-mMIMO. The measurement campaign was carried out at Aalborg University in a large indoor environment similar to a shopping mall with a staircase in the middle of the room. This location was chosen to study a 5G scenario called *shopping mall* in [1] Chapter 2.

The second measurement campaign uses 128 BS elements and we call it 128-mMIMO. The measurement campaign was carried out in an outdoor scenario at Aalborg University, Denmark. The environment has a large grass field in the center surrounded by buildings three floors high. In one side there is a road and a parking lot between the field and the building. LoS measurements are conducted in the middle of the field (at 30 m from the BS)

and NLoS measurements are conducted outside the field, behind a group of trees (at 60 m from the BS). This location was chosen to study a 5G scenario called *large outdoor event* in [1] Chapter 2.

2.2   64-mMIMO

This section outlines the main characteristics of 64-mMIMO. For more details refer to [17].

Three massive array shapes

Three BS arrays are tested, all consisting of 64 monopole elements. The monopoles are arranged in eight linear arrays, named sets in the following.

The array sets are grouped in three dispositions, shown in Fig. E.1:

VLA: The very large aperture array is 6 m long where the antenna sets are placed longitudinally separated 50 cm.

LA: The large aperture array is 2 m long where the antenna sets are placed longitudinally without separation.

C2D: The compact 2D array is a rectangular array of 25 cm by 28 cm where the antenna sets are placed next to each other, along the long edges.

Eight handsets with two antennas

The measurements involve eight mock-up handsets with four antennas (one at each corner), but only the two antennas in the top are active. Fig. E.2 shows the handset.

Eight users hold the handsets in front of them as if using a smartphone for browsing. During the measurements the users move randomly in a $1\,m^2$ area to generate small-scale changes in the channel.

Seven scenarios

In the following, *scenarios* denotes the dispositions of the users or handsets. Seven scenarios are tested, each one with specific propagation properties, with LoS and NLoS and with a specific distribution of the devices. Table E.1 summarizes the scenarios. Some scenarios are depicted in Fig. E.3. Fig. E.4 shows a floor map of some scenarios. Notice that ∥ refers to scenarios where the two antennas in the handset form an array parallel to the BS. On the other hand ⊥ means that the two antennas of the handset form an array perpendicular to the BS. F-InFront means that the handsets are deployed in front of the stairs, while F-Behind means the handsets are behind the stairs. A more detailed description of the scenarios can be found in [17].
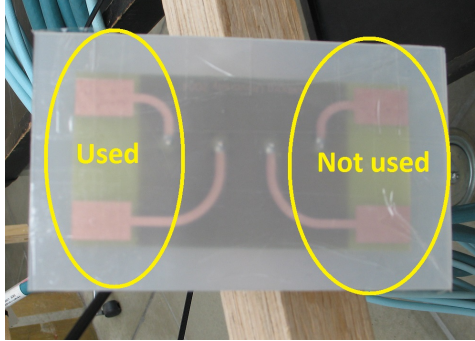
	LoS	NLoS
Spread Users	(**S-LoS ‖**) (**S-LoS ⊥**)	(**S-NLoS**)
Grouped Users	(**G-LoS**)	(**G-NLoS**)
Without Users	(**F-InFront**) (**F-Behind**)	

Table E.1: Scenario reference table.
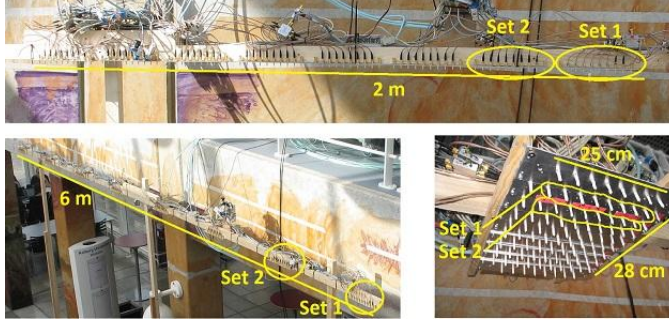
Fig. E.1: Antenna configurations. Bottom-left: VLA, Top: LA and Bottom-right: C2D

Fig. E.2: Handset with four antennas. Only two are used

2.3   128-mMIMO

This section outlines the main characteristics of 128-mMIMO.

Base station array

The BS array consists of 128 monopole elements. The monopoles are arranged in eight linear arrays, named sets in the following, each with sixteen elements separated by $\lambda/2$. Two dummy monopoles are added at the ends of each set so that all the active elements have similar properties. The sets are separated 0.34 m. The total length of the BS is 5.78 m and it is placed on the wall at

Fig. E.3: Top-left, S-LoS ‖. Top-right, S-NLoS. Bottom-left, F-InFront. Bottom-right, G-LoS
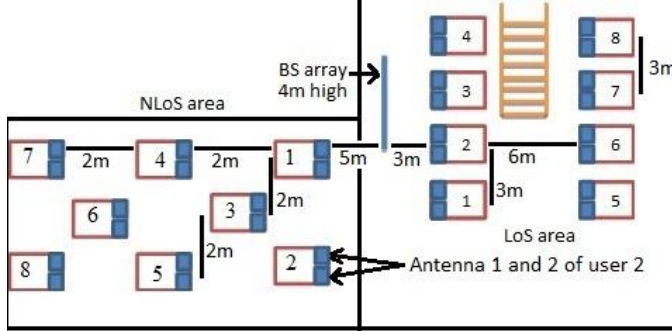

Fig. E.4: Floor map with location of BS array, LoS area, NLoS area and user numbering.

approx. 4.1 m from the ground. Fig. E.5 shows the BS array.

Two scenarios

In the following *scenarios* denotes the dispositions of the users. Two scenarios are tested, LoS and NLoS. Fig. E.6 show the two scenarios and their relative position to the BS.

Two handsets with two antennas

The measurements involve two mock-up handsets (the same as in the first campaign, showed in Fig. E.2). Two users hold the handsets in front of them

as if using a smartphone for browsing. They are allowed to have their own hand-grip to make the measurements more realistic. The users move the mock-up randomly in a $1\,\mathrm{m}^2$ area (i.e. approx. 20×20 wavelengths) to generate small-scale changes in the channel. In order to control the mean distance between users a 1.1 m stick is used. One end of the stick is placed in fixed positions marked on the ground, and the other end is held and moved by the users together with the mock-up. The stick can be seen in the hands of user 1 in Fig. E.7. The mean distance between users is modified by changing the position of the lower end of the stick. The positions marked on the ground are represented with blue dots in Fig. E.6.

1. LoS scenario: The users increase their separation in the parallel dimension of the array. The users are measured in 10 positions separated by: 0.2 m, 0.3 m, 0.4 m, 0.5 m, 0.6 m, 0.8 m, 1 m, 1.5 m, 2 m, and 4 m.

2. NLoS scenario: Each user is located on one of two orthogonal lines. The users are measured in 21 positions separated from the crossing point by: 4 m, 2 m, 1.5 m, 1 m, 0.8 m, 0.6 m, 0.5 m, 0.4 m, 0.3 m, 0.2 m, 0 m, 0.2 m, 0.3 m, 0.4 m, 0.5 m, 0.6 m, 0.8 m, 1 m, 1.5 m, 2 m, and 4 m.

Fig. E.7 shows the two users during a measurement.

3 Channel sounder and Normalization

3.1 Channel sounder: quasi-simultaneous measurements

The measurements were made with a correlation based channel sounder operating at 5.8 GHz and with a bandwidth of about 100 MHz. The sounder has 8 parallel receive channels and 16 parallel transmit channels. In the 64-mMIMO campaign the sounder measures the 8×16 MIMO channel fully in parallel, which is further extended by connecting the elements of each antenna set (defined in subsection 2.2) via a fast switch. The sounder measures the full system channel (64×16) semi-simultaneously (i.e. within 655 μs), so we can consider the channel to be static during the measurement interval. This remarkable characteristic of the sounder allows to measure dynamic channels. In the 128-mMIMO campaign the sounder uses only a subset of the transmit ports (i.e. 4) so it measures a 8×4 MIMO channel fully in parallel, which is further extended by connecting the elements of each antenna set (defined in subsection 2.3) via a fast switch. The sounder measures the full system channel (128×4) semi-simultaneously (i.e. within 1.31 ms). The massive MIMO channel is sampled at a rate of 60 Hz during 20 s, for a total of 1200 channel realizations in each measurement run. The measurement SNR averaged over scenarios, arrays, users positions, and all the antenna links is

Fig. E.5: BS array with 8 sets of 16 elements

estimated to be 27 dB and 20 dB for the 64-mMIMO and 128-mMIMO respectively with a 5 percentile of 13 dB and 6 dB respectively.

3.2   Narrowband channel and Normalization

We focus on the analysis of a narrow band channel obtained via Fourier transform of the measured impulse responses. We disregard all the frequencies except the central one with a bandwidth of 2 MHz. We denote $\mathbf{h}_k^{(n)}(r) \in \mathbb{C}^{M \times 1}$ as the channel vector from antenna $n \in \{a, b\}$ in the handset of user $k \in \{1, ..., 8\}$ in 64-mMIMO and $k \in \{1, 2\}$ in 128-mMIMO to the BS array at channel realization $r \in \{1, ..., R\}$, where $R = 1200$. $M = 64$ in 64-mMIMO and $M = 128$ in 128-mMIMO is the number of BS elements. $h_{mk}^{(n)}(r)$ is the mth entry of the vector, corresponding to the mth element of the BS array. We call $\mathbf{H}(r) \in \mathbb{C}^{M \times KN}$ the full 64×16 channel matrix in 64-mMIMO and 128×4 in 128-mMIMO. $K = 8$ is the number of users in 64-mMIMO and $K = 2$ in 128-mMIMO, $N = 2$ is the number of antennas per user. The two channel vectors of user k at realization r are placed in two consecutive columns of $\mathbf{H}(r)$.

Normalizing the channel we create a virtual power gain control, where the received energy from each user antenna is normalized as:

$$\overline{\mathbf{h}}_k^{(n)}(r) = \frac{\mathbf{h}_k^{(n)}(r)}{\sqrt{\sum\limits_{r=1}^{R} \left\| \mathbf{h}_k^{(n)}(r) \right\|^2}} \sqrt{MR} \tag{E.1}$$

where $\|\cdot\|$ is the Euclidean norm.

With this normalization, we remove the user impact and handset antenna power imbalance but we keep the differences among BS elements. We denote $\overline{\mathbf{H}}(r) \in \mathbb{C}^{M \times KN}$ as the channel matrix made out of the normalized vectors in (E.1).

4   Channel hardening

One of the most promising features of massive MIMO is its capability to harden the channel. In other words, the fast fading is reduced and the noise is
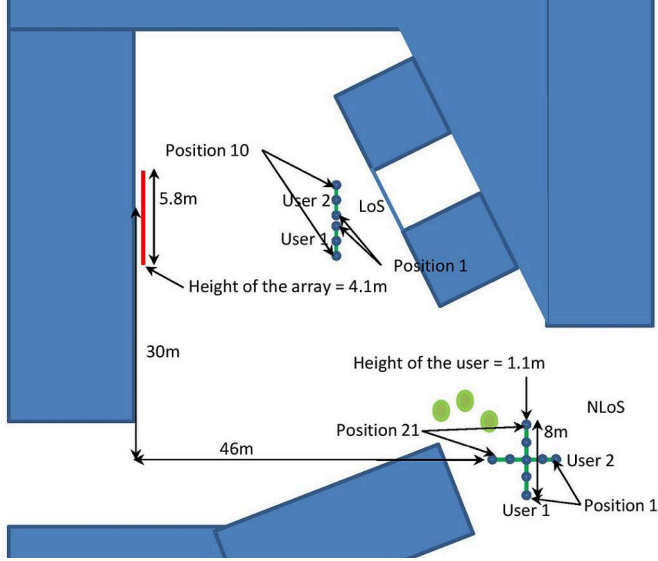
Fig. E.6: Scenario in LoS and scenario in NLoS

Fig. E.7: 2 users holding the sticks to keep the separation constant

averaged out as a result of the law of large numbers [20]. Channel hardening allows to allocate resources in a longer time period, since the fast variations of the channel vanishes. In addition, the signal power of each user is more stable, so the outage probability is reduced.

4.1 Standard deviation of the mean power

To study the channel hardening effect, we compute the standard deviation of the mean power across the antennas of the BS array. The mean power is

$$\overline{P}_k^{(n)}(r) = \frac{1}{M'} \sum_{m=1}^{M'} \left| \overline{h}_{mk}^{(n)}(r) \right|^2 \tag{E.2}$$

where M' is the selected number of BS elements. The standard deviation is computed over the R realizations of the channel as

$$Std_k^{(n)} = \sqrt{\frac{\sum_{r=1}^{R} \left(\overline{P}_k^{(n)}(r) - \mu \right)^2}{R - 1}} \tag{E.3}$$

where $\mu = \frac{1}{R} \sum_{r=1}^{R} \overline{P}_k^{(n)}(r)$ is the mean power over the realizations.

First we focus on 64-mMIMO. The results obtained are diverse for each scenario and each user. The reasons could be the shadowing, the number of scatterers, and the relative position of the user and the BS array. Here we give an example in Fig. E.8 that shows the standard deviation of the mean power for user 3, antenna a in the S-LoS $\perp$ scenario. The results for a theoretical Gaussian channel is used as a reference model. The number of elements in the BS array is increased adding consecutive elements, starting from the most right element in Fig.E.1.

The results show a decrease of channel variations when increasing the number of BS antennas. The VLA has the most hardening effect, followed by the LA which in turn is better than the C2D array. When the aperture of the array increases some of the antennas become more separated, likely creating less correlated channels and more hardening. Even if in this case the role of the array shape is clear, it is not like this for all the scenarios or users.

In order to have a broader view of the result, in Fig. E.9 we plot the same metric for the maximum number of elements in the BS array (i.e. 64 antennas), taking the statistics across the 16 user antennas, for each array and scenario measured, which gives 16 samples per box. The boxplot shows the first and third quartiles as the bottom and top of the box, and the line inside the box is the second quartile (i.e. the median). The median of the 16 user antennas shows that for all the scenarios, except the S-NLoS, the VLA has the strongest channel hardening, followed by the LA which in turn is better than the C2D. Thus, the conclusions obtained in Fig. E.8 can be generalized in a statistical sense for most of the scenarios.

Second we focus on 128-mMIMO. We use the same metric explained before. Fig. E.10 shows the standard deviation of the mean power for user 1 antenna a in both LoS and NLoS scenarios. The Gaussian channel is also plotted as a reference. The results are similar to the 64-mMIMO, and show a
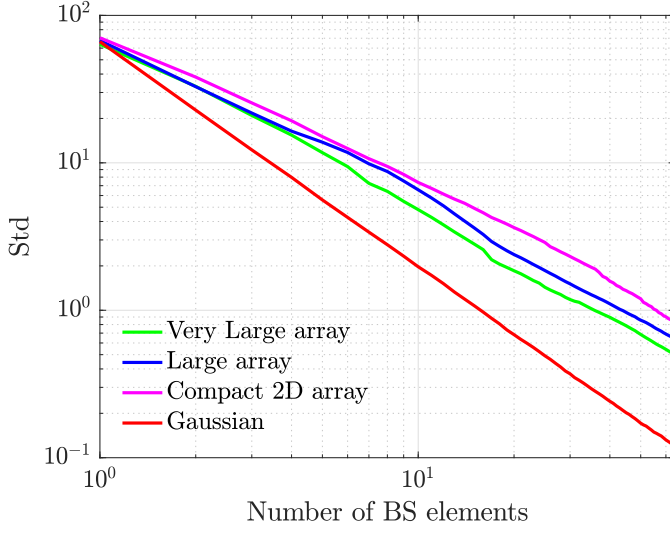
Fig. E.8: Standard deviation of the mean power, User 3 antenna a, S-LoS ⊥
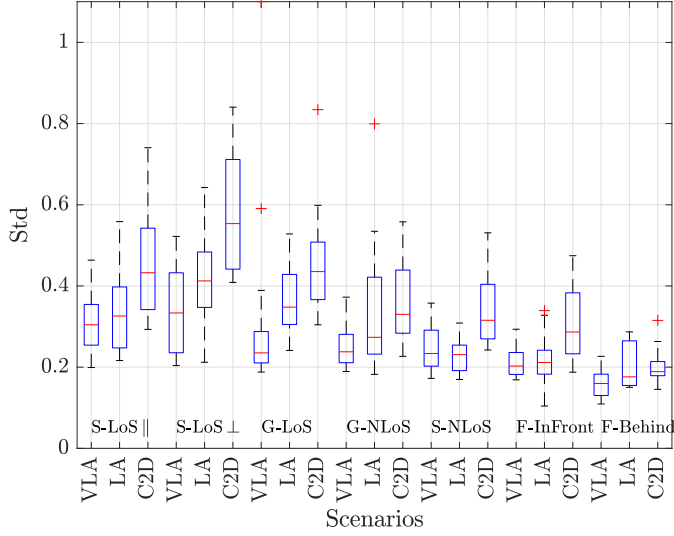
Fig. E.9: Boxplot of the standard deviation of the mean power with 64 BS antennas, all the scenarios

hardening effect in the channel. It is interesting to notice that both scenarios have similar performance. In order to generalize the results, we look at the statistics over users and their positions.

In Fig. E.11 we show the same metric for 128 BS antennas taking the statis-

tics over the 4 user antennas and all the measured positions of the users, which gives 84 samples for the NLoS scenario and the Gaussian channel boxes, and 40 samples for the LoS scenario box. We observe that the measured channels show a larger dispersion compared with the Gaussian channel as it is expected due to variation in the surroundings, hand grip, etc. We also observe the stronger hardening in the LoS scenario compared with the NLoS scenario. The NLoS scenario in some cases achieve as much hardening as the LoS but the median and the inter-quartile range is smaller for the LoS scenario.

To understand the reason why LoS and NLoS scenario behave so similarly we simulate a very simple scenario modeling the relative position of BS antennas and the users as in the LoS scenario in the measurements and we add a certain number of random scatterers. We model the channel between BS antenna i and user antenna j (with distance d_{ij}) as: $h_{ij} = \frac{\lambda}{4\pi d_{ij}}e^{-j\frac{2\pi}{\lambda}d_{ij}}$. This is not a model of the measured channel, but a tool to study the channel hardening in LoS conditions. We observe that when there are no scatterers the channel is already hardened even for a small number of BS antennas. This is because the LoS channel has no power variation across the antennas (also observed in the measurements), only a small variation due to the movement of the user. With a small number of scatterers, both with and without a LoS path, the results are similar to those of the measurements, so this is probably the situation we have measured. Finally when the number of scatterers is very high, the channel shows a strong hardening like the Gaussian channel as expected.

In order to understand the degree of scattering in the measurements we use the method of moments to calculate the Rician K factor [21]. Computing the statistics for all the antenna links, and distances between users, the 10 and 90 percentiles and the mean are: -0.8 dB, 8.2 dB, 4.1 dB, respectively for the LoS Parallel scenario and -3.1 dB, 7.1 dB, 2 dB for the NLoS scenario. Note the method of moments K factor estimation is known to be poor for low SNR [22]. Hence, a small fraction of clearly erroneous results were omitted from the statistics.

In order to quantify the hardening we look at the ratio of the median standard deviation obtained with 128 antennas to the median standard deviation obtained with 1 antenna. To avoid the differences of choosing different antennas, we take the average of the standard deviation of all the single antennas. In the Gaussian channel the ratio is 63 dB, while in the LoS it is 48 dB and in the NLoS it is 49 dB. Even if there is certain difference between the Gaussian channel and the measured channels, the measured hardening is still significant. To quantify the spread of the hardening, we use the ratio between the inter-quartile range obtained with 128 antennas to the inter-quartile range obtained with 1 antenna. For the NLoS the ratio is 40 dB, for the LoS it is
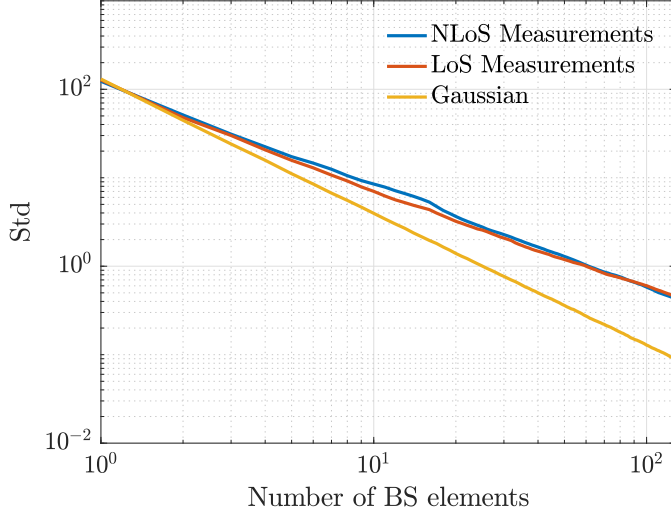
Fig. E.10: Standard deviation of the mean power, User 1 antenna a NLoS 0.57m and LoS 0.6m between users
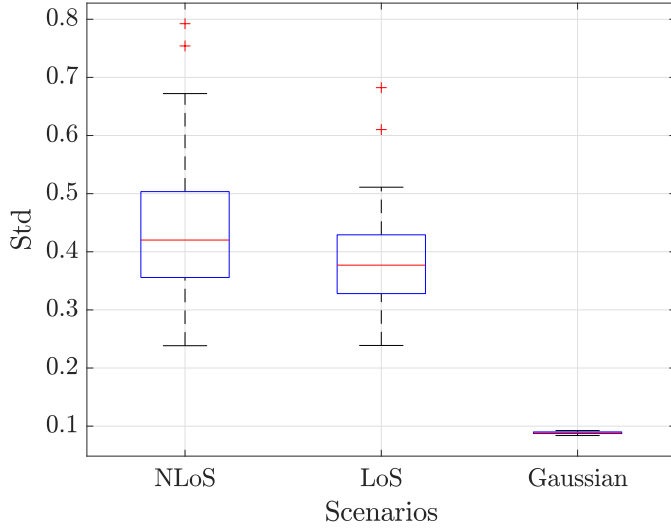
Fig. E.11: Boxplot of the standard deviation of the mean power with 128 BS antennas

49 dB and for the Gaussian channel it is 65 dB. We see that the ratio of spread is similar to the ratio of hardening, except for the NLoS scenario where the ratio of spread is lower.

As a conclusion, we observe the channel hardening effect when the number of BS antennas increases, but not as strong as the Gaussian channel. We

also showed the improvement brought by increasing the aperture of the array, and the small impact of the LoS or NLoS scenarios.

Finally we add that the random movement of the users brings high realism to the measurements, but it causes random polarisation mismatch, which is the same for all the antennas at the BS. This variation on the power can not be averaged out by the law of large numbers and it is reflected in the standard deviation.

5 Multi-user orthogonality and Sum-Rate

5.1 NLoS

The orthogonality between the channel vector of user k_1 and user k_2 is represented by its normalized scalar product,

$$SP(r) = \frac{\left|(\overline{\mathbf{h}}_{k_1}(r))^H \overline{\mathbf{h}}_{k_2}(r)\right|}{\left\|\overline{\mathbf{h}}_{k_1}(r)\right\| \left\|\overline{\mathbf{h}}_{k_2}(r)\right\|} \tag{E.4}$$

where $|\cdot|$ is the absolute value, and the superscript H denotes the conjugate transpose.

Fig. E.12 shows the mean scalar product over the R realizations of the channel. First we put our attention into the dependence of the channel vector orthogonality with the distance between users. When two users are placed in the same position their signals experience the same propagation phenomena (e.g. reflexion, diffraction, etc.). Therefore, the channels become highly correlated with a level up to 0.65. The channels are not exactly the same due to the handgrip of the users and small variations in the position since they cannot be at the same physical position. Increasing the distance between users decreases the inner product of their channel vectors. This result is complementary to the analysis in [17] section III.A. where the inner product between users is observed to decrease with the distance between users. About 0.2 correlation is observed for users separated more than approx. 1 m as also observed for well separated users and using 128 BS antennas in [4, 10].

The previous result on the inner product has a clear impact on the sum-rate of the system as linear precoders rely on the low correlation level of the users to simultaneously transmit independent data streams to them. Here we analyze the sum-rate of the system using the matched filter precoder.

The channel matrix is composed by the two channel vectors of the users using only one antenna

$$\overline{\mathbf{H}}(r) = [\overline{\mathbf{h}}_{k_1}^{(n_1)}(r) \quad \overline{\mathbf{h}}_{k_2}^{(n_2)}(r)] \tag{E.5}$$
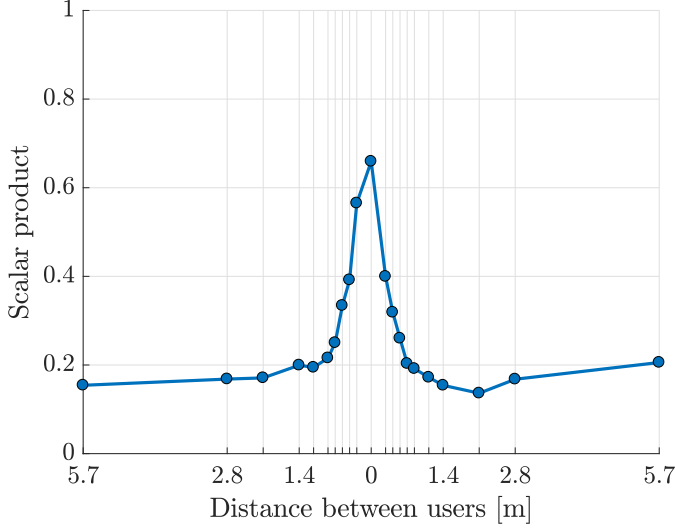
Fig. E.12: Multi-user orthogonality, User 1 antenna a, User 2 antenna b, NLoS, 128-mMIMO

The channel matrix $\overline{\mathbf{H}}(r)$ is normalized to achieve the desired average SNR.

$$\overline{\overline{\mathbf{H}}}(r) = \sqrt{\frac{R}{\sum_{r=1}^{R} \left\| \overline{\mathbf{H}}(r)^H \overline{\mathbf{H}}(r) \right\|_f^2}} \overline{\mathbf{H}}(r) \tag{E.6}$$

where $\|\cdot\|_f$ is the Frobenius norm.

We compute the SINR of each user considering an SNR of 15 dB as,

$$SINR_k = \frac{\alpha \left| \overline{\overline{\mathbf{H}}}_k \mathbf{W}_k \right|^2}{\alpha \left| \sum_{\substack{j=1 \\ j \neq k}}^{K} \overline{\overline{\mathbf{H}}}_k \mathbf{W}_j \right|^2 + \sigma^2} \tag{E.7}$$

where $\mathbf{W}_i$ is the precoding vector for user i, $\overline{\overline{\mathbf{H}}}_i$ is the channel vector for user i, α is the normalization factor, and σ^2 is the power of the noise. The throughput for user k is computed as $R_k = \log(1 + SINR_k)$. The sum rate is obtained summing the throughput R_k of all the users.

As expected, the sum-rate shown in Fig. E.13 is strongly related to the inner product between user's channel vectors. When the users are in the same location the sum-rate drops nearly 50 % of that when they are well separated.

In the same figure we investigate the effect of increasing the number of BS elements from 4 to 128 while increasing the aperture. The elements are
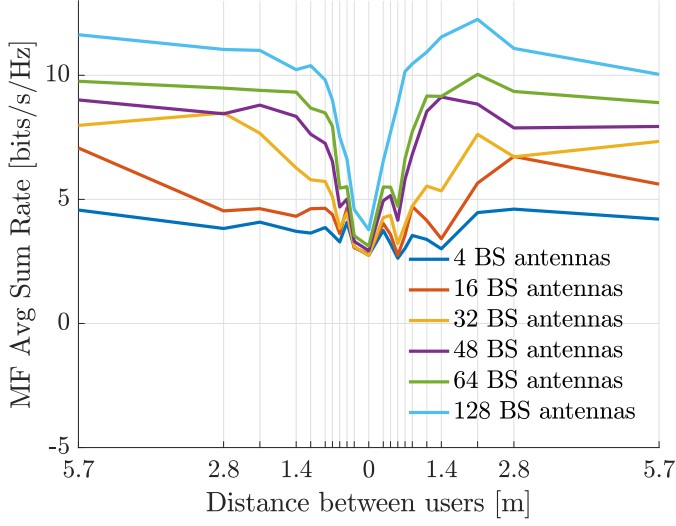
Fig. E.13: Average sum-rate, User 1 antenna a, User 2 antenna b, NLoS, consecutive elements

chosen in a consecutive order from the right side in Fig. E.5. In the worst scenario presented (i.e. 4 BS elements) there is hardly an improvement as the inter-user distance increases. When the users are well separated, the improvement brought by an increase number of antennas is visible. This holds also true for a relatively close users, up to around 1 m separation. When the users become very closely spaced (20 cm to 80 cm), the impact of increase the number of antennas becomes much less significant.

The position of the elements (specially the aperture of the array, defined as the maximum distance between any two elements) plays a key role in defining the users' orthogonality. In the previous example the aperture of the array was increased at the same time as the number of elements. Next, we keep the aperture constant when increasing the number of elements. The results are presented in Fig. E.14. In this figure two regions can be defined, namely an element limited region, and an aperture limited region. For arrays with more than 16 elements, the matched filter sum-rate is mainly defined by the aperture of the array, since the curves show a similar performance regardless the number of elements. The other region can be observed for the number of elements below 16. The matched filter sum-rate becomes limited by the number of elements, regardless the aperture of the array.

5.2 LoS

The matched filter sum-rate is also studied in the LoS scenario. In this scenario, the results are very related with the radiation pattern of the BS array,
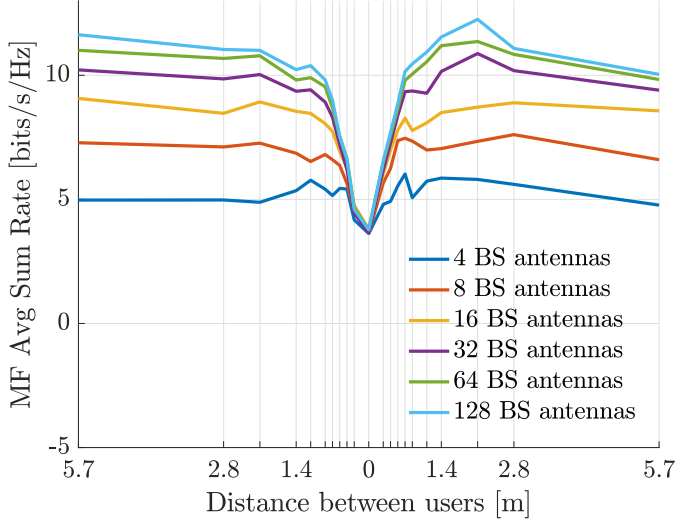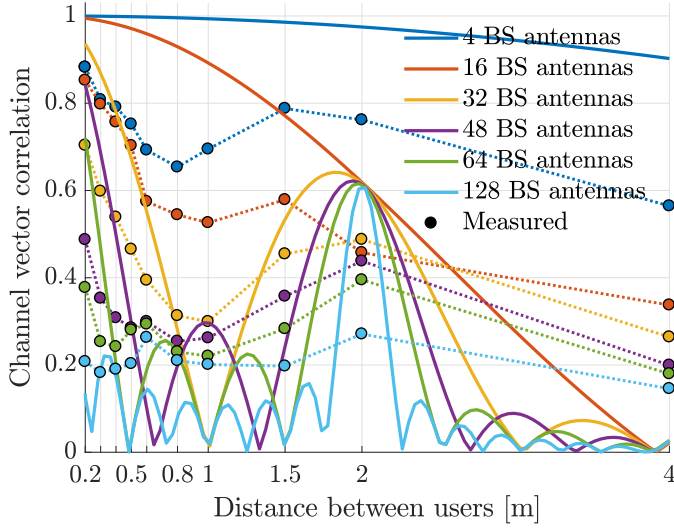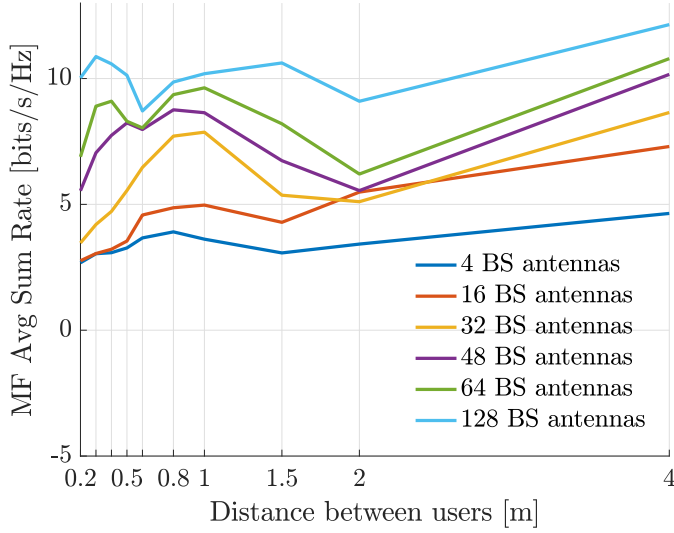
Fig. E.14: Average sum-rate, User 1 antenna a, User 2 antenna b, NLoS, equidistant elements and fix aperture

since the channel is dominated by the LoS component. For this reason, the sum-rate highly depends on the relative position of the users, with respect to the main beam and grating lobes. By observing Fig. E.15, where we show the channel vector scalar product (as described in Eq. E.4) of a simulated scenario and the measured one, we see that the position of the BS elements strongly impacts the result. In the simulation, for 16 elements or less, there are no grating lobes, because the separation between consecutive elements is half the wave length. When the number of elements includes two sets of 16 elements, a correlation peak appears at 2 m separation between users due to the grating lobe. For an array with three sets, another peak of correlation appears, and so on. The measurements follow a similar pattern, with high correlation at 2 m, lower correlation at 4 m, etc. 4 m separated users are well-separated for large arrays that have narrow beams, so we observe similar correlations to [4, 10] of about 0.2. Smaller arrays have larger correlation than [4, 10] because our 4 m separation is smaller than the beamwidth, but their tenths of meters separation is larger.

Fig. E.16 shows the matched filter sum-rate for the LoS scenario. First of all notice that for a user separation of 2 m the arrays with several sets (i.e. more than 16 elements) have a "valley" in the sum-rate due to the grating lobe, while the arrays with only one set (i.e. less or equal than 16 elements) do not see this effect. Especially in the curve of $32-$elements array, the symmetry with the previous figure (i.e. Fig. E.15) is very clear. At separation 1 m, the null in correlation translates to a high sum-rate. After these few examples

Fig. E.15: Channel vector correlation, measured and simulated, User 1 antenna a, User 2 antenna b, LoS, consecutive elements

Fig. E.16: Average sum-rate, User 1 antenna a, User 2 antenna b, LoS Parallel, consecutive elements

it seems that in LoS the sum-rate is related with the radiation pattern of the BS array.

6 Rank of the spatial covariance matrix

To investigate the rank of the spatial covariance matrix we compute the co-variance matrix from the BS side

$$\mathbf{C}_k^{(n)} = \frac{1}{R} \sum_{r=1}^{R} \mathbf{h}_k^{(n)}(r) \left(\mathbf{h}_k^{(n)}(r) \right)^H \qquad \text{(E.8)}$$

Using an eigenvalue decomposition of the covariance matrix we obtain a set of eigenvalues $\Lambda = [\lambda_1...\lambda_{M'}]$, where M' is the number of selected BS elements. Fig. E.17 shows the eigenvalue profile for user 1, antenna a, in all the 64-mMIMO measured scenarios with users.

For the LoS scenarios the total energy is generally concentrated on fewer eigenvalues, compared to the NLOS scenarios. For example a level of $-15\,\text{dB}$ is reached at about 10 eigenvalues or less for the LoS scenarios, whereas about 20 eigenvalues are needed to reach that level in the NLoS scenarios. However, all the profiles are decaying smoothly, so that determining the rank of the spatial covariance matrix effectively depends on the choice of threshold.

The smoothness of the curves can be attributed to limitations of practical measurements such as the limited number of measurements, a degree of non-stationarity of the channel, and inevitable imperfections like noise and spurious signals.

Insight into the channel rank properties can also be gained by analysing angle of arraivals. Fig. E.18 shows average beamforming spectra (Hamming weighted) obtained with the LA, Set 3 in both LoS and NLoS with different users. While it is possible to identify a main angle of arrival for the case of a nearby LOS user, it is also clear that the distribution over angle is much more even in the NLOS scenarios, as expected from the eigenvalue distributions in Fig. E.17. Even if the users have a dominant path, we observe energy scattered in other angles, as also reported in [3, 5].

7 Conclusion

This paper investigates three major characteristics of massive MIMO channels that are widely accepted and used in most of the theoretical studies, but they have, to the best of our knowledge, never been verified in measured prop-agation channels. These characteristics are the channel hardening in terms of mean power across the array, user orthogonality for specific distances be-tween users and the rank of the spatial covariance matrix.

The presented results confirm the channel hardening effect of the massive MIMO channels. The study shows how the standard deviation of the mean power across the BS array decreases when the number of elements in the
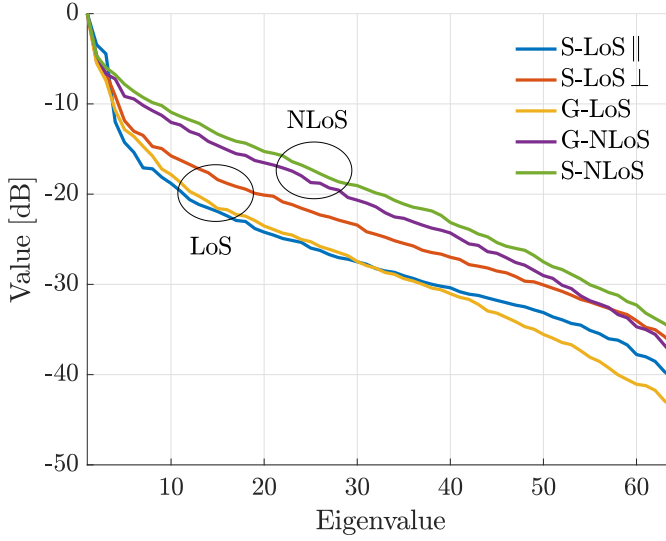
Fig. E.17: Normalized eigenvalues profile, User 1 antenna a, C2D, all scenarios with user
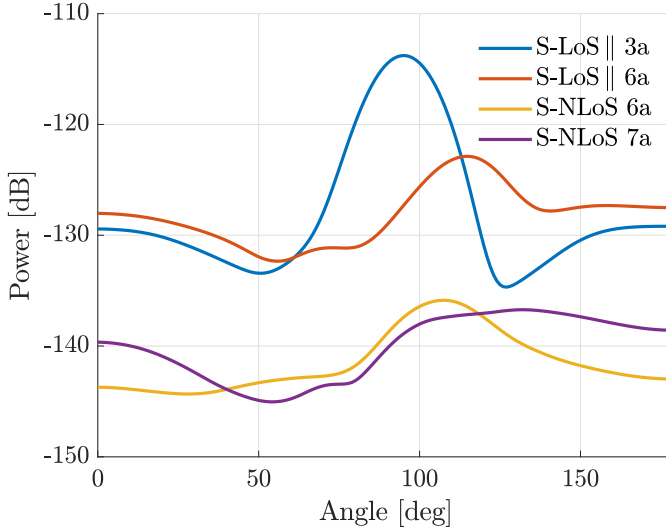
Fig. E.18: Beamforming angle of arrival averaged over channel realizations, Large Array, set 3

array increases. We also show the stronger hardening brought by increasing the aperture of the array.

This study also shows the sum-rate of the matched filter precoder of two users separated certain distances. The results show that in NLoS scenarios, the sum-rate decreases when the users are close to each other. In LoS sce-

narios the sum-rate depends on the exact position of the users respect to the beam created by the array. It makes clear the importance of taking into account the distance between users to model the system.

Finally in the study on the rank of the spatial covariance matrix, the profile of eigenvalues of the covariance matrix does not show a clear group of effective eigenvalues. Looking at the angle-of-arrival of the signal it is clear the energy is scattered in multiple directions, except in LoS with users very close to the BS array.

References

[1] A. Osseiran, J. F. Monserrat, and P. Marsch, *5G Mobile and Wireless Communications Technology*, 1st ed. Cambridge University Press, 2016.

[2] T. L. Marzetta, "Noncooperative cellular wireless with unlimited numbers of base station antennas," *IEEE Transactions on Wireless Communications*, vol. 9, no. 11, pp. 3590–3600, 2010.

[3] S. Payami and F. Tufvesson, "Channel measurements and analysis for very large array systems at 2.6 GHz," in *2012 6th European Conference on Antennas and Propagation (EUCAP)*. IEEE, 2012, pp. 433–437.

[4] J. Hoydis, C. Hoek, T. Wild, and S. ten Brink, "Channel measurements for large antenna arrays," in *2012 International Symposium on Wireless Communication Systems (ISWCS)*. IEEE, 2012, pp. 811–815.

[5] L. Wenjuan, L. Liu, T. Cheng, L. Yanping, X. Jingcheng, and L. Pengyu, "Channel measurements and Angle Estimation for Massive MIMO Systems in a Stadium," in *2015 17th International Conference on Advanced Communication Technology (ICACT)*. IEEE, 2015, pp. 105–108.

[6] D. Fei, R. He, B. Ai, B. Zhang, K. Guan, and Z. Zhong, "Massive MIMO Channel Measurements and Analysis at 3.33 GHz," in *2015 10th International Conference on Communications and Networking in China (ChinaCom)*. IEEE, 2015, pp. 194–198.

[7] H. Yu, Q. Zheng, Z. Zheng, L. Tian, and Y. Wut, "The Rationality Analysis of Massive MIMO Virtual Measurement at 3.5 GHz," in *CIC International Conference on Communications in China (ICCC Workshops)*. IEEE, 2016, pp. 1–5.

[8] J. Li, B. Ai, R. He, K. Guan, Q. Wang, D. Fei, Z. Zhong, Z. Zhao, D. Miao, and H. Guan, "Measurement-Based Characterizations of Indoor Massive MIMO Channels at 2 GHz, 4 GHz, and 6 GHz Frequency Bands," in *2016 IEEE 83rd Vehicular Technology Conference (VTC Spring)*. IEEE, 2016, pp. 1–5.

[9] C. M. Chen, V. Volskiy, A. Chiumento, L. Van Der Perre, G. A. Vandenbosch, and S. Pollin, "Exploration of User Separation Capabilities by Distributed Large Antenna Arrays," in *2016 IEEE Globecom Workshops (GC Wkshps)*. IEEE, 2016, pp. 1–6.

[10] X. Gao, O. Edfors, F. Rusek, and F. Tufvesson, "Linear Pre-Coding Performance in Measured Very-Large MIMO Channels," in *Vehicular Technology Conference (VTC Fall), 2011 IEEE*. IEEE, 2011, pp. 1–5.

[11] M. Gauger, J. Hoydis, C. Hoek, H. Schlesinger, A. Pascht, and S. ten Brink, "Channel Measurements with Different Antenna Array Geometries for Massive MIMO Systems," in *SCC 2015; 10th International ITG Conference on Systems, Communications and Coding*. IEEE, 2015, pp. 1–6.

[12] J. Flordelis, X. Gao, G. Dahman, F. Rusek, O. Edfors, and F. Tufvesson, "Spatial separation of closely-spaced users in measured massive multi-user MIMO channels," in *IEEE International Conference on Communications*. IEEE, 2015, pp. 1441–1446.

[13] X. Gao, F. Tufvesson, O. Edfors, and F. Rusek, "Measured propagation characteristics for very-large MIMO at 2.6 GHz," in *2012 Conference Record of the Forty Sixth Asilomar Conference on Signals, Systems and Computers (ASILOMAR)*. IEEE, 2012, pp. 295–299.

[14] X. Gao, O. Edfors, F. Rusek, and F. Tufvesson, "Massive MIMO Performance Evaluation Based on Measured Propagation Data," *IEEE Transactions on Wireless Communications*, vol. 14, no. 7, pp. 3899–3911, 2015.

[15] M. Teeti, J. Sun, D. Gesbert, and Y. Liu, "The Impact of Physical Channel on Performance of Subspace-Based Channel Estimation in Massive MIMO Systems," *IEEE Transactions on Wireless Communications*, vol. 14, no. 9, pp. 4743–4756, 2015.

[16] A. Adhikary, J. Nam, J.-Y. Ahn, and G. Caire, "Joint Spatial Division and Multiplexing," *IEEE Transactions on information theory*, vol. 59, no. 10, pp. 6441–6463, 2013.

[17] À. Oliveras Martínez, E. D. Carvalho, and J. Ø. Nielsen, "Towards Very Large Aperture Massive MIMO: a measurement based study," in *Globecom Workshops (GC Wkshps), 2014*. IEEE, 2014, pp. 281–286.

[18] À. Oliveras Martínez, E. De Carvalho, J. Ødum Nielsen, and L. Jing, "Frequency Dependence of Measured Massive MIMO Channel Properties," in *2016 IEEE 83rd Vehicular Technology Conference (VTC Spring)*, 2016, pp. 1–5.

[19] À. Oliveras Martínez, E. De Carvalho, and J. Ødum Nielsen, "Massive MIMO Properties based on Measured Channels: Channel Hardening , User Decorrelation and Channel Sparsity," in *Conference Record of the Fiftieth Asilomar Conference on Signals, Systems and Computers*, 2016.

[20] B. M. Hochwald, T. L. Marzetta, and V. Tarokh, "Multiple-antenna channel hardening and its implications for rate feedback and scheduling," *IEEE Transactions on Information Theory*, vol. 50, no. 9, pp. 1893–1909, 2004.

[21] L. J. Greenstein, D. G. Michelson, and V. Erceg, "Moment-Method Estimation of the Ricean K-factor," *IEEE Communications Letters*, vol. 3, no. 6, pp. 175–176, 1999.

[22] C. Tepedelenlioglu, A. Abdi, G. B. Giannakis, and M. Kaveh, "Performance analysis of moment-based estimators for the K parameter of the rice fading distribution," in *IEEE International Conference on Acoustics, Speech, and Signal Processing*, 2001.

References

Paper F

Experimental Study of the Benefits of a Second
Antenna at the User Side in a Massive MIMO System

Àlex Oliveras Martínez, Petar Popovski, Jesper Ødum Nielsen,
and Elisabeth De Carvalho

Abstract

Massive MIMO is commonly described as a large number of Base Station (BS) antennas serving a smaller number of single-antenna users. However, adding a second antenna to the user handset opens the possibility to exploit multiplexing techniques and obtain higher throughput. This study is based on a measurement campaign comprising a BS with 64 elements reconfigurable into 3 shapes: (1) a very large array with 6m aperture; (2) a large array with 2m aperture; (3) a compact 2 dimensional array with 25cm by 28cm sides. We study the throughput in single-user and multi-user scenarios using both non-linear optimal and linear precoders. The experimental results show that the throughput increases when adding a second antenna, but the increase is lower than in Gaussian channels due to the intra-user correlation. However, increasing the number of BS antennas, massive MIMO achieve more benefits from the second antenna. A large number of users in the system and the inter-user correlation reduce the benefits of a second antenna in the user handset.

1   Introduction

Massive MIMO was first described in the seminal work of Marzetta as a time-division-duplexing (TDD) cellular system comprising a very large number of Base Station (BS) antennas serving a smaller number of single-antenna users in the same time-frequency resource [1]. In the recent years it has been considered an essential technology for 5G, since it claims high gains in throughput, reliability and energy efficiency [2]. The excess number of BS antennas renders a large number of degrees of freedom in the system that can be exploited by signal processing techniques. For example, when the number of BS antennas grows large, the channel vectors of the users become asymptotically orthogonal, which makes linear precoding techniques to achieve close to optimal performance [3].

Extending the definition of massive MIMO to users with multiple antennas, the degrees of freedom of the system can be utilized to multiplex several data streams to the same user. Hence, the throughput gain of massive MIMO can be increased. However, the close distance between antennas in the same device can reduce the degrees of freedom of the channel and lead to only small improvements in multiplexing gain. Although most of the massive MIMO research has been focused on single-antenna users, some work derived the benefits of multiple antennas users in theoretical channels [4]. We go beyond those studies by focusing on multi-antenna handsets in measured massive MIMO propagation channels. Specifically, we study the broadcast channel where the BS serves multiple users simultaneously.

Several massive MIMO measurement campaigns have been performed recently, but due to the difficulty of measuring such a large number of antennas

simultaneously, most of them use virtual antenna arrays (e.g. [5]). The measurements for the current work were performed at 5.8 GHz in a large indoor environment similar to a shopping mall to reflect the new scenarios of 5G [2]. Such scenarios can integrate very large BS arrays into their structures. The measurement has 64 BS elements reconfigurable into three array shapes: A very long aperture (6 m) array, a long aperture (2 m) array, and a rectangular (25 cm by 28 cm) array. The array serves 8 users with 2 antennas each. Line-of-Sight (LoS) and Non-Line-of-Sight (NLoS) scenarios are measured. We focus on indoor scenarios where moving users hold a handset mockup. The study of multi-antenna users' throughput is only possible because of the simultaneous user antenna measurements achieved by the Aalborg University channel sounder. The data of the measurements was also analyzed in [6–8].

Another measurement campaign studying user handsets with multiple antennas was performed in [9]. It uses 100 BS antennas, but only one static handset with 3 antennas, from which only 2 are used at a time. The main difference from our present work is that [9] focus on the uplink pilot transmission schemes to achieve diversity gain, whereas here the focus is on the downlink broadcast multiplexing. Also, in [9] user antenna power imbalance is studied, while here the throughput is evaluated versus SNR and the number of antennas. In addition, we consider dynamics in the channel generated by the movement of the users and their handgrip.

1.1 Contribution

The data from the measurement campaign used in this study was previously analysed in [6–8]. These publications focus on the characteristics of the massive MIMO channel without giving results on the throughput performance. These publications present results on the degree of multi-user multiplexing, the orthogonality of the channel vectors, the channel hardening, etc. Although, most of the results are for single-antenna users, they also show the condition number of the channel with the two antennas in the same user handset.

In contrast here we study the benefit of adding a second antenna to the user handset. This is a novel result because the analysed measured channels are the only ones having multiple users with multiple antennas each. In addition, this publication presents results on the performance of the system using various linear and non-linear precoders. We compare the throughput of the system with single-antenna users and double-antenna users and we study the impact of the number of antennas and the signal-to-noise ratio (SNR). We also show statistics of the sum rate for different users.

The results show that dual-antenna users have higher throughput than single-antenna ones, but the improvement is smaller than that for Gaussian channels due to the higher correlation between the antennas in the user hand-

set. In single-user systems the improvement of adding a second antenna to the handset is larger than in multi-user systems, because in multi-user systems the load is higher and the channel experiences a saturation effect. In addition, multi-user systems suffer from intra-user interference. We observe that in massive MIMO increasing the number of antennas at the BS reduces the correlation and inter-user interference and makes the performance of measured channels similar to the performance of Gaussian channels. For example, for 32 BS antennas, the results show a 37 % average increase in dirty paper coding capacity at 10 dB SNR when adding the second antenna, compared to a 55 % increase in Gaussian channels. Doubling the number of BS antennas to 64, the improvement becomes 53 % and 65 % for the measured channels and the Gaussian ones respectively. In the indoor measured channels with 8 double-antenna users and an SNR range from −10 to 14 dB, massive MIMO achieves more benefits from adding a second antenna to the user due to the large number of BS antennas.

2   Measurements and Data

In the following we briefly depict the measurement campaign. For more details refer to [6].

2.1   Set-up

Three BS arrays are tested, all consisting of 64 monopole elements. The monopoles are arranged in eight linear arrays, named sets in the following, each with eight elements separated by $\lambda/2$.

The array sets are grouped in three dispositions. The VLA (i.e. very large aperture) array is a linear 6 m long array where the antenna sets are placed longitudinally with a separation of 50 cm between them. The LA (large aperture) array is a linear 2 m long array where the antenna sets are placed longitudinally with no separation between them. The C2D (i.e. compact 2D array) is a square array of dimension 25 cm by 28 cm where the antenna sets are placed next to each other, along the long edges. The C2D array is shown in Fig. F.1(b).

The measurements involve eight mock-up handsets with two antennas separated $\lambda/2$. The total of 16 channels originating at the user side are all measured simultaneously. Eight users hold the handsets in front of them imitating "data mode" as if using a smartphone for browsing.

In the following *scenarios* denotes the dispositions of the users or handsets. Seven scenarios are tested, each one with specific propagation properties, with LoS and NLoS and with a specific distribution of the devices. The details of the scenarios are descibed in [6]. Fig. F.1(a) shows the NLoS scenario with

spread users.

2.2 Channel sounder: quasi-simultaneous measurements

The measurements were made with a correlation based channel sounder operating at 5.8 GHz and with a bandwidth of about 100 MHz. The sounder measures a 8×16 MIMO channel fully in parallel, which is further extended by connecting the elements of each antenna set (see above) via a fast switch, so that the 64 elements are multiplexed onto the 8 parallel Rx channels of the channel sounder. During the measurements the users move randomly in a 1 m² area while the massive MIMO channel is sampled at a rate of 60 Hz during 20 s, for a total of 1200 time realizations of the channel in the measurement run.

2.3 Narrowband channel and Normalization

We focus on the analysis of a narrowband channel of 2 MHz bandwidth obtained via Fourier transform of the measured impulse responses. We denote $\mathbf{h}_k^{(n)}(r) \in \mathbb{C}^{M \times 1}$ as the channel vector from antenna $n \in \{a, b\}$ in the handset of user $k \in \{1, ..., K\}$ to the BS array at channel realization $r \in \{1, ..., R\}$, where $M = 64$ is the number of BS elements, $K = 8$ is the number of users and $R = 1200$ is the number of channel realizations.

Normalizing the channel we create a virtual power gain control, where the received energy from each user is normalized as:

$$\overline{\mathbf{h}}_k^{(n)}(r) = \frac{\mathbf{h}_k^{(n)}(r)}{\sqrt{\sum\limits_{r=1}^{R} \sum\limits_{n=1}^{N} \left\| \mathbf{h}_k^{(n)}(r) \right\|^2}} \sqrt{MRN} \qquad \text{(F.1)}$$

where $\|\cdot\|$ is the Euclidean norm, and N ($N = 1$ or 2) is the number of antennas per user.

With this normalization, we remove the user power imbalance but we keep the differences among BS elements, channel realizations, and handset antennas' power imbalance. We denote $\overline{\mathbf{H}}^{(1)}(r) \in \mathbb{C}^{M \times K}$ the channel made out of concatenating the normalized vectors in (F.1) using antenna a of each user. $\overline{\mathbf{H}}_k(r) \in \mathbb{C}^{M \times N}$ is the channel of user k using 1 or 2 antennas and $\overline{\mathbf{H}}(r) \in \mathbb{C}^{M \times KN}$ is the whole system channel matrix concatenating the channel of the users using both antennas.

3 Channel throughput

Channel throughput is used as a mean to quantify the performance of the system. We compare sub-optimal linear precoders with capacity achieving

(a) Scenario with spread users in NLoS, S-NLoS

(b) Compact 2D array, C2D

Fig. F.1: Scenario and array shown in the results

techniques (i.e. dirty paper coding) in the broadcast channel where the BS serves multiple users simultaneously.

3.1 Dirty paper coding

Dirty paper coding is a capacity achieving non-linear precoding technique first described in [10]. We compute such capacity using the waterfilling algorithm described in [11] which exploits the multiple access channel (MAC) - broadcast channel (BC) duality to obtain the optimal transmission policies. The achieved capacity becomes

$$C_{\text{DPC}}^{\text{sum rate}}(P, \overline{\mathbf{H}}(r)) =$$

$$\max_{\left\{ P_j \geq 0, \sum_{i=1}^{K} \text{Tr}(P_i) \leq P \right\}} \log \left| I + \sum_{i=1}^{K} \overline{\mathbf{H}}_i(r)^{\dagger} P_i(r) \overline{\mathbf{H}}_i(r) \right| \quad \text{(F.2)}$$

as described in [12]. P is the total transmitted power, P_j is the MAC covariance matrix of user j, I is the identity matrix, $|\cdot|$ is the determinant operator and $\cdot^{\dagger}$ is the transpose conjugate operator.

3.2 Zero-forcing precoder

We use a Zero-forcing precoder (ZF) to compute the linear precoder throughput for single-antenna users. ZF eliminates the inter-user interference by nulling the signal to unintended users [13]. Such precoder is defined as:

$$\mathbf{W}_{ZF}(r) = \overline{\mathbf{H}}^{(1)}(r)^{\dagger} (\overline{\mathbf{H}}^{(1)}(r) \overline{\mathbf{H}}^{(1)}(r)^{\dagger})^{-1} \quad \text{(F.3)}$$

Each column of $\mathbf{W}_{ZF}$ (i.e. $\mathbf{W}_{ZF,i}$) is normalized to unit power [13] $\overline{\mathbf{W}}_{ZF,i}(r) = \frac{\mathbf{W}_{ZF,i}(r)}{\sqrt{\left\|\mathbf{W}_{ZF,i}(r)\right\|_F^2}}$.

The system model becomes:

$$\mathbf{y}(r) = \overline{\mathbf{H}}^{(1)}(r)^\dagger \overline{\mathbf{W}}_{ZF}(r)\mathbf{P}(r)\mathbf{x}(r) + \mathbf{n}(r) \qquad \text{(F.4)}$$

With $\mathbf{y}(r)$ the receive signal, $\mathbf{x}(r)$ the transmit signal, $\mathbf{P}(r)$ a diagonal matrix with the power allocated to each user using water filling algorithm, and $\mathbf{n}(r)$ an additive white Gaussian noise. The sum rate of this system is computed as the sum of the throughput for each user $R_k = \log(1 + \text{SINR}_k)$. Where SINR_k is the signal power to noise plus interference ratio of user k ($\text{SINR}_k = \frac{P_k}{I_k + N_0}$).

3.3 Block diagonalization precoder

In systems with multiple antenna users the goal is to reduce the inter-user interference at the same time that several data streams are multiplexed for each user. The solution is a block-diagonal precoder [14]. A block diagonalization precoder (BD) transmits the signal for the intended user into the null space of the interfering user, and projects this signal to the channel of the intended user. Hence, the multiplexing gain is exploited while the inter-user interference is reduced. The power is allocated to the data streams using a water filling algorithm.

We use BD to compute the linear precoder throughput for double-antenna users.

4 Results

4.1 Single user

We begin the analysis by considering a channel with a single user in order to keep the load of the system low (i.e. the number of user antennas is much lower than the number of BS antennas). In this way we also avoid the effects of inter-user interference and we can focus on the impact of other properties of the channel, such as the intra-user correlation.

Fig. F.2 shows the DPC capacity averaged over 1200 channel realizations of two correlated channels with independent identically distributed (i.i.d.) Gaussian entries. We refer to these simulated channels for comparison purposes.

In the following we plot the results of measured channels together with the results of simulated channels with independent identically distributed (i.i.d.) Gaussian entries, which we call "Gaussian channels". We show results
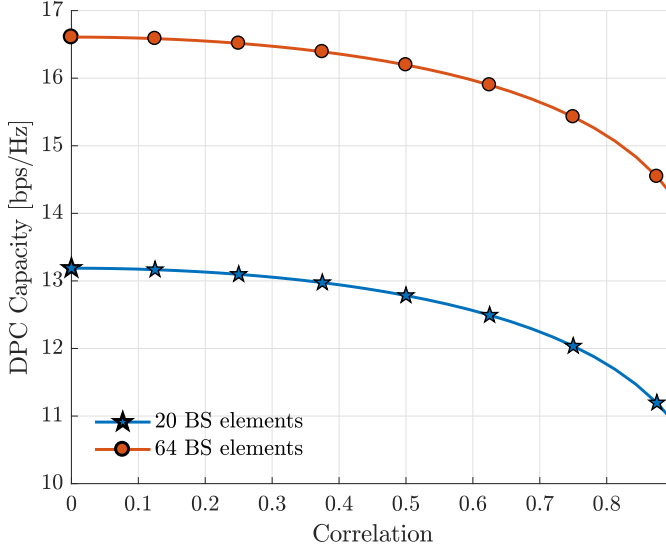
Fig. F.2: DPC capacity averaged over 1200 realizations of simulated correlated Gaussian channels

considering 20 consecutive antennas at the BS and all 64 antennas to show the effects of the number of antennas and the array aperture. The capacity is computed for a 10 dB SNR, unless otherwise stated.

Fig. F.3 shows the cumulative distribution function (CDF) of the DPC capacity over the 1200 channel realizations. The results presented here are for the S-NLoS scenario, C2D, user 7, but they are very similar to other users, arrays and scenarios.

The results in Fig. F.3 show a smaller difference between measured channels and Gaussian channel when increasing the number of BS antennas. This is in accordance with the theoretical result that increasing the number of BS antennas makes the channel vectors of different users asymptotically orthogonal, and therefore more similar to the Gaussian channel [1]. For a fixed number of BS antennas, a second antenna in the handset increases the differences between measured channels and Gaussian channels. This is due to the large correlation between the antennas that can not be compensated by increasing the number of BS antennas.

The steepness of the curves shows the channel hardening effect. The more hardened channel, experiences less fading and the capacity has small variations over time. In Fig. F.3 we observe that the measured channels have less hardening than the Gaussian channel, due to the intra-user correlation.

We also notice that the measured channels can achieve higher DPC capacity than the Gaussian channel. This can happen due to the fading, because even if the total gain of the measured channel and the Gaussian channel is the
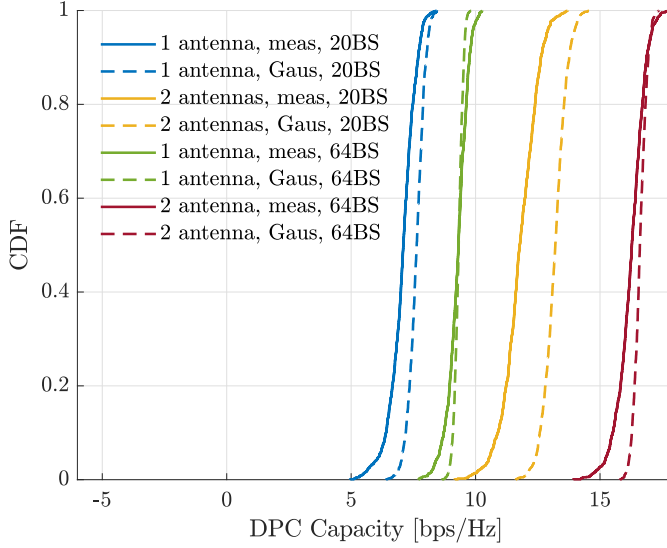
Fig. F.3: CDF of the DPC capacity at 10dB with 1 and 2 antennas, S-NLoS, C2D, User 7

same, the amount of fades and their deepness can be different. Due to the non-linearity of the logarithm function of the DPC capacity equation, even if the average power is the same for measured and Gaussian channels, the average DPC capacity does not need to be the same.

In terms of DPC capacity there is a clear benefit of adding a second antenna to the user handset. Although the curves show some variations on the capacity due to the fading, the double-antenna users have always a higher capacity than single-antenna users with the same number of BS antennas.

For the rest of the results we show the ergodic capacity averaging the instantaneous capacity over the 1200 channel realizations.

For a better understanding of the diversity of results among different users Fig. F.4 shows the statistics over the 8 users of the DPC capacity in the S-NLoS scenario and C2D. The boxplot shows the quartiles, whiskers and outliers. It divides the data in 4 regions each one containing 25 % of the results (i.e. 25th, 50th and 75th percentiles), the whiskers contain the values 1.5 times the inter-quartile range, above or below the 75th and 25th percentiles, and the rest of the data are outliers (i.e. crosses in red).

The results show that all the 8 users benefit of adding a second antenna in their handset regardless the number of antennas in the BS. The median capacity for channels with 20 BS antennas and users with two antennas is 13.2 bps/Hz for the Gaussian channel and 11.7 bps/Hz for the measured one corresponding to the case of 0 and 0.8 correlation respectively, as observed in Fig. F.2. For channels with 64 BS antennas, the median capacity is
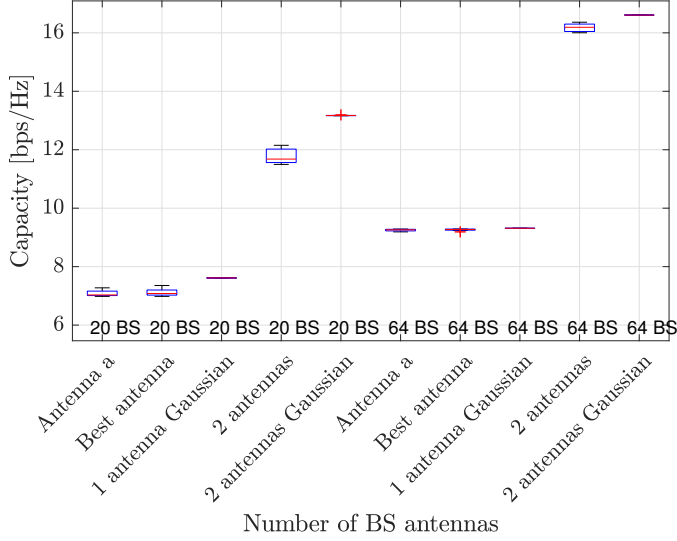
Fig. F.4: Throughput at 10dB with 1 and 2 antennas users expanding the BS array, S-NLoS, C2D array

16.6 bps/Hz and 16.2 bps/Hz for the Gaussian and the measured channels respectively which correspond to 0 and 0.5 correlation. Fig. F.5. shows that the correlation is 0.41 and 0.36 for 20 and 64 antennas respectively so the capacity not only depends on the correlation but also depends on other factors. For example, unequal branch powers will have an impact on the capacity.

The results in Fig. F.4 also show a higher dispersion in the users with 2 antennas. The position and handgrip of the users has a high impact in the orthogonality of its antennas. There is a decrease in the spread of the results when increasing the number of BS antennas. This is more evident in LoS scenarios and it shows the effects of channel hardening. Also by increasing the number of BS antennas the results of measured channels become more similar to the Gaussian channel. This is due to the asymptotic orthogonality achieved by increasing the number of BS antennas in massive MIMO.

Fig. F.4 also shows the DPC using the best antennas (i.e. a or b for all the channel realizations), however the results are very similar to always using antenna a. This means that there is no consistent difference in the channel of both antennas. For a single channel realization the fading properties of the channel can make the capacity in one antenna much better than in the other. However the randomness of the channel makes the ergodic capacity after 1200 channel realizations very similar for both antennas.

To compare single-antenna users and double-antenna users Fig. F.5 shows the DPC capacity averaged over the 8 users when increasing the number of BS antennas and increasing the aperture of the array. The results presented here
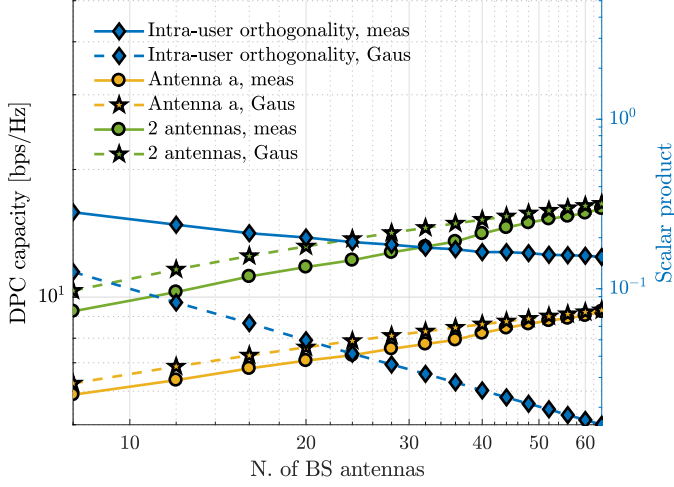
Fig. F.5: Scalar product and DPC capacity at 10dB with 1 and 2 antenna users expanding the BS array, S-NLoS, C2D array

are for the S-NLoS scenario, C2D, but they are very similar to other measured scenarios and arrays. Notice that both axes are in logarithmic scale.

To evaluate the impact of the channel vector orthogonality of the two antennas in the same handset of the user we add to the plot the intra-user scalar product squared and averaged over channel realizations and users, which is computed as

$$SPS = \frac{1}{KR} \sum_{k=1}^{K} \sum_{r=1}^{R} \left(\frac{\left| \mathbf{h}_k^{(a)}(r) \mathbf{h}_k^{(b)}(r) \right|}{\left\| \mathbf{h}_k^{(a)}(r) \right\| \left\| \mathbf{h}_k^{(b)}(r) \right\|} \right)^2 \tag{F.5}$$

Since the Gaussian channel has zero mean, this metric shows the variance of the sample correlation and it is equal to $\frac{1}{M}$ [3]. The results of the measured channels are also proportional to $\frac{1}{M}$ but with less slope than the Gaussian channel, because the short distance between the antennas in the same handset makes their channel vectors highly correlated.

The capacity shows a direct proportionality with the number of BS antennas. This is a clear effect of the array gain. To double the antennas in the handset, doubles the slope of the capacity. The single-antenna users present a slope of 0.05 bps/Hz per antenna and the double-antenna users present a slope of 0.1 bps/Hz per antenna. The effect of the orthogonality between antennas is reflected on the distance between the capacity of the measured channel and the Gaussian channel.

To compare the different measured scenarios, Fig. F.6 shows the DPC ergodic capacity averaged over the 8 users. The results presented here are for
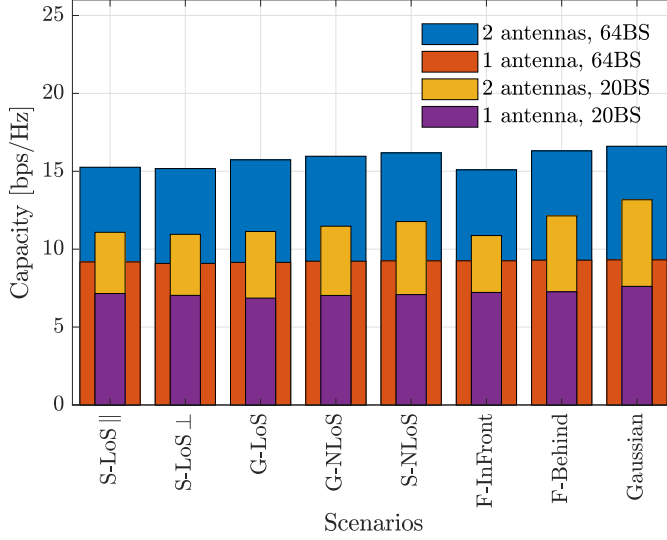
Fig. F.6: DPC capacity averaged over users with 1 and 2 antennas at 10dB, C2D array

the C2D array but they are very similar to other arrays. Notice that only the length of the bar shows the DPC capacity, whereas the width is set to improve the visualization.

When considering single-antenna users, all the scenarios lead to very similar results. The reason is that in single-antenna single-user channels the capacity depends on the attenuation of the channel. Since the measured channels are normalized to remove the users' power imbalance using eq. F.1, the averaged capacity presents small fluctuations among the scenarios. These fluctuations are due to the fading.

For dual-antenna users we observe higher variations of the DPC capacity among the measured scenarios. Although the variations are larger than for single-antenna users, the results are similar to the Gaussian channel. The reason for the variations is the correlation between the antennas in the same handset. The amount of scatterers in the environment and their distribution have an impact on decorrelating the channel vectors. This effect is even more visible in multi-user channels like the ones presented in Fig. F.11, discussed below.

Finally we focus on the conditions of the channel for which the two antennas of the handset are active. For this purpose we study the waterfilling power allocation to the antennas when performing eigenvalue decomposition. Due to the fading characteristics of the channel the power allocation to the antennas varies in each channel realization, therefore we compute the proportion of channel realizations that both antennas are allocated power. In

order to avoid the effect of the array gain we scale the transmitted power by the number of links in the system.

$$\mathbf{y} = \sqrt{\beta} \sqrt{\frac{P_t}{\text{numel}(\overline{\overline{\mathbf{H}}}_k)}} \overline{\overline{\mathbf{H}}}_k \mathbf{x} + \mathbf{n} \qquad \text{(F.6)}$$

$\mathbf{y}$ denotes the received signal by the user, β is the path loss, P_t is the transmitted power before removing the array gain, $\text{numel}(\cdot)$ is the number of elements of a matrix, $\mathbf{x}$ is the transmitted signal after precoding and $\mathbf{n}$ is an additive white Gaussian noise.

The results are averaged over the users and they are presented in Fig. F.7. This figure presents the results for the S-NLoS scenario and VLA. Other scenarios and arrays present different results according to the different correlation characteristics.

The results show an increase of number of channel snapshots where 2 antennas are active when increasing the number of BS antennas for a fixed SNR. For example at 6 dB SNR with 8 BS antennas only 22 % of the channel realizations use 2 antennas, while this percentage grows to 30 % and 93 % for 20 and 64 antennas respectively. This is the consequence of decorrelating the two antennas in the handset which makes the eigenvalues more similar to each other and the waterfilling algorithm allocates power to both antennas. This result can be seen in Fig. F.5, as the number of BS antennas increases the capacity of the measured channels becomes more similar to the Gaussian channel, because the two antennas become more uncorrelated and power is allocated to both of them.

4.2   Multiple users

In the following we consider a system with 8 users. In such scenario a small number of BS antennas means a large load of the system and it can have an impact on the result. The throughput is affected by the inter-user interference.

To illuminate the benefits of a second antenna in the user handset Fig. F.8 shows the throughput for DPC and linear precoders for single-antenna users and double-antenna users in the S-NLoS scenario and C2D. As the difference between curves changes for each SNR, we take 10 dB as a reference point for the following comparisons.

In this figure we observe an improvement of 50 % DPC sum rate when adding a second antenna to the users. Although the signal in the second antenna of the device is not completely orthogonal with the first antenna, there is a benefit of adding it. The improvement is smaller than the observed in single user systems. For example Fig. F.4 shows a 75 % increase in capacity. This is because multi-user systems are limited by the inter-user correlation, apart from the intra-user correlation. For linear precoders the result is similar with
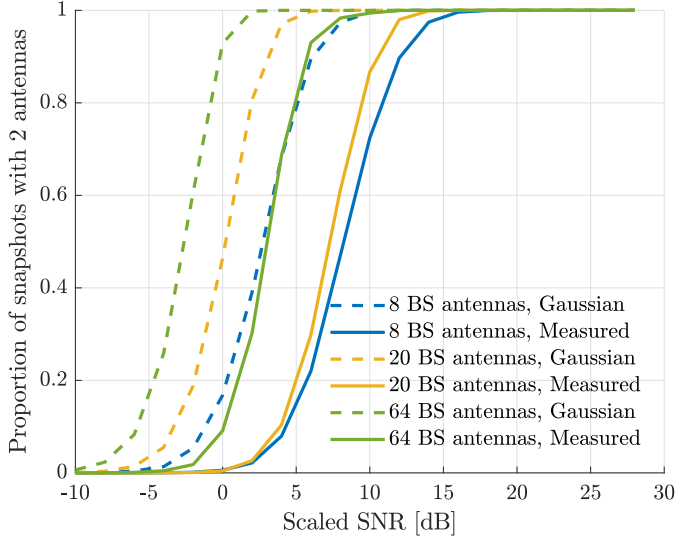
Fig. F.7: Proportion of snapshots that 2 antennas of the user are active, averaged over the users, removing the array gain, S-NLoS, VLA array

a sum rate increase of 36 %. In average, among all the scenarios and arrays (i.e. $7 \times 3 = 21$ combinations), there is an improvement of adding a second antenna of 53 % and 43 % for non-linear and linear precoders, respectively. For less than -4 dB SNR the performance of single stream per user is similar to the double stream per user, using linear precoders.

In comparison, the improvement in the Gaussian channels is 65 %, which is a larger percentage due to the larger orthogonality between the two antennas of the user. Although the theoretical Gaussian channels present a lower correlation between antennas, the throughput of the measured channel is similar, showing the benefit of the massive number of antennas decorrelating the user channels. Nevertheless this improvement is still lower than the 75 % achieved in single user systems observed in Fig. F.4 , it is a result of the saturation effect of the high load of the system.

In the same Fig. F.8 it is interesting to compare the sum rate achieved by linear precoders and DPC for a fixed number of user antennas. Both for single-antenna users and double-antenna users there is a small gap between linear precoders and optimal ones. This is due to the asymptotically orthogonal user channels achieved by an excess of BS antennas, which renders linear precoders close to optimal. However, we observe a larger difference for double-antenna users, where the ratio between BS antennas and total number of user antennas is lower (i.e. $\frac{64}{16} = 4$ compared to $\frac{64}{8} = 8$).

Additionally we compute the capacity for a time division multiplexing (TDMA) system instead of the broadcast channel in order to compare to the
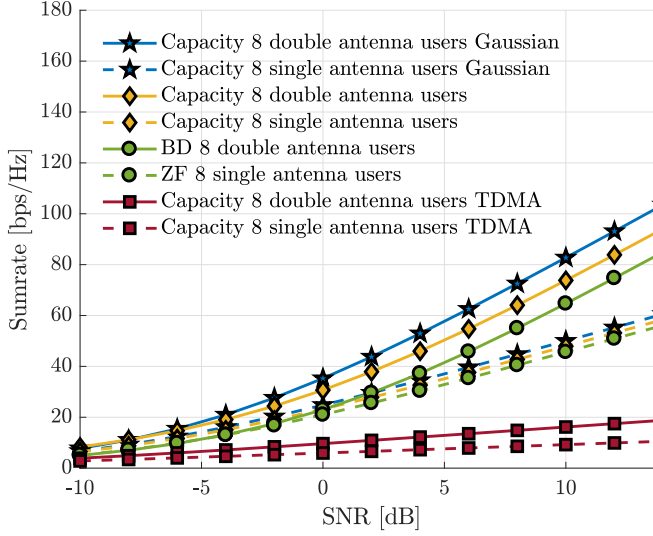
Fig. F.8: Throughput with 1 and 2 antenna users, S-NLoS, C2D

results without the effect of the load of the system. These results correspond to the results presented in section 4.1.

In order to investigate the impact of the number of antennas, and more specifically, the ratio between BS antennas and user antennas, Fig. F.9 shows the sum rate achieved at 10 dB SNR when increasing the number of BS antennas in the S-NLoS scenario and C2D. The antennas are selected in a consecutive order starting from the antennas closer to the bridge, and the aperture of the array is increased with the number of antennas. The TDMA curves are the same as presented in Fig. F.5.

First we observe that adding a second antenna to the user has more benefits when the number of BS antennas is large. Increasing the number of BS antennas decorrelates the two antennas in the handset and more information can be transmitted to the second antenna. For example, using 32 BS antennas there is a 37 % increase averaged over the scenarios and arrays in DPC capacity, whereas the Gaussian channel presents a 55 % capacity increase. The difference between measured and Gaussian channels is larger than when using 64 BS antennas that the increase in DPC is 53 % and 65 % for measured and Gaussian channels respectively.

As expected from the results in Fig. F.8, Fig. F.9 shows, for the linear precoders, a better performance of single-antenna users compared to the double-antenna users when the number of BS antennas is low. This is due to the ratio between BS antennas and user antennas. To fully exploit the benefits of massive MIMO, an excess of BS antennas is necessary. Hence, double-antenna

users need more BS antennas than single-antenna users. The crossing point of the two linear precoder curves corresponds to the ratios $\frac{25}{16} = 1.6$ compared to $\frac{25}{8} = 3.1$. Hence, in this scenario, to achieve massive MIMO performance, the number of BS's antennas has to be around 60 % higher than the number of user antennas. The linear precoders rely on the extra degrees of freedom to eliminate the inter-user interference. If the number of BS antennas is similar to the number of interfering users there are not enough degrees of systems to eliminate the inter-user interference. If the number of BS antennas is smaller then the number of user antennas the precoders can not work and the capacity becomes 0, as observed for less than 16 antennas in the BD curve. Other scenarios present similar results, however the crossing point varies among scenarios and arrays.

The impact of the number of antennas ratio is smaller in the DPC capacity than in the linear precoders. The double-antenna users have a better performance regardless the number of BS antennas. In addition, the DPC capacity increases at a higher rate for double-antenna users. Therefore, the benefit of the second user antenna increases with the number of BS antennas. It is also important to notice that increasing the number of BS antennas reduces the gap between the linear precoders and the DPC. Again, this is the effect of achieving asymptotically orthogonal user channels.

For small number of BS antennas, the correlation between user antennas in the measured channel is high, and the sum rate is lower than for the Gaussian channels. Increasing the number of BS antennas reduces the correlation and the sum rate of measured channels approaches the sum rate of the Gaussian channel. Specially for single-antenna users, the performance of the linear precoders becomes close to the DPC and Gaussian channel. For double-antenna users the difference in performance is larger, because of the smaller ratio between number of BS antennas and user antennas.

Fig. F.10 compares systems with the same load. First a system with 16 user antennas; grouped in 8 users so multiplexing is possible, or separated in 16 users so user antennas can not cooperate. The antennas used are the same in both cases so there are no difference in correlation. Second a system with 8 user antennas; chosen from 4 users so there is high correlation in the two antennas in the same user, or chosen from 8 users so there is low correlation between the antennas. Under this comparison, BD and ZF are almost the same, which means that neither the collaboration of antennas grouped two-by-two (BD) nor the decorrelated user antennas (ZF) shows a dominant performance. Reducing the number of BS antennas reduces the sum rate in both systems, but increases the difference between BD and ZF for the 'multiplexing' cases.

Fig. F.11 compares the mean DPC capacity of the measured scenarios. The figure shows the results with double-antenna users and single-antenna users as well as with 20 BS antennas and 64 BS antennas.
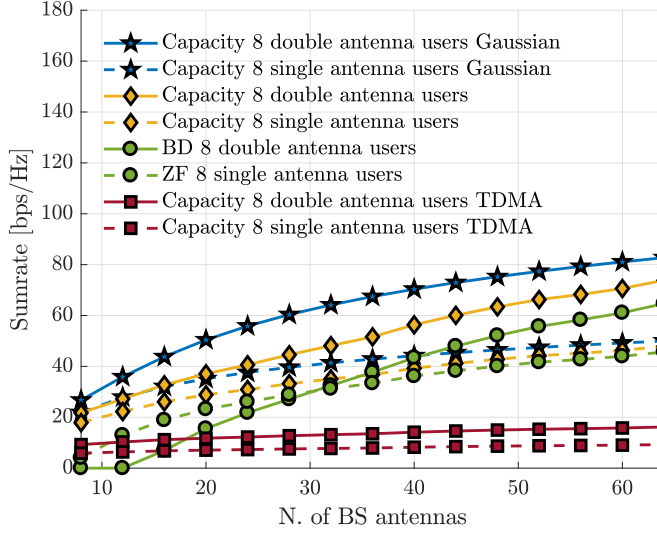
Fig. F.9: Multi-user throughput at 10dB with 1 and 2 antenna users expanding the BS array, S-NLoS, C2D
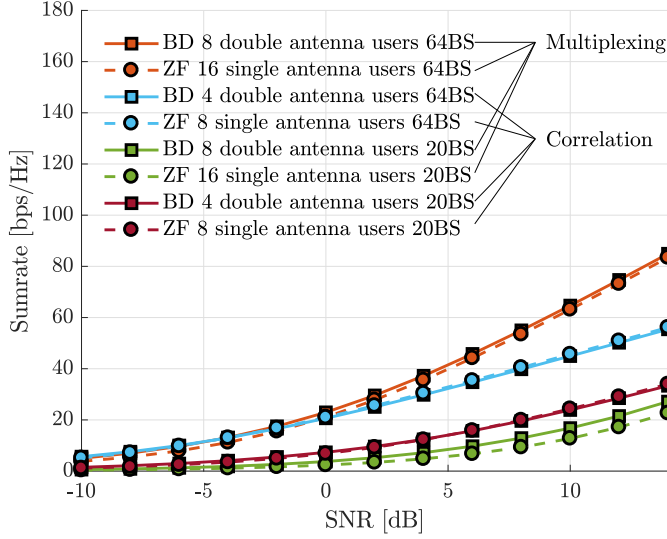
Fig. F.10: Mean multi-user throughput at 10dB with 1 and 2 antenna users and fixed load of the system, S-NLoS, C2D array

First, we observe a larger variation of the results compared with the single user scenario presented in Fig. F.6 because the multiuser scenario is affected by the inter-user interference, so the position of the users has a higher impact.
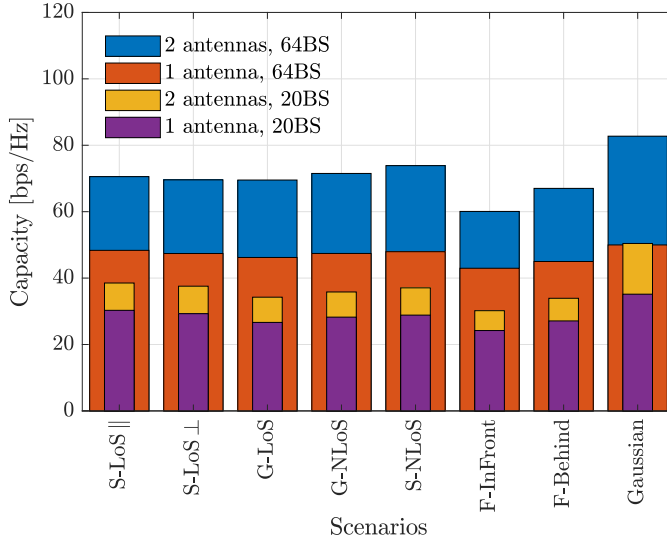
Fig. F.11: Mean multi-user DPC Capacity with 1 and 2 antenna users at 10dB, C2D array

Both for single-antenna users and double-antenna users the Free space scenarios show the lowest capacity. This is due to the short distance between the devices tied to the table. In addition the F-InFront scenario already presented high intra-user correlation in Fig. F.6 .

There is an increase of capacity in NLoS scenarios because the large amount of scatterers decorrelates the channel vectors of the users, even if they are grouped. This result is the same for the LA, however the VLA shows a decrease in capacity in NLoS scenarios, probably because some parts of the array are far away from the entrance of the room where the users are located.

5   Conclusion

A massive MIMO measurement campaign has been used to investigate the benefits of having two antennas in the user handset. The measurement campaign was carried out in a large indoor environment and involved 3 array shapes with 64 elements each, 8 users holding a double-antenna mockup handset, and 7 scenarios including LoS, NLoS, spread users, grouped users, and without users.

Considering a single user scenario we observe the benefits of adding a second antenna to the handset. The second antenna increases the capacity, but it also increases the variation of the results. A larger number of BS antennas makes the two antennas in the handset more orthogonal and the measured channels becomes more similar to the simulated Gaussian channel.

In multi-user scenarios the results show a 53 % average increase in dirty paper coding capacity at 10 dB SNR when adding the second antenna. There is also an improvement using linear precoders, though slightly less (43 %). We also show the importance of the ratio between the number of BS antennas and user antennas in linear precoders. Even though the user antennas in the measurements can be correlated, increasing the number of BS antennas achieves the massive MIMO asymptotic orthogonality and the gap between the throughput of i.i.d. Gaussian channels, non-linear precoders, and linear precoders asymptotically vanishes.

We conclude that the benefits of adding a second antenna to the user vary in each channel realization due to the fading, but in massive MIMO, by increasing the number of BS antennas, the proportion of channel realizations that allocate power to both antennas increases. Overall the sum-rate improves by adding a second antenna.

References

[1] T. L. Marzetta, "Noncooperative cellular wireless with unlimited numbers of base station antennas," *IEEE Transactions on Wireless Communications*, vol. 9, no. 11, pp. 3590–3600, 2010.

[2] A. Osseiran, J. F. Monserrat, and P. Marsch, *5G Mobile and Wireless Communications Technology*, 1st ed.   Cambridge University Press, 2016.

[3] H. Q. Ngo, E. Larsson, and T. Marzetta, "Aspects of Favorable Propagation in Massive MIMO," in *Signal Processing Conference (EUSIPCO), 2014 Proceedings of the 22nd European*, no. 2.   IEEE, 2014, pp. 76–80.

[4] X. Li, E. Björnson, S. Zhou, and J. Wang, "Massive MIMO with Multi Antenna Users: When are Additional User Antennas Beneficial?" in *23rd International Conference on Telecommunications (ICT)*.   IEEE, 2016, pp. 1–6.

[5] J. Hoydis, C. Hoek, T. Wild, and S. ten Brink, "Channel measurements for large antenna arrays," in *2012 International Symposium on Wireless Communication Systems (ISWCS)*.   IEEE, 2012, pp. 811–815.

[6] À. Oliveras Martínez, E. D. Carvalho, and J. Ø. Nielsen, "Towards Very Large Aperture Massive MIMO: a measurement based study," in *Globecom Workshops (GC Wkshps), 2014*.   IEEE, 2014, pp. 281–286.

[7] À. Oliveras Martínez, E. De Carvalho, J. Ødum Nielsen, and L. Jing, "Frequency Dependence of Measured Massive MIMO Channel Properties," in *2016 IEEE 83rd Vehicular Technology Conference (VTC Spring)*, 2016, pp. 1–5.

[8] À. Oliveras Martínez, E. De Carvalho, and J. Ødum Nielsen, "Massive MIMO Properties based on Measured Channels: Channel Hardening , User Decorrelation and Channel Sparsity," in *Conference Record of the Fiftieth Asilomar Conference on Signals, Systems and Computers*, 2016.

[9] E. L. Bengtsson, P. C. Karlsson, F. Tufvesson, J. Vieira, S. Malkowsky, L. Liu, F. Rusek, and O. Edfors, "Transmission schemes for multiple antenna terminals in real massive MIMO systems," in *2016 IEEE Global Communications Conference (GLOBECOM)*. IEEE, 2016, pp. 1–6.

[10] M. H. M. Costa, "Writing on Dirty Paper," *IEEE Transactions on Information Theory*, vol. 29, no. 3, pp. 439–441, 1983.

[11] N. Jindal, W. Rhee, S. Vishwanath, S. A. Jafar, and A. Goldsmith, "Sum power iterative water-filling for multi-antenna Gaussian broadcast channels," *IEEE Transactions on Information Theory*, vol. 51, no. 4, pp. 1570–1580, 2005.

[12] S. Vishwanath, N. Jindal, and A. Goldsmith, "Duality, achievable rates, and sum-rate capacity of Gaussian MIMO broadcast channels," *IEEE Transactions on Information Theory*, vol. 49, no. 10, pp. 2658–2668, 2003.

[13] A. Paulraj, R. Nabar, and D. Gore, *Introduction to Space-Time Wireless Communications*, 1st ed. New York, NY, USA: Cambridge University Press, 2008.

[14] Q. H. Spencer, A. L. Swindlehurst, and M. Haardt, "Zero-forcing methods for downlink spatial multiplexing in multiuser MIMO channels," *IEEE Transactions on Signal Processing*, vol. 52, no. 2, pp. 461–471, 2004.

References

148

Paper G

Geometry-Based Stochastic Channel Models for 5G:
Extending Key Features for Massive MIMO

Àlex Oliveras Martínez, Patrick Eggers, Elisabeth De Carvalho

Abstract

This paper introduces three key features in geometry-based stochastic channel models in order to include massive MIMO channels. Those key features consists of multi-user (MU) consistency, non-stationarities across the base station array and inclusion of spherical wave modelling. To ensure MU consistency, we introduce the concept of "user aura", which is a circle around the user with radius defined according to the stationarity interval. The overlap between auras determines the share of common clusters among users. To model non-stationarities across a massive array, sub-arrays are defined for which clusters are independently generated. At last, we describe a procedure to incorporate spherical wave modelling, where a cluster focal point is defined to account for distance between user and cluster.

1 Introduction

In a massive MIMO (Multiple-Input Multiple-Output) system, the base station is equipped with a very large number of antenna elements and serves multiple users in the same time-frequency resource [1]. Under certain favorable propagation conditions (e.g. [2]), fast fading and uncorrelated noise at the receiver vanish, bringing huge gains in throughput, reliability and energy efficiency [3]. Massive MIMO is considered a key technology for the development of 5G [4].

The characteristics of the massive MIMO channel bring some challenges for inclusion in the existing geometry-based stochastic channel models (GSCM). The existing GSCM can be divided into two groups. We name them Winner-type and COST-type. The first ones are the main focus of this work and examples are the 3GPP spatial channel model (SCM), extended SCM (SCME) [5], Winner (WIM1), Winner II (WIM2) [6], Winner+ (WIM+) and QuaDRiGa [7]. Their main characteristic consists of the definition of the scatterers based on the angles of departure and angles of arrival, i.e. terminal perspective. On the other hand COST-type GSCM [8] defines the physical position of the scatterers in the simulation area.

Existing work proposes an extension of COST-type GSCM for massive MIMO [9]. The COST-type GSCM channel models defines the physical position of the scatterers, not directly angles of departure or arrival as seen from terminal. Consequently, it is difficult to extract parameters for the COST model using measurements (contrary to the case of the Winner type GSCM channel model). Those reasons explain why Winner-type GSCM is currently more widespread and is the preferred candidate for 5G channel modelling in standardization efforts.

One major drawback of Winner-type GSCM is that it does not support multi-user (MU) consistency. MU consistency refers to the generation of

channels for each users that are consistent with the distance between users in terms of observed clusters and their correlation. Winner-type GSCM fails to represent scenarios where the users are in close proximity, as the channels are generated independently for each user, regardless of the distance between users. As the performance of massive MIMO is related to the user channel vectors orthogonality [2], Winner-type GSCM models results in over-optimistic performance.

With the increase in the number of antennas, the size of the arrays also increases. Although compact array designs are desirable for operators, some papers argue that the real advantages of massive MIMO appear when the size of the array become large [10]. Non-stationarities have been observed in measurements [10, 11] for large but also compact arrays [10], so that it would appear that even for compact arrays, it becomes important to model non-stationarities. The non-stationarities are of different nature: the power can vary, the directions of departure/arrival varies, different parts of the array see different clusters, etc.
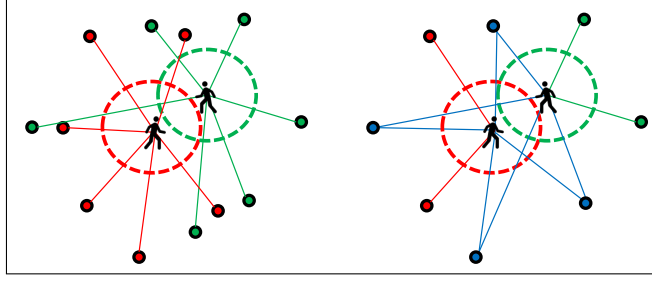
Winner-type GSCM define the clusters by their angles of departure and angles of arrival and rely on a planar wave approximation. When the array becomes larger or the clusters are at close proximity to the users, the planar wave approximation becomes inexact calling for a spherical wave modelling and a modification of Winner-type GSCM models.

The present study proposes solutions to extend Winner-type GSCM to include MU consistency, non-stationarities across the base station array and spherical wave modelling. We introduce the concept of "aura" associated to each user, which is a circle centered on the user with radius defined by the stationarity interval. When users are at close proximity, their auras overlap and the overlapping surface defines the common clusters shared among users. An example is presented in Fig. G.1. We propose an algorithm to compute the number of clusters to be shared among pairs of users, then groups of multiple users. As a pre-step, an algorithm to divide the users into connected groups is used to increase the speed of the process. The large scale parameters (LSP) of one of the users sharing the cluster are used to compute the parameters of the cluster. Finally the cluster parameters are shared with the other users sharing the cluster. Then the parameters or the position of the clusters (depending on the distance between user and cluster) is recalculated according to the position of the new user.

To account for non-stationarity effects, the base station is divided into sub-arrays with size defined by the stationarity distance (i.e. correlation or coherence distance with regard to visible clusters). Different realizations of the LSP at each sub-array are used to generate the clusters.

Spherical wave modeling, (similarly to QuaDRiGa's drifting procedure [7]) supports near field clusters at the base station side, by fixing focal points derived from the delays and angles of the clusters.

Fig. G.1: Left: Existing GSCM with independent clusters for users closely located. Right: Proposed extension with multiuser consistency where closely located users have common clusters

This work uses QuaDRiGa, a Winner-type GSCM, as a reference model on top of which to build the proposed extensions. However the ideas in the paper can also be applied to other Winner-type GSCM.

2 Definition of basic concepts

2.1 Segments

From WIM1 onwards the trajectory of the users is divided into smaller segments. These segments are defined such as the LSP of the channel remain constant (i.e. the segment length equals the stationarity interval). Therefore the number of clusters that each user has and the correspondent parameters can only change segment wise. This paper proposes an algorithm that checks the relative position of the users at the beginning of each segment and defines the number of common cluster for the rest of the segment. The proposed extension of the GSCM can only be applied if the user segment transitions are synchronized.

2.2 Clusters

In GSCM, physical objects are modeled as scatterers where the transmitted waves are reflected. These scatterers are divided into groups according to their delay and angle of departure or arrival, forming clusters. Each cluster is composed by 20 scatterers. The angles of the scatterers are samples of a Laplacian function, as shown in Fig. G.2. The parameters of the clusters of each user define the channel properties of that user. The proposed extension proposes to share some of the clusters between users that are near to each other to achieve the desired multiuser consistency. The number of shared clusters is related to the distance between users, but which clusters are shared can vary according to the implementation.
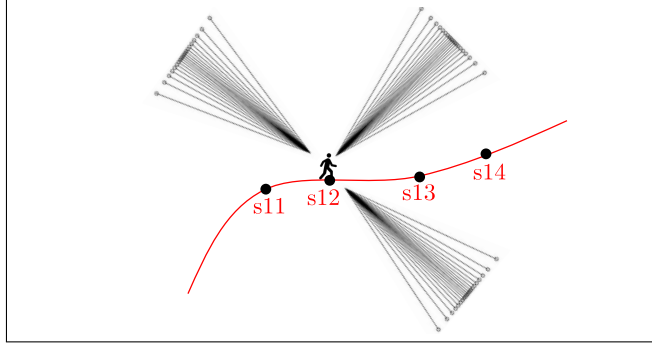
Fig. G.2: Angular representation of the clusters in Winner-type GSCM. The AoA defines the mean angle of the cluster and the angles of the scatters have a deterministic offset from this angle. All the scatterers in the cluster have the same delay (Not represented in this figure)

The common clusters between users have been observed in a massive MIMO channel measurement described in [10]. Due to lack of space the measurement campaign is not described here (for detail see [10]). In the measurement campaign the base station array has 64 elements divided in sets of 8 elements. There are 8 users holding a handset with 2 elements called *a* and *b*. The angle of arrival is estimated using steering-vector beamforming at each set of 8 elements. The 8 element set has a $13°$ -3 dB beamwidth and max. sidelobe level of -14.7 dB. We focus on the maximum power cluster to avoid a misinterpretation of the side lobes. This cluster is marked with a red dot. In Fig. G.3 the power angular spectrum for the 8 users in a non-Line-of-Sight scenario (called S-NLoS in [10]) is presented. Fig. G.3 shows that user 1 and user 3 separated 2.2 m have a cluster at $104°$ and $110°$ respectively. Due to the $13°$ resolution of the beamforming this can be considered a common cluster.

2.3 User aura

Where COST-type GSCM provide natural cluster sharing as it is cluster centric, the Winner-type GSCM are user centric. Despite QuaDRiGa made a mapping of the parameters to geometric positions to provide time evolution of the channel, it is still local to each user. To facilitate a possible sharing of clusters between users, we introduce the concept of an aura. The user aura is defined as the circle surrounding the users with radius equal to the stationarity interval. When two users are separated more than the stationarity interval they have independent channel vectors and their auras are disjoint. If two users are close to each other their auras overlap. The amount of overlapping area is proportional to the distance between the users. This proportion is used to define the amount of clusters that need to be shared
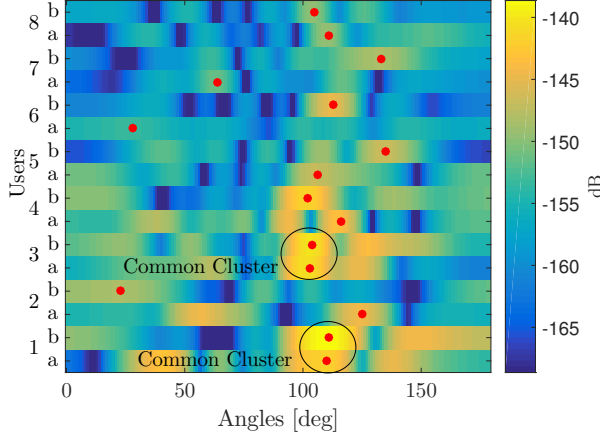
Fig. G.3: Common cluster observed between user 1 and 3 in an indoor NLoS scenario. Red dots mark the angle of maximum power
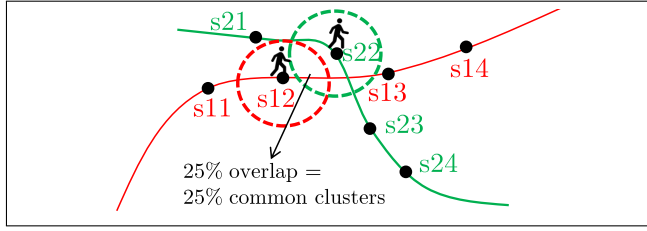

Fig. G.4: Track of two users divided into segments. sUX is the first position of user U in segment number X

between users. The overlapping of the auras is computed in the first position of each segment and the number of common clusters is kept constant along the segment. Fig. G.4 shows an example users' layout.

2.4 Aura at the base station

To generate non-stationaries from the base station perspective, the array is divided into sub-arrays in the same way the user trajectory is divided into segments. In the same way each user has defined an aura, the sub-arrays in the base station have also defined an aura of radius equal to the stationarity interval. The sub-arrays have the length of the stationarity interval, and the aura is centered at the center of the sub-array. Notice that the stationarity interval along the base station array might differ from the user perspective. To generate the non-stationarities over the array, the exposed extension proposes to chose different parameters of the cluster at the transmitter for each sub-array. See an example in Fig. G.5. The auras of adjacent sub-arrays can
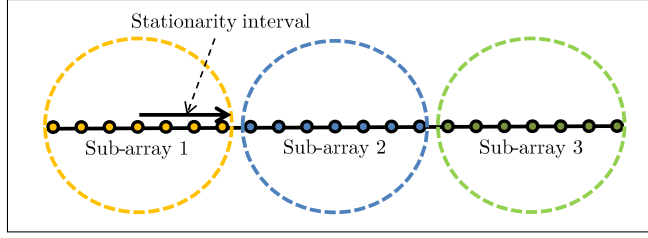
Fig. G.5: Division of the base station array into sub-arrays according to the stationarity interval

be overlapped to produce a gradual share of the clusters. However, in this work it is not implemented.

2.5 Drifting

One contribution of QuaDRiGa is the time evolution channel consistency. It means that in each snapshot the channel is consistent with the previous and the following snapshot. At the initial position of the segment the parameters of the clusters are calculated. These parameters are updated according to the movement of the user in the subsequent snapshots of the channel. To achieve this time evolution the position of the scatterers has to be defined and kept constant through the segment. Then, the relative position between the user and the scatter can be computed, and the new parameters of the scatter can be updated. The proposed extension uses this concept to define the position of the scatters both at the receive and the transmit side and therefore the spherical waves can be used.

3 Extension of GSCM

3.1 Simulation flow

Winner-type GSCM channel model follows nine steps to generate the channel coefficients [7]:

1. Define the parameters of the simulation (Positions of the users and base stations, Antenna arrays, Tracks of the users, Segments, Scenarios)

2. Generation of the correlation maps using the scenarios configuration files

3. Generation of clusters for each segment

4. Generation of the scatterers inside the clusters and calculation of the vector for each scatterer and each position of the user
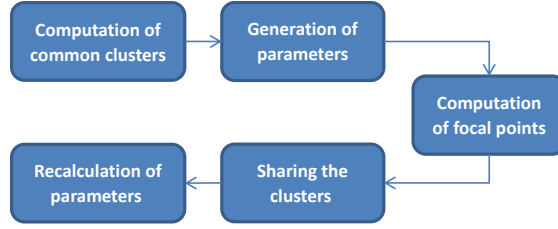
Fig. G.6: Modification of the QuaDRiGa step 3 into 5 sub-steps

5. Calculate antenna response for each angle

6. Calculate the phases using the position of the clusters and the antennas

7. Sum of the coefficients of the 20 scatterers. The channel matrix for each cluster is created

8. Merge the adjacent segments (birth/death process)

9. Formatting of channel coefficients and delays

To obtain the multi-user consistency, non-stationarities across the array and the spherical waves propagation, Aalborg University (AAU) modifies step 3 of the nine steps.

3.2 Description of extensions

The modified step 3 has 5 sub-steps. These sub-steps are presented in Fig. G.6:

1. Calculate proportion of common clusters

2. Generation of initial parameters

3. Computation of the focal points of the clusters

4. Sharing the clusters

5. Recalculating parameters

3.3 Calculate proportion of common clusters

The proposed solution uses a simple preprocessing algorithm and an algorithm designed by AAU to compute the number of common cluster between users depending on their proximity. These algorithms are simple to implement. We want to remark that an algorithm for computing the overlapping of circles with exact precision already exist in [12]. The implementation of such
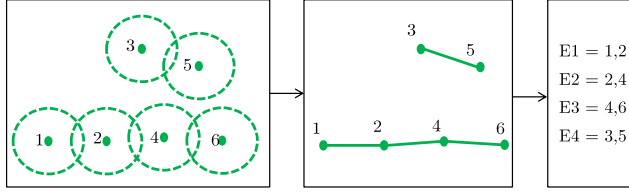
Fig. G.7: Simulation layout with six users converted into a graph and an edges description

algorithm can be complex and the processing time long. The accuracy provided by such algorithm is not necessary. Therefore we develop a simplified method.

First there is a preprocessing of the layout to cluster the users in connectivity groups. This algorithm makes groups of users whose auras are overlapping [13]. This step is necessary to increase the efficiency of the algorithm to compute the number of common clusters. This algorithm uses graph theory to find connected components. Each user is represented as a vertex of the graph. If the distance between two users is smaller than the sum of its radius their auras are overlapping and there is an edge between the two vertices representing the two users. An example can be seen in Fig. G.7. The algorithm performs a deep search on each connected component. Each new vertex reached is marked. When no more vertices can be reached along edges from marked vertices, a connected component has been found. An unmarked vertex is then selected, and the process is repeated until the entire graph is explored. This algorithm requires memory space linear with $max(V, E)$, and time linear with $max(V, E)$. Where V is the number of vertices (i.e. users in the layout) and E is the number of edges of the graph (i.e. overlapping auras in the layout).

The algorithm to compute the common clusters is designed by AAU and it is based on finding the mean distance of the groups of users to the centroid of the groups. Then using a linear relationship (or another relationship) this distance gives a proportion of clusters to be shared among the group of users. This procedure is repeated for groups of two, three, four, etc. users until the maximum is reached. This algorithm is presented in Algorithm 1 and Fig. G.8 shows an example.

In the previous algorithm the centroid of the group of users (i.e. m) is computed as,

$$m = \frac{(x_1, y_1, z_1) + \cdots + (x_N, y_N, z_N)}{N} \tag{G.1}$$

where (x_n, y_n, z_n) is the position of user n in Cartesian coordinates (lets call it Pos_n).

foreach *group of N users (N ∈ {1, ..., max(users)})* **do**
    if $N = 1$ **then**
        proportion of clusters for the individual users $= 1$;
    else
        find centroid of the group of users: m;
        if *(all distances to m)<R* **then**
            find mean distance to m: md;
            proportion of clusters $= \frac{-md}{R+1}$: p;
            subtract $\frac{p}{N-1}$ from the groups containing $N-1$ users;
        else
            the users with (distance to m)>R are too far away and no
            clusters are shared in this group;
        end
    end
end

Algorithm 1: Compute the number of common clusters
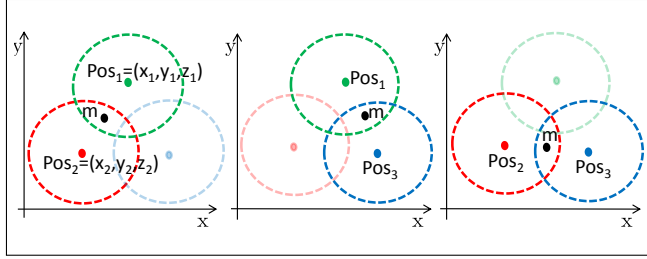
Fig. G.8: Example of the clustering algorithm for groups of 2 users (N = 2). User 1 in green, user 2 in red and user 3 in blue

Compute the distances from the users to the centroid and find if the auras are overlapping using:

$$\|m - Pos_n\| < R \tag{G.2}$$

To compute the mean distance of the group of users to the centroid use:

$$md = \frac{\|m - Pos_1\| + \cdots + \|m - Pos_N\|}{N} \tag{G.3}$$

The proportion of clusters to share corresponds to a linear relationship with the mean distance to the centroid (proportion of clusters $p = \frac{-md}{R+1}$). This linear function has been chosen for its simplicity. However, empirically derived cluster sharing functions can easily be substituted here.
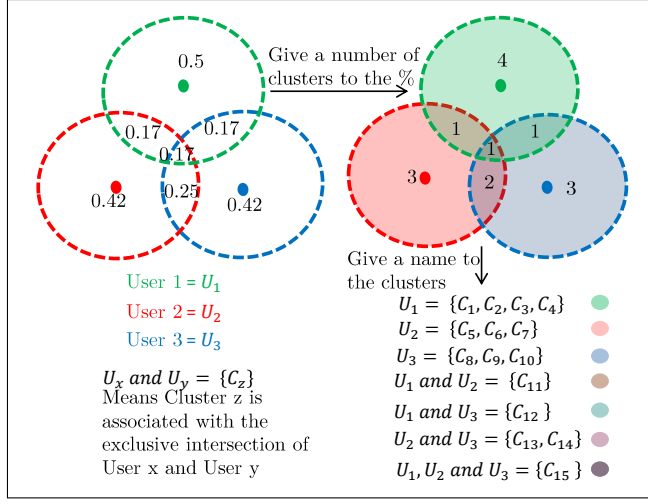
Fig. G.9: Example of the clustering algorithm with 7 clusters (C) per user(U). First compute the proportion of common clusters for each group, then compute the number of clusters and finally assign a set of cluster names

After the explained algorithm, each user has a proportion of individual clusters and each intersection of auras has a proportion of common clusters. Knowing the proportion of clusters to share and the total number of clusters, each user and group of users is assigned with a number of clusters as seen in Fig. G.9. Notice that the parameters defining each cluster (i.e. angles, delay, position) have not been computed yet. The clusters are only defined by its number, and the parameters are computed in the following sub-step.

3.4 Generation of initial parameters

The initial delays, powers and angles (i.e. azimuth of departure and arrival, elevation of departure and arrival) are generated for each cluster (Cx) in each segment following QuaDRiGa's procedure explained in [7]. To create non-stationarities across the array, we modify this procedure to have one azimuth angle and one elevation angle of departure for each sub-array. There are $4 + 2A$ parameters for each cluster (being A the number of sub-arrays). This procedure uses user (Ux) specific parameters (drawn from the large scale parameter maps) to generate the cluster parameters. If the cluster belongs only to one user (e.g. C_3 in Fig. G.9) the parameters of that user are used to generate the cluster. On the other hand if the cluster belongs to more than one user (e.g. C_{11} in Fig. G.9) one of the users is picked to use its parameters to generate the cluster. We propose to pick the users randomly with a uniform distribution, but other methods are possible. The values of the departure

angles are drawn independently for each sub-array.

3.5 Computation of the focal points of user side clusters

QuaDRiGa's drifting procedure determines the position of the Last Bounce Scatterer (LBS) and keeps it fixed during the whole segment, [7], global step 4. In this sub-step only the first part of the QuaDRiGa's drifting procedure is used to find the focal point of the LBS and add it to the table of parameters for each cluster. Even if the cluster belongs to more than one user (e.g. C_{11} in Fig. G.9) the focal point is referenced to the user used to generate the parameters of the cluster.

Then it is necessary to find the focal point at the transmitter side. We call the focal point at the transmit side First Bounce Scatterer (FBS) analogous to the QuaDRiGa nomenclature. We propose to use the same procedure used by QuaDRiGa to find the focal point of the clusters at the transmit side. Next we explain how to adapt their procedure to the transmit side. Fig. G.10 shows the parameters used.

First the total length (from transmitter, to cluster, to receiver) is obtained from the delay,

$$d_c = \tau_c c_0 + |r_{0,a,k}| \tag{G.4}$$

where $|r_{0,a,k}|$ is the distance between sub-array a and user k (i.e. $||APos_a - Pos_{k,s}||$, where $APos_a$ is the central position of the sub-array a and $Pos_{k,s}$ is the first position of the user k in the segment s), τ_c is the excess delay and c_0 is the speed of light. Then the departure angles of the cluster are converted into Cartesian coordinates. $\hat{e}_{c,a,s}$ is the vector defining the direction of the cluster c of sub-array a at segment s.

$f_{c,a,s}$ defines the vector from the user to the cluster. Considering the triangle with vertices at the center of the sub-array, at the user position, and at the focal point of the cluster, and using the cosine theorem we can compute the distance from the sub-array to the cluster.

$$f_{c,a,s}^2 = |r_{0,a,k}|^2 + |e_{c,a,s}|^2 - 2|r_{0,a,k}||e_{c,a,s}|cos(\beta_{c,a,s}) \tag{G.5}$$

$$(d_c - |e_{c,a,s}|)^2 = |r_{0,a,k}|^2 + |e_{c,a,s}|^2 + 2|e_{c,a,s}|r_{0,a,k}^T \hat{e}_{c,a,s} \tag{G.6}$$

$$|e_{c,a,s}| = \frac{d_c^2 - |r_{0,a,k}|^2}{2(d_c r_{0,a,k}^T \hat{e}_{c,a,s})} \tag{G.7}$$

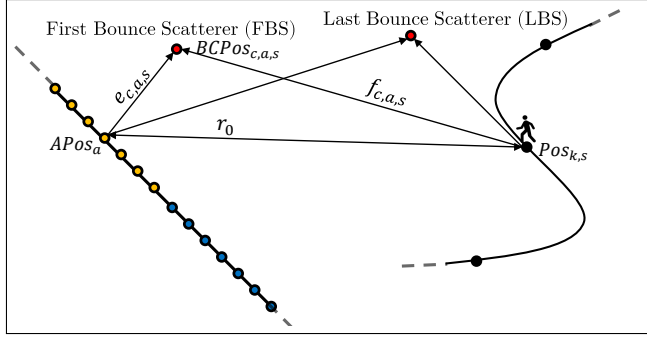The vector from the transmitter position to the focal point of the cluster at the transmit side is,

Fig. G.10: Computation of the focal point of the cluster at the transmitter side

Fig. G.11: Example of the cluster sharing

$$e_{c,a,s} = |e_{c,a,s}|\hat{e}_{c,a,s} \tag{G.8}$$

And using this vector and the position of the transmit array we can find the position of the focal point of the cluster at the transmit side (FBS) as

$$BCPos_{c,a,s} = e_{c,a,s} + APos_a \tag{G.9}$$

After adding the focal points, the clusters have 5+3A parameters in their tables (i.e. power, delay, azimuth of arrival, elevation of arrival, focal point at receiver and for each sub-array: azimuth of departure, elevation of departure and focal point at transmitter).

3.6 Sharing the clusters

In sub-step 3.3 we showed that each cluster could have more than one owner, but in sub-step 3.4 the parameters of only one user have been used to generate the cluster. In this sub-step the clusters are shared with the other users that they belong to, according to the results of 3.3. In other words, the clusters and their generated parameters are duplicated to the parameter tables of the corresponding users. See an example in Fig. G.11.
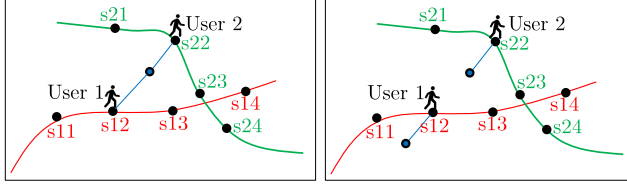
Fig. G.12: If the cluster is near to the users to share the parameters can result in very different clusters (right). It is better to share the focal point (left)

3.7 Recalculating parameters

As some clusters have been generated using the parameters of one user, but after sub-step 3.6 they have been shared with another user, it is necessary to recalculate the parameters for the new user. The reason is because the focal point of the cluster has been calculated using the angles and positions of one user, but the position of the other user can be different. There are two options to recalculate the parameters, both shown in Fig. G.12. The first option is to keep the same parameters generated in sub-step 3 and recalculate the two focal points of the cluster for the new user. The second option is to keep the same focal point and recalculate the other parameters (including the angles of departure). If the clusters are far away from the users it is possible to keep the same parameters and avoid recalculating the focal point because the relative position does not change very much. However, if the cluster is near the users, we have to recalculate the focal point, else it would result in effectively different clusters for the users. We propose that if the clusters are less than 3 segment lengths away the focal point is kept and the other parameters are recalculated. Otherwise, the opposite happens.

4 Conclusion

This paper extends the framework of the existing Winner-type GSCM towards the evolution of 5G channel models for massive MIMO. Winner-type GSCM are heavily employed by the industry, so a modification is necessary to continue build on existing knowledge base. The paper focuses on the three main limitations of the existing models that prevents the proper simulation of massive MIMO systems. First of all the lack of a method to model the multiuser consistency. Then, the impossibility to generate non-stationarities over the base station array. Finally the limitation of using the planar wave approximation. Using QuaDRiGa as a reference model, several modifications are proposed to overcome these limitations.

References

[1] T. L. Marzetta, "Noncooperative cellular wireless with unlimited numbers of base station antennas," *IEEE Transactions on Wireless Communications*, vol. 9, no. 11, pp. 3590–3600, 2010.

[2] H. Q. Ngo, E. Larsson, and T. Marzetta, "Aspects of Favorable Propagation in Massive MIMO," in *Signal Processing Conference (EUSIPCO), 2014 Proceedings of the 22nd European*, no. 2.   IEEE, 2014, pp. 76–80.

[3] E. G. Larsson, O. Edfors, F. Tufvesson, and T. L. Marzetta, "Massive MIMO for Next Generation Wireless Systems," *IEEE Communications Magazine*, vol. 52, no. 2, pp. 186–195, 2014.

[4] F. Boccardi, R. Heath, A. Lozano, T. L. Marzetta, and P. Popovski, "Five disruptive technology directions for 5G," *IEEE Communications Magazine*, vol. 52, no. 2, pp. 74–80, 2014.

[5] D. Baum, J. Hansen, and J. Salo, "An interim channel model for beyond-3G systems: extending the 3GPP spatial channel model (SCM)," in *2005 IEEE 61st Vehicular Technology Conference*, vol. 5.   IEEE, 2005, pp. 3132–3136.

[6] P. Kyösti, J. Meinilä, L. Hentilä, X. Zhao, T. Jämsä, C. Schneider, M. Narandzi, M. Milojevi, A. Hong, J. Ylitalo, V.-M. Holappa, M. Alatossava, R. Bultitude, Y. D. Jong, and T. Rautiainen, "IST-4-027756 WINNER II D1. 1.2 V1. 2 WINNER II Channel Models," Tech. Rep., 2007.

[7] S. Jaeckel, L. Raschkowski, K. Borner, and L. Thiele, "QuaDRiGa: A 3-D multi-cell channel model with time evolution for enabling virtual field trials," *IEEE Transactions on Antennas and Propagation*, vol. 62, no. 6, pp. 3242–3256, 2014.

[8] L. Liu, C. Oestges, J. Poutanen, K. Haneda, P. Vainikainen, F. Quitin, F. Tufvesson, and P. Doncker, "The COST 2100 MIMO channel model," *IEEE Wireless Communications*, vol. 19, no. 6, pp. 92–99, 2012.

[9] X. Gao, J. Flordelis, G. Dahman, F. Tufvesson, and O. Edfors, "Massive MIMO Channel Modeling - Extension of the COST 2100 Model," Tech. Rep., 2015.

[10] À. Oliveras Martínez, E. D. Carvalho, and J. Ø. Nielsen, "Towards Very Large Aperture Massive MIMO: a measurement based study," in *Globecom Workshops (GC Wkshps), 2014*.   IEEE, 2014, pp. 281–286.

[11] X. Gao, F. Tufvesson, O. Edfors, and F. Rusek, "Measured propagation characteristics for very-large MIMO at 2.6 GHz," in *2012 Conference Record of the Forty Sixth Asilomar Conference on Signals, Systems and Computers (ASILOMAR).* IEEE, 2012, pp. 295–299.

[12] F. Librino, M. Levorato, and M. Zorzi, "An algorithmic solution for computing circle intersection areas and its applications to wireless communications," in *2009 7th International Symposium on Modeling and Optimization in Mobile, Ad Hoc, and Wireless Networks*, 2009, pp. 1–10.

[13] J. Hopcroft and R. Tarjan, "Efficient Algorithms for Graph Manipulation," *Communications of the ACM*, vol. 16, no. 6, pp. 372–378, 1973.